REGIONAL HYDROLOGY CAPTURED IN NORTHERN BORNEO

RAINWATER AND DRIPWATER ISOTOPE VARIABILITY

A Dissertation
Presented to
The Academic Faculty

by

Jessica Woods Moerman

In Partial Fulfillment
of the Requirements for the Degree
Doctor of Philosophy in the
School of Earth and Atmospheric Sciences

Georgia Institute of Technology
May 2015

Approved by:

Dr. Kim Cobb, Advisor
School of Earth and Atmospheric Sciences
Georgia Institute of Technology

Dr. Peter Webster
School of Earth and Atmospheric Sciences
Georgia Institute of Technology

Dr. Jean Lynch-Stieglitz
School of Earth and Atmospheric Sciences
Georgia Institute of Technology

Dr. Jess Adkins
Division of Geological and Planetary Sciences
California Institute of Technology

Dr. Chris Reinhardt
School of Earth and Atmospheric Sciences
Georgia Institute of Technology

Date Approved: February 10, 2015

For my grandfather, Dr. Pietro Pasqua

ACKNOWLEDGEMENTS

I begin, first and foremost, by thanking Dr. Kim Cobb for her dedicated guidance as my Ph.D. advisor. Through her example and expert advice, she has trained me not only in how to be a scientist but also how to balance my passion for research and discovery with being a wife and mother. I can't thank you enough for this and for giving me the opportunity to visit beautiful Borneo, twice! I also want to thank the members of my dissertation committee, Drs. Peter Webster, Jean Lynch-Steiglitz, Chris Reinhardt, and Jess Adkins for their guidance not only with respect to my thesis but also in my professional development. I especially want to thank Jess for allowing me to come out to Caltech and learn the ropes in the clean lab.

A huge thanks goes out to the Mulu Gang: Stacy Carolin, Jud Partin, Syria Lejau, Jenny Malang, and all the staff at Gunung Mulu National Park. Exploring the jungles and caves of Mulu with y'all has been a transformative experience. Despite the exhausting work of lugging huge rocks out of the depths of the caves, habitual lack of sleep, and encounters with snakes, leeches, fire centipedes, and the dreaded rattan, my time spent with you during our expeditions have been among the best of my life. Syria and Jenny, thank you so much for collecting the hundreds of dripwaters that made this dissertation possible and for always keeping me safe in the caves. Jud, thank you for training me up, both as a cave explorer and in the ways of the stalagmite. Stacy, thank you for all the laughs, amazing science chats, and for keeping me sane out in the field and in the lab.

I also want to thank my wonderful labmates, office mates, and friends at Georgia Tech. To Stacy, Hussein, Jess, Pam, and Bronwen, you made the long hours at the office

a surprising delight. Thank you for all the many favors throughout the years, help with organizing field expeditions, and scientific insights. Jake, Morris, and Keaton: thank you for keeping me well caffeinated, on top of current events, and my cupboard stocked with Taco Mac beer glasses. Mary, thank you for being such a kind and wonderful friend since the beginning. Our writing sessions helped me keep everything on track, and our long chats catching up over coffee and Highland Bakery lunch have meant so much to me.

And finally, the biggest thanks goes out to my family. Thank you mom and dad for always encouraging me to go after my dreams and passions. I wouldn't be here without your love and support. And Chris, my loving supportive husband, I can't thank you enough for journeying step-by-step through this PhD with me. Thank you for your tremendous support and for all the trips to the grocery, delicious meals, dishes washed, and floors swept while I was stuck in my study hole. Thank you for being my rock and cheerleader when I felt like giving up. Thank you for your patience and hands-on help during all the paper and proposal writing and expedition prep. Thank you for always encouraging me to go after the difficult but important things, even though you knew it would be tough on both of us but always worth it in the end. And most of all, thank you for our beautiful son, Liam. He couldn't be more perfect, and I'm so excited to embark on this next leg of our journey together as a family.

TABLE OF CONTENTS

LIST OF TABLES

LIST OF FIGURES

LIST OF SYMBOLS AND ABBREVIATIONS

$\delta^{18}O$	Oxygen isotopic composition
δD	Hydrogen isotopic composition
‰	Per mil or per thousand
1σ	One standard deviation
AMOC	Atlantic meridional overturning circulation
dpm	drips per minute
ENSO	El Niño – Southern Oscillation
GCM	General circulation model
GMWL	Global meteoric water line
GNIP	Global Network of Isotopes in Precipitation
IAEA	International Atomic Energy Agency
ITCZ	Intertropical convergence zone
JJA	June-July-August
ka	Thousand years ago
L2	Drip site “Lang’s Cave”
LMWL	Local meteoric water line
MJO	Madden-Julian Oscillation
NINO3	Boxed region of 150°W-90°W and 5°N-5°S
NINO3.4	Boxed region of 170°W-120°W and 5°N-5°S
NINO4	Boxed region of 160°E-150°W and 5°N-5°S
NIST	National Institute of Standards and Technology
NOAA	National Oceanic and Atmospheric Administration
OISST	Optimum interpolation sea surface temperature

OLR	Outgoing longwave radiation
SLP	Sea level pressure
SOI	Southern Oscillation Index
SON	September-October-November
SST	Sea surface temperature
SSTa	Sea surface temperature anomaly
TRMM	Tropical Rainfall Measuring Mission
U/Th	Uranium/thorium series
V-GISP	Vienna-Greenland Ice Sheet Precipitation
V-PDB	Vienna-Pee Dee Belemnite
V-SMOW	Vienna-Standard Mean Ocean Water
V-SLAP	Vienna-Standard Light Antarctic Precipitation
WPWP	West Pacific Warm Pool
WF	Drip site “Wind Fast”
WS	Drip site “Wind Slow”

SUMMARY

Oxygen and hydrogen isotopes ($\delta^{18}O$, δD) are increasingly powerful tools for reconstructing past hydroclimate variability. The utility of $\delta^{18}O$- and δD-based paleoclimate records, however, depends on our understanding of how well these tracers reflect past climate conditions. The dynamics controlling the relationship between climate and water isotope variability are highly complex and often poorly constrained, especially in the tropics, where many key high-resolution paleoclimate records rely on past rainfall isotopes as proxies for hydroclimate. In this dissertation, I use multi-year timeseries of daily rainfall and biweekly dripwater $\delta^{18}O$ from northern Borneo – a site for stalagmite $\delta^{18}O$-based paleoclimate reconstruction in the heart of the West Pacific Warm Pool – to track the cloud-to-calcite transformation of $\delta^{18}O$ and its relationship to large-scale climate variability.

Chapter 2 investigates the variability of rainfall $\delta^{18}O$ from northern Borneo on diurnal to interannual timescales and its relationship with local and regional climate. Rainfall $\delta^{18}O$ is observed to vary inversely with precipitation amount during a single storm event and on monthly and longer timescales. Robust relationships are also found between northern Borneo rainfall $\delta^{18}O$ variability and the intraseasonal Madden-Julian Oscillation (MJO) and interannual El Nino Southern Oscillation (ENSO), with lower rainfall $\delta^{18}O$ values corresponding with wetter conditions in agreement with the 'tropical amount effect'. Comparisons with satellite-derived precipitation and convective activity further reveal that rainfall $\delta^{18}O$ is best interpreted as a reflection of regional-scale, rather than local, hydrological variability.

Chapter 3 investigates the rainfall-to-dripwater transformation of climate-related isotopic signals following water transit through the Borneo cave system. ENSO-related interannual $\delta^{18}O$ variability is preserved in cave dripwaters but MJO-related intraseasonal variations are largely homogenized and therefore absent in dripwater $\delta^{18}O$. Water mixing within the vadose zone is revealed as the primary rainfall-to-dripwater transformation process. Using a simple dripwater mixing model, dripwater residence times of 3-10 months are constrained. Different groundwater residence times and flow pathways are found to produce different dripwater $\delta^{18}O$ timeseries from the same rainfall $\delta^{18}O$ input. The preservation of large ENSO-related interannual variability in Borneo dripwater $\delta^{18}O$ bolsters the prospect of reconstructing past ENSO change from fast-growing northern Borneo stalagmites. A statistical stalagmite forward model further demonstrates that amplitudes of El Niño-related anomalies are inversely correlated to dripwater residence time in high-resolution stalagmite $\delta^{18}O$ records and the interaction of ENSO and dripwater residence times can lead to significant offsets in low-resolution records. This comprehensive analysis illustrates the influence of karst hydrology on the climate-related $\delta^{18}O$ signals that are ultimately archived in stalagmite $\delta^{18}O$.

Overall, this dissertation provides empirical support for the interpretation of northern Borneo stalagmite $\delta^{18}O$ as a robust indicator of regional-scale hydroclimate variability, where higher $\delta^{18}O$ reflects regional drying. More generally, this research provides a roadmap for obtaining more nuanced interpretations of speleothem $\delta^{18}O$ records from multi-year, high-resolution, paired timeseries of rainfall and dripwater $\delta^{18}O$.

CHAPTER 1

INTRODUCTION

1.1 Stable water isotopes

Stable isotopologues of water (e.g. $H_2{}^{16}O$, $HD^{18}O$) are powerful tracers of the hydrologic cycle due to their differential fractionation during condensation and evaporation processes. Given their unique relationship with geography and climate, the isotopic composition of natural waters provides insight into many complex systems and thus has wide-ranging applications across multiple fields including climate science, forensic science, water resource management, agriculture, and many others. In the field of paleoclimatology, oxygen and hydrogen isotopes ($\delta^{18}O$, δD) are used to reconstruct past variability in temperature and hydrology. Until recently, long, continuous records of past climate conditions were limited to reconstructions from marine sediments and high-latitude ice cores. As such, developments in measuring water isotopes in low-latitude archives, such as speleothem $\delta^{18}O$, leaf wax δD, and tropical ice cores, have greatly advanced the field. Over the last decade, speleothems in particular have emerged as a key terrestrial, low-latitude link to marine and high-latitude records due to their broad geographical prevalence, often-continuous deposition at high rates, and absolute age control [e.g. *Cruz et al.*, 2005; *Fleitmann et al.*, 2003; *Wang et al.*, 2001]. The utility of these records, however, depends on our ability to accurately interpret them, which in turn ultimately relies on our understanding of the relationship between climate and stable water isotope variability. The following sub-sections review the fundamentals of water isotope geochemistry, the relationship between water isotope variability and hydrological

processes, how the climate-isotope relationship may be altered during water transport through cave systems, and an overview of the climate, geology, and stalagmite $\delta^{18}O$ reconstructions of northern Borneo.

1.1.1. Water isotope systematics

Water has five stable isotopologues (e.g. molecules that differ only in their isotopic composition), which are comprised of two of the two different stable isotopes of hydrogen (^{1}H, ^{2}H) and one of the three different isotopes of oxygen (^{16}O, ^{17}O, ^{18}O). Given the relatively low abundance of ^{17}O, most water cycle and paleoclimate studies have exclusively utilized ^{1}H, ^{2}H (or D), ^{16}O, and ^{18}O, although recent theoretical and analytical advances have made the measurement of ^{17}O in water and carbonates and its possible use as a paleo-proxy feasible [e.g. *Angert et al.*, 2004; *Landais et al.*, 2010; *Luz and Barkan*, 2000; *Passey et al.*, 2014]. For simplicity, I primarily focus on the isotopes of oxygen for the remainder of this section – though all discussion also applies to hydrogen isotope systematics. I also refer to the isotopologues of water in general as 'water isotopes.'

The use of water isotopes in hydrologic studies began with the recognition that the isotopic compositions of oxygen and hydrogen in precipitation varied in tandem [*Friedman*, 1953] and that meteorological processes fractionate oxygen and hydrogen isotopes in water in a predictable and well-correlated manner [*Craig*, 1961]. Mass-dependent isotopic fractionation is characterized by the preferential partitioning of isotopes between two substances (e.g. water versus carbonate) or physical phases (e.g. liquid versus vapor) based on their mass-based properties, such as atomic or molecular velocity, diffusivity, and bond strength. During chemical reactions and phase transitions,

lighter isotopes are more readily incorporated into higher energy substances or phases, due to (1) the relatively lower energy required to break bonds given their smaller mass and (2) higher diffusion velocities given their lighter weight [*Clark and Fritz*, 1997]. The degree of partitioning is expressed by the fractionation factor (α), defined below as

$$\alpha_{A\text{-}B} = R_A/R_B \tag{1.1}$$

where R is the ratio of the heavy to light isotope (e.g. $^{18}O/^{16}O$) of the respective substance or phase, A and B [*Hoefs*, 2004]. Variation in oxygen isotopic composition is conventionally expressed in 'delta' notation ($\delta^{18}O$) as defined in Eqn. 2 and reported relative to the $^{18}O/^{16}O$ ratio of an international standard in units of per mil (‰).

$$\delta^{18}O = \left(\frac{{}^{18}O/{}^{16}O_{sample} - {}^{18}O/{}^{16}O_{\text{standard}}}{{}^{18}O/{}^{16}O_{\text{standard}}} \right) \times 1000 \tag{1.2}$$

The reference standard for water samples is Vienna Standard Mean Ocean Water (V-SMOW) and Vienna Pee Dee Belemnite (V-PDB) for carbonates. Both standards by definition have a $\delta^{18}O$ value of 0‰. As such, positive (negative) sample $\delta^{18}O$ values indicate that the sample has a higher (lower) $^{18}O/^{16}O$ ratio than the standard. The terms 'lighter' and 'more depleted' are also commonly used to signify more negative $\delta^{18}O$ values and 'heavier' and 'more enriched' for more positive $\delta^{18}O$ values. These terms are used interchangeably throughout this dissertation.

Phase transitions mediated by condensation and evaporation are the most relevant water isotope fractionation processes for studies of the hydrologic cycle. During condensation, the heavier isotope is preferentially incorporated into the condensate, leaving the residual vapor pool relatively depleted in the heavy isotope. Condensation is typically considered an equilibrium fractionation process, whereby phase transitions

between vapor and liquid in a closed environment are fully reversible and the forward and backward reaction rates are uniform, as denoted by the double arrow in the equation below,

$$H_2O_{(l)} + H_2{}^{18}O_{(v)} \Leftrightarrow H_2{}^{18}O_{(l)} + H_2O_{(v)} \quad (1.3)$$

Equilibrium fractionation is a temperature-dependent process [*Mook*, 2001]. In the case of condensation, greater fractionation occurs at lower condensation temperatures given the larger difference in vibrational and rotational energy of water molecules between heavy versus light isotopes in colder conditions [*Criss*, 1999]. Under equilibrium conditions, $\delta^{18}O$ and δD values of meteoric water co-vary in a well-correlated fashion [*Craig*, 1961; *Dansgaard*, 1964], represented by the following linear equation

$$\delta D = 8*\delta^{18}O + 10 \quad (1.4)$$

This empirical linear relationship, known as the Global Meteoric Water Line (see Figure 2.2) reflects that, when in equilibrium, hydrogen isotopic fractionation is ~8x more efficient than oxygen isotopic fractionation owing to hydrogen's smaller molecular size and binding energy [*Majoube*, 1971].

During evaporation, the lighter isotope is preferentially incorporated into the vapor phase, leaving the residual liquid relatively enriched in the heavy isotope. Evaporation often occurs as a non-equilibrium or "kinetic fractionation" process. Under kinetic fractionation, one side of the reaction is favored over the other,

$$H_2{}^{16}O_{(l)} \rightarrow H_2{}^{16}O_{(v)} \quad (1.5)$$

Kinetic fractionation occurs when the rate of the forward reaction accelerates, often stemming from an abrupt change in temperature or the removal of evaporated vapor by turbulent processes creating open rather than closed system behavior [*Clark and Fritz*,

1997]. Since the diffusion velocity of $H_2{}^{18}O$ is slower than that of HDO, the ~1:8 equilibrium ratio of $\delta^{18}O$ versus δD in precipitation will increase as a higher relative proportion of ^{18}O to ^{2}H remains in the liquid phase. The degree of deviation from equilibrium fractionation is expressed by the secondary parameter deuterium-excess, or d-excess, whereby

$$\text{d-excess} = \delta D - 8*\delta^{18}O \quad (1.6)$$

The value of d-excess depends on the humidity and temperature at the place of evaporation [*Mook*, 2001]. The below-cloud evaporation of raindrops typically yields small to negative d-excess values. Meteoric water lines with $\delta D/\delta^{18}O$ slopes less than the equilibrium slope of 8 are also commonly used to fingerprint the occurrence of kinetic evaporative fractionation [*Gat*, 1971].

To better characterize mechanisms driving the hydrologic cycle and global circulation patterns, the International Atomic Energy Agency (IAEA) launched a worldwide observational survey of oxygen and hydrogen isotopes in precipitation in 1961, which is now known as the Global Network of Isotopes in Precipitation (GNIP). In a comprehensive report of the initial findings, Dansgaard [1964] identified several empirical 'effects' that describe broad relationships observed between precipitation isotopic composition and geographical and climatological features. Namely, these include the latitude effect, altitude effect, continental effect, and amount effect, whereby rainfall $\delta^{18}O$ becomes progressively lighter with increasing latitude, elevation, distance from the ocean or evaporation source, and precipitation amount, respectively [*Dansgaard*, 1964]. A simple Rayleigh distillation or 'progressive rainout' model is often invoked to explain these isotope effects [*Mook*, 2001]. Under this framework, one can consider a single

reservoir (e.g. an air parcel) with a single flux out (e.g. condensation). The first condensate to precipitate from this air parcel will preferentially incorporate the heavier isotope, leaving the residual vapor relatively depleted. As condensation proceeds and the fraction of vapor remaining in the parcel decreases, both the condensate and residual vapor become increasingly more depleted.

While the Rayleigh distillation model describes the primary features of these isotope effects fairly effectively to a first order degree, factors such as topography, climate regime, and air mass mixing, among others, complicate these seemingly straightforward relationships, particularly when the isotopic variability at a single station is considered. This is especially true for the amount effect, which is governed by a range of mechanisms. The next section discusses the amount effect and its contributing processes in greater detail.

1.1.2. Amount effect

The amount effect describes the empirical inverse relationship observed between precipitation amount and rainfall $\delta^{18}O$ at low latitudes, where temperature variations are relatively small. Dansgaard [1964] first recognized this empirical relationship, noting that average rainfall $\delta^{18}O$ tends to be lower (higher) at tropical sites with high (low) annual precipitation amounts. This seemingly simple relationship, however, is generated by complex interactions between multiple, oft-competing processes. The primary processes contributing to the amount effect include (1) progressive rainout [*Dansgaard*, 1964], (2) isotopic exchange between falling raindrops and the unsaturated air column [*Dansgaard*, 1964; *Gedzelman and Arnold*, 1994], (3) sub-cloud evaporation of falling raindrops [*Dansgaard*, 1964; *Risi et al.*, 2008a]; and (4) reinjection of already depleted vapor into

cloud system [*Lawrence et al.*; *Risi et al.*, 2008b]. Isotopic exchange and secondary evaporation mechanisms are dependent on the size of rain droplets and the relative humidity of the surrounding air, which in turn vary directly with precipitation intensity [*Ciais and Jouzel*, 1994; *Field et al.*, 2010; *Lee and Fung*, 2008]. Since the ambient air overall is typically more enriched than the rainfall and evaporation preferentially removes light isotopes from the liquid phase, these two processes act to increase the $\delta^{18}O$ of falling raindrops when precipitation rates are low, creating an 'amount effect' relationship. On the other hand, the reinjection of already depleted vapor back into a convective system acts to produce successively more depleted rainfall $\delta^{18}O$. With stronger convective recycling, vapor is reinjected more efficiently into the system and rainfall $\delta^{18}O$ becomes progressively more depleted [*Lawrence et al.*, 2004; *Risi et al.*, 2008b].

Although the amount effect was first characterized as a spatial relationship, it has been widely used as an interpretive framework for reconstructing past temporal changes in tropical hydroclimate in $\delta^{18}O$- and δD-based proxy records, with drier (wetter) conditions inferred from higher (lower) archived isotopic compositions. Models equipped with isotopic tracers, however, suggest that such spatial relationships may not adequately reflect temporal isotopic variability [e.g. *Schmidt et al.*, 2007]. This likely stems from the fact that numerous processes contribute to the amount effect, as discussed above. As originally noted by Dansgaard [1964], the dominant mechanism responsible for producing the amount effect varies from site-to-site. The relative dominance of a given process not only varies by location but also likely with timescale. The amount effect was originally characterized using monthly averages and long-term means of precipitation

amount and rainfall isotopic compositions [*Dansgaard*, 1964; *Rozanski*, 1993] but has also been observed on synoptic timescales during tropical cyclones and well-organized convective systems [e.g. *Lawrence et al.*, 2004]. As such, whether the same processes at a given site drive the amount effect on these different timescales remains unclear. With respect to paleoclimate interpretations, it is also uncertain if and how climate-isotope relationships may change over time and with forcing mechanism. Finally, it must be noted that processes unrelated to the amount effect also influence rainfall $\delta^{18}O$ at tropical sites. These include, among others, shifts in moisture source and/or trajectory, hydrological variability at the moisture source, and changes in precipitation seasonality. A generalized, 'one-size fits all' approach to interpreting $\delta^{18}O$-based records, therefore, may lead to inaccurate interpretations of past tropical hydroclimate variability. Indeed, Mook [2001] explicitly recommends that the amount effect be explored on a case-by-case basis via special local water isotope sampling programs. In this way, a process-based understanding of how the amount effect manifests at individual paleoclimate sites can be obtained, thus reducing uncertainty in interpretations of past climate variability.

1.1.3. Karst influences on cave dripwater isotopes

Paleoclimate reconstructions from speleothems rely upon the assumption that the isotopic composition of dripwater, and ultimately that of calcite, reflects surface climate variability. While this assumption appears to be upheld at many reconstruction sites [e.g. *Cruz et al.*, 2005; *Fleitmann et al.*, 2003; *Wang et al.*, 2001], extreme cases are documented in which karst hydrology rather than climate predominantly controls speleothem $\delta^{18}O$ variability [*Baker et al.*, 2012]. As water flows from the ground surface to the cave drip site, several non-climatic processes can alter the isotopic composition of rainfall and its climate-related signal. At or near the surface, the primary transformation

mechanisms include evaporation and biases towards wet seasons and/or high-volume precipitation events. Within the karst itself, the extent of water mixing as well as variability in flow path greatly influence dripwater, and ultimately stalagmite, $\delta^{18}O$.

Within the karst system, water flows along interconnected voids. The intergranular pore space inherent to the carbonate host rock represents the primary porosity. Water movement through the primary porosity is classified as 'matrix' or 'diffuse' flow. Fractures and joints constitute secondary porosity, with water movement classified as 'fracture' or 'preferential' flow. Flow along bedrock fractures delivers water to the inner reaches of the cave more rapidly and discretely than matrix flow. Finally, solution-enhanced conduits represent tertiary porosity. Flow through these conduits is typically rapid and high in volume, often creating underground streams and rivers.

Speleothems primarily form from waters traveling via matrix or fracture flow (i.e. primary or secondary porosity, respectively), as water transit times are typically slow enough to allow for calcite saturation. Water, however, may flow along any combination of these pathways, and flow may switch in an unpredictable, nonlinear fashion, introducing discrepancies in the temporal variability between rainfall and dripwater $\delta^{18}O$ [*Baker et al.*, 2013; *Bradley et al.*, 2010]. Water may also be stored for some time in karst reservoirs, allowing waters of different ages to mix and causing temporal smoothing of isotopic signals. Based on water store geometry, the flux out of the reservoir may be sensitive to volume thresholds, below which outflow ceases. Such thresholds further increase the likelihood of nonlinear flow behavior.

The relative dominance of a given isotopic transformation process varies with geographic location and climate regime. Additionally, flow behavior may be highly complex at a single drip site and heterogeneous between different drip sites, cave chambers, and karst systems. As such, monitoring dripwater $\delta^{18}O$ at speleothem reconstruction sites is essential for constraining how speleothem $\delta^{18}O$ records may be influenced by karst hydrology. Monitoring at arid region sites reveals that cave dripwater

$\delta^{18}O$ is often more positive than rainfall $\delta^{18}O$, which is typically attributed to evaporation within the soil and/or epikarst layers [e.g. *Ayalon et al.*, 1998; *Bar-Matthews et al.*, 1996; *Bradley et al.*, 2010]. Dripwater $\delta^{18}O$ in regions with prominent seasonality in precipitation amount is more likely to be influenced by biases in hydrologically effective recharge, with long-term isotopic means weighted towards high-volume rainfall events and/or wet seasons [e.g. *Jex et al.*, 2010; *Pape et al.*, 2010; *Partin et al.*, 2012]. The hydrological pathway along which water flows within the karst is a significant control on dripwater $\delta^{18}O$ at most cave sites, due to its influence of water residence time, mixing, and nonlinear flow behavior [e.g. *Baker et al.*, 2012; *Jex et al.*, 2013; *Partin et al.*, 2012; *Treble et al.*, 2013].

Over the last decade, linear regression analysis has been increasingly employed to calibrate the isotopic composition of rainfall, dripwater, and/or young stalagmites with instrumental records of climate parameters of interest [*Fairchild and Baker*, 2012; *Lachniet*, 2009]. The slope of the calibration equation yields a quantitative estimate of the amount of change in isotopic composition per unit of climatic variability. The robustness of the derived isotope-climate relationship is provided by the correlation coefficient, which assesses the calibration equation reflects the proxy data. Model skill can be assessed via validation analyses, whereby the isotope-climate relationship is applied to a period of time not used in the calibration but during which both proxy and instrumental data is available. The smaller the residual difference between the instrumental record and reconstructed climate parameter, the greater the skill of the model.

Although the quantitative estimates of past climate variability derived from modern calibrations indeed improve upon qualitatively based interpretations, there are several limitations to this approach. First, application of the modern calibration relationship to stalagmite $\delta^{18}O$ outside the calibration-validation period assumes that climate-isotope relationship is constant over time. However, recent work suggests that proxies may have a non-stationary response to climatic variability under different

boundary conditions [e.g. *Schmidt et al.*, 2014]. Secondly, only high-resolution (e.g. annual or higher) stalagmite records with robust age control are suitable for calibration against instrumental records [*Lachniet*, 2009], and young, fast-growing stalagmite samples with well-constrained age models are often difficult to come by. Finally, temporal integration of the climate-related isotope signal by the mixing of water within the karst system and nonlinearities in water flow behavior further complicate direct, linear comparisons between instrumental climate records and stalagmite $\delta^{18}O$ timeseries [*Fairchild and Baker*, 2012].

To overcome the limitations of statistical calibration, the development of proxy system models has recently been adopted [e.g. *Evans et al.*, 2013]. This approach involves the generation of process-based forward models that account for the dominant mechanisms influencing the climate-related isotopic signal prior to its incorporation within the paleoclimate archive (e.g. stalagmite calcite). The ultimate goal of proxy system modeling is often the generation of synthetic or "pseudoproxy" timeseries. Models can be designed to simulate nonlinearities inherent to the proxy system, and by using GCM-derived climate data as input, nonstationarity in climate-isotope relationship can also be addressed [*Evans et al.*, 2013]. Given the range of non-climatic processes that influence speleothem $\delta^{18}O$, speleothem proxy system models in the existing literature vary in levels of complexity and scope. For example, the speleothem forward model of Bradley *et al.* [2010] primarily consists of a karst hydrological model capable of simulating nonlinearities in flow pathway and water storage and mixing within the karst. In contrast, the model presented by Wackerbarth *et al.* [2010] focuses on surface processes, such as the evaporative enrichment of soil water and biases in effective recharge. Both models transform modeled dripwater $\delta^{18}O$ into pseudostalagmite $\delta^{18}O$ by accounting for temperature-dependent equilibrium isotopic fractionation associated with calcite precipitation but use different fractionation equations. In addition to continued

refinement of forward model design, the next advance for proxy system modeling is the direct coupling to GCMs.

1.2. Borneo speleothem $\delta^{18}O$ climate records

1.2.1. Northern Borneo study site

This dissertation presents rainfall and dripwater $\delta^{18}O$ timeseries from 2006-2012 from Gunung Mulu National Park located in the northwestern region of the maritime island of Borneo (4°N, 114°E) in the heart of the West Pacific Warm Pool (WPWP). The following subsections describe the climate and geology of northern Borneo and Gunung Mulu National Park.

1.2.1.1. Climatology

Gunung Mulu National Park receives approximately 5m of rainfall annually, and temperatures range between 26-27°C year-round. Since northern Borneo remains within the annual migration pathway of the Intertropical Convergence Zone (ITCZ), rainfall at Mulu is distributed fairly evenly throughout the year. This is in stark contrast to most other sites in the Indo-Pacific region, which experience distinct monsoon-related wet and dry seasons. Surface wind speed and direction over northern Borneo, however, does display marked seasonality, with more northerly (southerly) winds in boreal summer (winter) and relatively quiescent winds during the fall/spring shoulder seasons [*Cobb et al.*, 2007].

1.2.1.2. Interannual variability

As the dominant mode of tropical as well as global interannual variability (~2-7 years), the El Niño-Southern Oscillation (ENSO) produces the largest changes in northern Borneo climate. During warm ENSO phases (e.g. El Niño events), northern

Borneo typically experiences anomalously dry conditions that persist from boreal fall to spring [*Lau and Nath*, 2003; *Ropelewski and Halpert*, 1987], with the 1997/1998 El Niño event reducing precipitation by more than 50% [*Cobb et al.*, 2007] and generating widespread fires throughout Borneo [*Murdiyarso and Adiningsih*, 2007]. Conversely, during cold ENSO phases (e.g. La Niña events), northern Borneo experiences anomalously wet conditions and flooding.

Perturbations to the mean state of the tropical Pacific cause spontaneous variability between the two end-member states (e.g. warm versus cold phases) on interannual timescales. Under ENSO neutral conditions, the easterly trade winds drive a 4-10°C east-west sea surface temperature (SST) gradient by inducing a shoaling of the thermocline and upwelling of cold deep waters in the eastern equatorial Pacific and causing warm waters to amass in the western equatorial Pacific [*Cane*, 2005]. High SSTs in the WPWP facilitate enhanced evaporation and precipitation, which strengthens deep convection associated with the ascending branch of the zonal atmospheric Walker circulation. The subsiding branch of the Pacific Walker cell, conversely, delivers dry air to the east Pacific. As a result, sea level pressure (SLP) is higher in the east than the west. The zonal SST gradient, thus, partially regulates the strength of the easterly trade winds, linking the ocean and atmosphere in a positive coupled feedback, commonly referred to as the Bjerknes feedback [*Bjerknes*, 1969].

The coupled tropical ocean-atmosphere system is sensitive to modest perturbations [e.g. *Dijkstra*, 2006], with a slackening of the easterly trade winds capable of initiating an El Niño event. The weakened trade winds cause a reduction in upwelling and deepening of the thermocline in the east Pacific, thus relaxing the cross-equatorial

SST gradient and further weakening the easterly trade winds and Walker circulation [*Lindzen and Nigam*, 1987]. Tracking positive SST anomalies, the center of deep convection, previously in the west Pacific, migrates eastward to the central Pacific. This reorganization of the Walker circulation reduces (enhances) precipitation in the western (eastern) Pacific basin, resulting in regional drought (flooding). La Niña events represent the reversal of this feedback, with a strengthening of the Walker circulation and easterly winds amplifying the zonal SST gradient and causing anomalously warm and wet (cool and dry) conditions in the west (east) Pacific. La Niña events, however, are not mirror images of El Niño events [e.g. *Okumura and Deser*, 2010]. El Niño-related anomalies are typically larger in magnitude than those associated with La Niña [*Burgers and Stephenson*, 1999], whereas La Niña events tend to persist longer (~2 years) than El Niño events (~1 year) [*McPhaden and Zhang*, 2009].

1.2.1.3. Intraseasonal variability

Northern Borneo climate is also very sensitive to intraseasonal variations in precipitation, particularly those associated with the Madden-Julian Oscillation (MJO). The MJO is the dominant mode of intraseasonal tropical variability (30-90 days) [*Madden and Julian*, 1971]. MJO-related variability accounts for approximately 20% of total variance in precipitation at Mulu [*Cobb et al.*, 2007], causing anomalies that exceed ±10 mm/day at the site.

Central to the dynamics of the MJO is the coupling of large-scale eastward propagating circulation and a deep convective center. This center of enhanced convection and anomalously high precipitation is known as the 'active phase' and travels west-to-east across the equatorial Indian and Pacific ocean basins at a speed of approximately 5

ms^{-1}, resulting in a local intraseasonal period of 30-90 days [*Zhang*, 2005]. Weak convection and anomalously dry conditions flank the convective center to both the east and west and are referred to as 'suppressed phases.' The suppressed phase west (east) of the convective center is characterized by anomalously strong westerly (easterly) winds resembling an equatorial Rossby (Kelvin) wave. Warm SSTs sustain the enhanced convection associated with the active phase. Deep convection, therefore, often weakens and becomes less spatially coherent when the active phase passes over the large landmasses of the Maritime Continent [*Zhang*, 2005]. This relative weakening over land is also attributed to (1) competition with strong local diurnal cycles of convection, (2) interference by local topography, and (3) reduction of surface evaporation over land [*Maloney and Sobel*, 2004; *Wang and Li*, 1994; *Zhang and Hendon*, 1997]. The MJO may also influence interannual ENSO variability, as particularly strong active MJO phases often coincide with the onset and growth of strong El Niño events [*Lau and Chan*, 1988; *McPhaden*, 1999].

1.2.1.4. Geology

The caves of Gunung Mulu National Park are found within the Melinau Limestone Formation – a Late Eocene to Early Miocene shallow marine carbonate platform [*Wannier*, 2009; *Wilford*, 1961]. The Melinau Formation has a spatial footprint of ~300 km^2 and is characterized by a series of NE-SW trending carbonate mounds – the tallest of which, Gunung Api, rises 1710 m above sea level. The majority of sampling efforts since 2003 have been undertaken at Gunung Api, Gunung Benerat, and the Southern Hills, as well as at Gunung Buda, which is located within nearby Gunung Buda National Park. The caves of Gunung Api, Benerat, and Buda formed within Late

Oligocene limestone, which is comprised primarily of packstone-to-mudstone carbonates rich in foraminifera and non-reefal corals [*Wannier*, 2009]. The Southern Hills cave, Lang's Cave, where long-term dripwater δ monitoring is ongoing, however, formed within a Late Eocene grainstone carbonate deposit consisting of high-energy bioclastics dominated by red algae and foraminifera.

The region supports lush tropical rainforests with relatively thin topsoil. Groundwater recharge for the Mulu karst system can be broadly divided into three categories: (1) autogenic infiltration of precipitation falling directly onto the Melinau limestone; (2) allogenic runoff from the nearby sandstone mountain of Gunung Mulu (2377 m); and occasional flooding off the Melinau River alluvial plain [*Waltham and Brook*, 1980].

1.2.2. Borneo speleothem $\delta^{18}O$ records

The modern Indo-Pacific is a climatically complex region, influenced by the Asian and Australian monsoon systems, the annual migration of the ITCZ, interannual variations in the Indian and Pacific Walker cells associated with the Indian Ocean Dipole and ENSO, and intraseasonal variability associated with the MJO, among other intraseasonal oscillations. Each of these systems is cited as a possible mechanism driving past Indo-Pacific hydroclimate variability [*Ayliffe et al.*, 2013; *Carolin et al.*, 2013; *Denniston et al.*, 2013; *Griffiths et al.*, 2009; *Lewis et al.*, 2010; *Partin et al.*, 2007; *Tierney et al.*, 2012]. Northern Borneo's high sensitivity to ENSO-related precipitation anomalies and lack of appreciable seasonal cycle makes it a unique and valuable site for reconstructing Indo-Pacific paleoclimate and deconvolving the role of these phenomena

in past climatic change in the tropics and beyond. Owing to its extensive cave network, Gunung Mulu National Park provides a wealth of speleothem samples, which can be combined to create very long, highly replicated, continuous records.

Currently, reconstructions of northern Borneo speleothem $\delta^{18}O$ span the last 500ka nearly continuously [*Carolin et al.*, 2013; submitted; *Meckler et al.*, 2012; *Partin et al.*, 2007]. Uranium-series dating yields absolute age control and age errors typically less than ±500 years (2σ). Multi-decadal resolutions are achieved for records covering the past 200ka, allowing for the resolution of centennial-scale variations [*Carolin et al.*, 2013; submitted; *Partin et al.*, 2007]. The resolution of records older than 200ky range from 100-1000 years per sample, sufficient to resolve glacial-interglacial variability [*Meckler et al.*, 2012]. Speleothem $\delta^{18}O$ is the primary proxy used for reconstructing northern Borneo climate; however, studies investigating the feasibility of other proxies, such as trace elements (e.g. Mg[Sr]/Ca) and paleo-temperature indicators (e.g. clumped isotopes, fluid inclusions), are ongoing [*Meckler et al.*, submitted; *Partin et al.*, 2013].

Records of Borneo speleothem $\delta^{18}O$ indicate that west Pacific hydroclimate is sensitive to both high- and low-latitude forcings (e.g. North Atlantic freshwater hosing as well as precession-related local insolation variability) but responds in a complex, non-uniform manner to each. Significant periodicity exists at ~23ky over the last 160ky [*Carolin et al.*, submitted; *Meckler et al.*, 2012] and is best correlated with precession-driven local boreal fall (SON) insolation variability. This low-latitude forcing produces more negative speleothem $\delta^{18}O$ under higher SON insolation [*Carolin et al.*, 2013; submitted; *Partin et al.*, 2007]. Although not unprecedented [e.g. *Rafter and Charles*, 2012], the match with SON insolation differs from other nearby terrestrial records, which

show sensitivity to local summer insolation [e.g. *Ayliffe et al.*, 2013; *Wang et al.*, 2008]. Changes in zonal rather meridional circulation may plausibly drive precession-related hydroclimate variability at Borneo [*Carolin et al.*, 2013; *Koutavas and Joanides*, 2012; *Tierney et al.*, 2012].

Borneo speleothem $\delta^{18}O$ is generally more positive during glacial periods than interglacials, suggesting regional drying in the WPWP under glacial boundary conditions [*Carolin et al.*, 2013; submitted; *Meckler et al.*, 2012; *Partin et al.*, 2007]. While drier glacial conditions in the northern hemisphere tropics are typically attributed to a southward shift of the ITCZ under strong northern hemisphere cooling [*Chiang et al.*, 2009; *Denton et al.*, 2010], multiple lines of evidence suggest that low-latitude precessional forcing may have a greater influence on orbital-scale variability at Borneo than high-latitude glacial boundary conditions [*Carolin et al.*, submitted; *Meckler et al.*, 2012]. Borneo speleothem $\delta^{18}O$, however, is highly sensitive to abrupt changes in high-latitude climate – most notably to north Atlantic freshwater forcing during Heinrich events. Large, abrupt positive excursions in Borneo speleothem $\delta^{18}O$ coincide with ice-rafted debris in north Atlantic marine records, which mark the occurrence of Heinrich events, and suggest millennial-scale regional drying [*Carolin et al.*, 2013; *Partin et al.*, 2007]. Southward displacement of the ITCZ driven by a weakening of Atlantic meridional overturning circulation (AMOC) due to high-latitude freshwater influx is often invoked to explain abrupt drying in the northern hemisphere tropics associated with Heinrich events [*Broecker*, 1998]. This mechanism is well-supported within the WPWP region for Heinrich 1 (~17ka) by a north-south transect of Southeast Asia and Australasian speleothem $\delta^{18}O$ records, which show anomalous drying in the northern

hemisphere and anomalously wet conditions in the southern hemisphere [e.g. *Ayliffe et al.*, 2013; *Denniston et al.*, 2013; *Partin et al.*, 2007; *Wang et al.*, 2001]. Interestingly, the Borneo record lacks clear evidence of Dansgaard–Oeschger events – abrupt millennial-scale northern hemisphere warming episodes that are prominent throughout the Greenland ice core records [*Carolin et al.*, 2013].

1.2.2.3. Improving paleoclimate interpretations

The usefulness of the Borneo speleothem $\delta^{18}O$ record, and paleoclimate reconstructions in general, relies on our ability to interpret past climate conditions from them. The multiple climatic forcings, myriad proposed dynamical mechanisms, and complex interactions between them highlight the possibility of interpreting the Borneo speleothem $\delta^{18}O$ record in many different ways. To achieve more accurate interpretations of the Borneo records, the isotope-climate relationship at Borneo must be better constrained. This dissertation aims to do so by comprehensively examining (i) the connection between local and regional climate and a multi-year, daily resolved timeseries of local Borneo rainfall $\delta^{18}O$ (Chapter 2) and (ii) how the isotopic climate signal is preserved in dripwater $\delta^{18}O$ following groundwater transport through the karst system (Chapter 3). Beyond applications to paleoclimatology, the results presented in this dissertation provide important observational benchmarks for isotope-equipped global climate models and proxy system models.

1.3. REFERENCES

Angert, A., C. D. Cappa, and D. J. DePaolo (2004), Kinetic O-17 effects in the hydrologic cycle: Indirect evidence and implications, *Geochim. Cosmochim. Acta*, *68*(17), 3487-3495.

Ayalon, A., M. Bar-Matthews, and E. Sass (1998), Rainfall-recharge relationships within a karstic terrain in the eastern Mediterranean semi-arid region, Israel: delta O-18 and delta D characteristics, *J. Hydro.*, *207*(1-2), 18-31.

Ayliffe, L. K., et al. (2013), Rapid interhemispheric climate links via the Australasian monsoon during the last deglaciation, *Nat Commun*, *4*, 2908.

Baker, A., C. Bradley, S. J. Phipps, M. Fischer, I. J. Fairchild, L. Fuller, C. Spötl, and C. Azcurra (2012), Millennial-length forward models and pseudoproxies of stalagmite δ18O an example from NW Scotland, *Clim. Past.*, *8*(4), 1153-1167.

Baker, A., C. Bradley, and S. J. Phipps (2013), Hydrological modeling of stalagmite δ18O response to glacial-interglacial transitions, *Geophys. Res. Lett.*, *40*(12), 3207-3212.

Bar-Matthews, M., A. Ayalon, A. Matthews, E. Sass, and L. Halicz (1996), Carbon and oxygen isotope study of the active water-carbonate system in a karstic Mediterranean cave: Implications for paleoclimate research in semiarid regions, *Geochim. Cosmochim. Acta*, *60*(2), 337-347.

Bjerknes, J. (1969), Atmospheric teleconnections from equatorial Pacific, *Mon. Weather Rev.*, *97*(3), 163-&.

Bradley, C., A. Baker, C. N. Jex, and M. J. Leng (2010), Hydrological uncertainties in the modelling of cave drip-water δ18O and the implications for stalagmite palaeoclimate reconstructions, *Quat. Sci. Rev.*, *29*(17-18), 2201-2214.

Broecker, W. S. (1998), Paleocean circulation during the last deglaciation: A bipolar seesaw?, *Paleoceanography*, *13*(2), 119-121.

Burgers, G., and D. B. Stephenson (1999), The "normality" of El Nino, *Geophys. Res. Lett.*, *26*(8), 1027-1030.

Cane, M. A. (2005), The evolution of El Niño, past and future, *Earth Planet. Sci. Lett.*, *230*(3-4), 227-240.

Carolin, S. A., K. M. Cobb, J. F. Adkins, B. Clark, J. L. Conroy, S. Lejau, J. Malang, and A. A. Tuen (2013), Varied response of western Pacific hydrology to climate forcings over the last glacial period, *Science*, *340*(6140), 1564-1566.

Carolin, S. A., K. M. Cobb, J. Lynch-Stieglitz, J. W. Moerman, S. Lejau, J. Malang, A. A. Tuen, and J. Adkins (submitted), Walker and Hadley circulation dynamics in a 0-160 kybp stalagmite record of WPWP hydrology.

Chiang, J. C. H., Y. Fang, and P. Chang (2009), Pacific Climate Change and ENSO Activity in the Mid-Holocene, *J. Clim.*, *22*(4), 923-939.

Ciais, P., and J. Jouzel (1994), Deuterium and oxygen-18 in precipitation - isotopic model, including mixed cloud processes, *J. Geophys. Res.-Atmos.*, *99*(D8), 16793-16803.

Clark, I., and P. Fritz (1997), *Environmental Isotopes in Hydrogeology*, CRC Press LLC, Boca Raton, FL.

Cobb, K. M., J. F. Adkins, J. W. Partin, and B. Clark (2007), Regional-scale climate influences on temporal variations of rainwater and cave dripwater oxygen isotopes in northern Borneo, *Earth Planet. Sci. Lett.*, *263*(3-4), 207-220.

Craig, H. (1961), Isotopic variations in meteoric waters, *Science*, *133*(346), 1702-&.

Criss, R. E. (1999), *Principles of Stable Isotope Distribution*, Oxford University Press, New York.

Cruz, F. W., S. J. Burns, I. Karmann, W. D. Sharp, M. Vuille, A. O. Cardoso, J. A. Ferrari, P. L. S. Dias, and O. Viana (2005), Insolation-driven changes in atmospheric circulation over the past 116,000 years in subtropical Brazil, *Nature*, *434*(7029), 63-66.

Dansgaard, W. (1964), Stable isotopes in precipitation, *Tellus*, *16*(4), 436-468.

Denniston, R. F., Y. Asmerom, M. Lachniet, V. J. Polyak, P. Hope, N. An, K. Rodzinyak, and W. F. Humphreys (2013), A Last Glacial Maximum through middle Holocene stalagmite record of coastal Western Australia climate, *Quat. Sci. Rev.*, *77*, 101-112.

Denton, G. H., R. F. Anderson, J. R. Toggweiler, R. L. Edwards, J. M. Schaefer, and A. E. Putnam (2010), The Last Glacial Termination, *Science*, *328*(5986), 1652-1656.

Dijkstra, H. A. (2006), The ENSO phenomenon: theory and mechanisms, *Advances in Geosciences*, *6*, 3–15.

Evans, M. N., S. E. Tolwinski-Ward, D. M. Thompson, and K. J. Anchukaitis (2013), Applications of proxy system modeling in high resolution paleoclimatology, *Quat. Sci. Rev.*, *76*, 16-28.

Fairchild, I., and A. Baker (2012), *Speleothem Science: From Process to Past Environments*, Wiley-Blackwell, Hoboken, NJ.

Field, R. D., D. B. A. Jones, and D. P. Brown (2010), Effects of postcondensation exchange on the isotopic composition of water in the atmosphere, *J. Geophys. Res.*, *115*(D24).

Fleitmann, D., S. J. Burns, U. Neff, A. Mangini, and A. Matter (2003), Changing moisture sources over the last 330,000 years in Northern Oman from fluid-inclusion evidence in speleothems, *Quat. Res.*, *60*(2), 223-232.

Friedman, I. (1953), Deuterium content of natural waters and other substances, *Geochim. Cosmochim. Acta*, *4*(1-2), 89-103.

Gat, J. R. (1971), Comments on stable isotope method in regional groundwater investigations, *Water Resources Research*, *7*(4), 980-&.

Gedzelman, S. D., and R. Arnold (1994), Modeling the isotopic composition of precipitation, *J. Geophys. Res.-Atmos.*, *99*(D5), 10455-10471.

Griffiths, M. L., et al. (2009), Increasing Australian–Indonesian monsoon rainfall linked to early Holocene sea-level rise, *Nature Geoscience*, *2*(9), 636-639.

Hoefs, J. (2004), *Stable Isotope Geochemistry*, 5th ed., Springer, New York, NY.

Jex, C. N., A. Baker, I. J. Fairchild, W. J. Eastwood, M. J. Leng, H. J. Sloane, L. Thomas, and E. Bekaroğlu (2010), Calibration of speleothem δ18O with instrumental climate records from Turkey, *Global Planet. Change*, *71*(3-4), 207-217.

Jex, C. N., S. J. Phipps, A. Baker, and C. Bradley (2013), Reducing uncertainty in the climatic interpretations of speleothem δ18O, *Geophys. Res. Lett.*, *40*(10), 2259-2264.

Koutavas, A., and S. Joanides (2012), El Niño-Southern Oscillation extrema in the Holocene and Last Glacial Maximum, *Paleoceanography*, *27*(4), n/a-n/a.

Lachniet, M. S. (2009), Climatic and environmental controls on speleothem oxygen-isotope values, *Quat. Sci. Rev.*, *28*, 412-432.

Landais, A., C. Risi, S. Bony, F. Vimeux, L. Descroix, S. Falourd, and A. Bouygues (2010), Combined measurements of 17Oexcess and d-excess in African monsoon precipitation: Implications for evaluating convective parameterizations, *Earth Planet. Sci. Lett.*, *298*(1-2), 104-112.

Lau, K. M., and P. H. Chan (1988), Intraseasonal and interannual variations of tropical convection - A possible link between the 40-50 day oscillation and ENSO, *Journal of the Atmospheric Sciences*, *45*(3), 506-521.

Lau, N. C., and M. J. Nath (2003), Atmosphere-ocean variations in the Indo-Pacific sector during ENSO episodes, *J. Clim.*, *16*(1), 3-20.

Lawrence, J. R., S. D. Gedzelman, D. Dexheimer, H. K. Cho, G. D. Carrie, R. Gasparini, C. R. Anderson, K. P. Bowman, and M. I. Biggerstaff (2004), Stable isotopic composition of water vapor in the tropics, *J. Geophys. Res.-Atmos.*, *109*(D6), 16.

Lee, J.-E., and I. Fung (2008), "Amount effect" of water isotopes and quantitative analysis of post-condensation processes, *Hydrological Processes*, *22*(1), 1-8.

Lewis, S. C., A. N. LeGrande, M. Kelley, and G. A. Schmidt (2010), Water vapour source impacts on oxygen isotope variability in tropical precipitation during Heinrich events, *Clim. Past.*, *6*(3), 325-343.

Lindzen, R. S., and S. Nigam (1987), On the role of sea-surface temperature-gradients in forcing low-level winds and convergence in the tropics, *Journal of the Atmospheric Sciences*, *44*(17), 2418-2436.

Luz, B., and E. Barkan (2000), Assessment of oceanic productivity with the triple-isotope composition of dissolved oxygen, *Science*, *288*(5473), 2028-2031.

Madden, R. A., and P. R. Julian (1971), Detection of a 40-50 day oscillation in zonal wind in tropical Pacific, *Journal of the Atmospheric Sciences*, *28*(5), 702-&.

Majoube, M. (1971), Oxygen-18 and deuterium fractionation between water and steam, *J. Chim. Phys.-Chim. Biol.*, *68*(10), 1423-&.

Maloney, E. D., and A. H. Sobel (2004), Surface fluxes and ocean coupling in the tropical intraseasonal oscillation, *J. Clim.*, *17*(22), 4368-4386.

McPhaden, M. J. (1999), Genesis and Evolution of the 1997-98 El Niño, *Science*, *283*(5404), 950-954.

McPhaden, M. J., and X. B. Zhang (2009), Asymmetry in zonal phase propagation of ENSO sea surface temperature anomalies, *Geophys. Res. Lett.*, *36*, 6.

Meckler, A. N., M. O. Clarkson, K. M. Cobb, H. Sodemann, and J. F. Adkins (2012), Interglacial hydroclimate in the tropical West Pacific through the Late Pleistocene, *Science*, *336*(6086), 1301-1304.

Meckler, A. N., H. Vogel, D. Leuenberger, S. A. Carolin, K. M. Cobb, J. W. Moerman, J. Adkins, and D. Fleitmann (submitted), Glacial-interglacial temperature change in the tropical West Pacific:

A comparison of stalagmite-based paleo-thermometers, *Quat. Sci. Rev.*

Mook, W. (2001), *Environmental Isotopes in the Hydrological Cycle: Principles and Applications*, UNESCO/IAEA Series, http://www.-naweb.iaea.org/napc/ih/volumes.asp.

Murdiyarso, D., and E. S. Adiningsih (2007), Climate anomalies, Indonesian vegetation fires and terrestrial carbon emissions, *Mitigation and Adaptation Strategies for Global Change*, *12*(1), 101-112.

Okumura, Y. M., and C. Deser (2010), Asymmetry in the Duration of El Niño and La Niña, *J. Clim.*, *23*(21), 5826-5843.

Pape, J. R., J. L. Banner, L. E. Mack, M. Musgrove, and A. Guilfoyle (2010), Controls on oxygen isotope variability in precipitation and cave drip waters, central Texas, USA, *J. Hydro.*, *385*(1-4), 203-215.

Partin, J. W., K. M. Cobb, J. F. Adkins, B. Clark, and D. P. Fernandez (2007), Millennial-scale trends in west Pacific warm pool hydrology since the Last Glacial Maximum, *Nature*, *449*(7161), 452-455.

Partin, J. W., et al. (2012), Relationship between modern rainfall variability, cave dripwater, and stalagmite geochemistry in Guam, USA, *Geochem. Geophys. Geosys.*, *13*(3), n/a-n/a.

Partin, J. W., K. M. Cobb, J. F. Adkins, A. A. Tuen, and B. Clark (2013), Trace metal and carbon isotopic variations in cave dripwater and stalagmite geochemistry from northern Borneo, *Geochem. Geophys. Geosys.*, *14*(9), 3567-3585.

Passey, B. H., H. T. Hu, H. Y. Ji, S. Montanari, S. N. Li, G. A. Henkes, and N. E. Levin (2014), Triple oxygen isotopes in biogenic and sedimentary carbonates, *Geochim. Cosmochim. Acta*, *141*, 1-25.

Rafter, P. A., and C. D. Charles (2012), Pleistocene equatorial Pacific dynamics inferred from the zonal asymmetry in sedimentary nitrogen isotopes, *Paleoceanography*, *27*, 8.

Risi, C., S. Bony, and F. Vimeux (2008a), Influence of convective processes on the isotopic composition (δ18O andδD) of precipitation and water vapor in the tropics: 2. Physical interpretation of the amount effect, *J. Geophys. Res.*, *113*(D19).

Risi, C., S. Bony, F. Vimeux, L. Descroix, B. Ibrahim, E. Lebreton, I. Mamadou, and B. Sultan (2008b), What controls the isotopic composition of the African monsoon precipitation? Insights from event-based precipitation collected during the 2006 AMMA field campaign, *Geophys. Res. Lett.*, *35*(24).

Ropelewski, C. F., and M. S. Halpert (1987), Global and regional scale precipitation patterns associated with the El-Niño Southern Oscillation, *Mon. Weather Rev.*, *115*(8), 1606-1626.

Rozanski, K. A.-A., L.; Gonfiantini, R. (1993), Isotopic patterns in modern global precipitation, *Geophys. Monogr. Ser.* , *78*, 1-36.

Schmidt, G. A., A. N. LeGrande, and G. Hoffmann (2007), Water isotope expressions of intrinsic and forced variability in a coupled ocean-atmosphere model, *J. Geophys. Res.*, *112*(D10).

Schmidt, G. A., et al. (2014), Using palaeo-climate comparisons to constrain future projections in CMIP5, *Clim. Past.*, *10*(1), 221-250.

Tierney, J. E., D. W. Oppo, A. N. LeGrande, Y. Huang, Y. Rosenthal, and B. K. Linsley (2012), The influence of Indian Ocean atmospheric circulation on Warm Pool

hydroclimate during the Holocene epoch, *Journal of Geophysical Research: Atmospheres*, *117*(D19), n/a-n/a.

Treble, P. C., C. Bradley, A. Wood, A. Baker, C. N. Jex, I. J. Fairchild, M. K. Gagan, J. Cowley, and C. Azcurra (2013), An isotopic and modelling study of flow paths and storage in Quaternary calcarenite, SW Australia: implications for speleothem paleoclimate records, *Quat. Sci. Rev.*, *64*, 90-103.

Wackerbarth, A., D. Scholz, J. Fohlmeister, and A. Mangini (2010), Modelling the δ18O value of cave drip water and speleothem calcite, *Earth Planet. Sci. Lett.*, *299*(3-4), 387-397.

Waltham, A. C., and D. B. Brook (1980), Symposium on the geomorphology of the Mulu Hills.8. Cave development in the Melinau limestone of the Gunung-Mulu National-Park, *Geogr. J.*, *146*, 258–266.

Wang, B., and T. M. Li (1994), Convective interaction with boundary-layer dynamics in the development of a tropical intraseasonal system, *Journal of the Atmospheric Sciences*, *51*(11), 1386-1400.

Wang, Y., H. Cheng, R. L. Edwards, X. Kong, X. Shao, S. Chen, J. Wu, X. Jiang, X. Wang, and Z. An (2008), Millennial- and orbital-scale changes in the East Asian monsoon over the past 224,000 years, *Nature*, *451*(7182), 1090-1093.

Wang, Y. J., H. Cheng, R. L. Edwards, Z. S. An, J. Y. Wu, C. C. Shen, and J. A. Dorale (2001), A high-resolution absolute-dated Late Pleistocene monsoon record from Hulu Cave, China, *Science*, *294*(5550), 2345-2348.

Wannier, M. (2009), Carbonate platforms in wedge-top basins: An example from the Gunung Mulu National Park, Northern Sarawak (Malaysia), *Mar. Petrol. Geol.*, *26*(2), 177-207.

Wilford, G. E. (1961), The geology and mineral resources of Brunei and adjacent parts of Sarawak, with description of the Seria and Miri oilfields., *British Borneo Geological Survey Memoirs*, *10*.

Zhang, C. (2005), Madden-Julian Oscillation, *Rev. Geophys.*, *43*(2).

Zhang, C. D., and H. H. Hendon (1997), Propagating and standing components of the intraseasonal oscillation in tropical convection, *Journal of the Atmospheric Sciences*, *54*(6), 741-752.

CHAPTER 2

DIURNAL TO INTERANNUAL RAINFALL $\delta^{18}O$ VARIATIONS IN NORTHERN BORNEO DRIVEN BY REGIONAL HYDROLOGY

This chapter is published in:

J.W. Moerman, Cobb, K.M., Adkins, J.F., Sodemann, H., Clark, B., Tuen, A.A. (2013) Diurnal to interannual rainfall $\delta^{18}O$ variations in northern Borneo driven by regional hydrology. *Earth and Planetary Science Letters.* **369-370**, 108-119.

2.1. Abstract

The relationship between climate variability and rainfall oxygen isotopic ($\delta^{18}O$) variability is poorly constrained, especially in the tropics, where many key paleoclimate records rely on past rainfall isotopes as proxies for hydroclimate. Here we present a daily-resolved, 5-yr-long timeseries of rainfall $\delta^{18}O$ from Gunung Mulu National Park, located in northern Borneo (4° N, 114° E) in the heart of the West Pacific Warm Pool, and compare it to local and regional climatic variables. Daily rainfall $\delta^{18}O$ values range from +0.7 to -18.5‰ and exhibit a weak but significant inverse relationship with daily local precipitation amount ($R = -0.19$, $p < 0.05$), consistent with the tropical amount effect. Day-to-day $\delta^{18}O$ variability at Mulu is best correlated to regional precipitation amount averaged over the preceding week ($R = -0.64$, $p < 0.01$). The inverse relationship between Mulu rainfall $\delta^{18}O$ and local (regional) precipitation amount increases with increased temporal averaging, reaching $R = -0.56$ ($R = -0.72$) on monthly

timescales. Large, negative, multi-day rainfall $\delta^{18}O$ anomalies of up to 16‰ occur every 30-90 days and are closely associated with wet phases of the intraseasonal Madden-Julian Oscillation. A weak, semi-annual seasonal cycle in rainfall $\delta^{18}O$ of 2-3‰ bears little resemblance to seasonal precipitation variability, pointing to a complex sequence of moisture sources and/or trajectories over the course of the year. Interannual rainfall $\delta^{18}O$ variations of 6-8‰ are significantly correlated with indices of the El Niño Southern Oscillation, with increased rainfall $\delta^{18}O$ during relatively dry El Niño conditions, and vice versa during La Nina events. We find that Mulu rainfall $\delta^{18}O$ outperforms Mulu precipitation amount as a tracer of basin-scale climate variability, highlighting the time- and space-integrative nature of rainfall $\delta^{18}O$. Taken together, our results suggest that rainfall $\delta^{18}O$ variability at Mulu is significantly influenced by the strength of regional convective activity. As such, our study provides further empirical support for the interpretation of $\delta^{18}O$-based paleo-reconstructions from northern Borneo stalagmites as robust indicators of regional-scale hydroclimate variability, where higher $\delta^{18}O$ reflects regional drying.

2.2. Introduction

The inverse relationship between tropical precipitation amount and rainfall isotopic values, known as the 'amount effect' (Dansgaard, 1964; Rozanski *et al*., 1993; Araguas-Araguas *et al*., 1998), has provided the basis for numerous reconstructions of tropical paleohydrology from lake deposits (e.g. Sachs *et al*., 2009; Tierney *et al*., 2010), alpine ice cores (e.g. Hoffmann *et al.,* 2003; Vimeux *et al*., 2009) and stalagmite calcite (e.g. Bar-Matthews *et al*., 1997; Burns *et al*., 1998; Wang *et al*., 2001). Such

reconstructions play a key role in resolving past tropical climate changes, as continuous, high-resolution paleoclimate archives are relatively rare in the tropics. Stalagmite $\delta^{18}O$ records, in particular, have been used to probe hydroclimate variability over the last hundred years (Treble *et al*., 2005; Frappier *et al*., 2007), the last glacial cycle (Dykoski *et al*., 2005; Partin *et al*., 2007; Griffiths *et al*., 2009), and the last million years (Wang *et al*., 2001; Meckler *et al*., 2012).

Despite robust observations of the amount effect across tropical latitudes, the climatic controls on rainfall $\delta^{18}O$ at any given site remain highly uncertain as numerous processes contribute to rainfall $\delta^{18}O$ variability. Rayleigh distillation, whereby cumulative fractionation during condensation and rainout leaves the residual atmospheric vapor depleted in $\delta^{18}O$, has long been recognized as a first-order mechanism driving the amount effect and rainfall $\delta^{18}O$ variability (Dansgaard, 1964; Rozanski *et al*., 1993). The Rayleigh mechanism operates both locally, in the case of rainfall $\delta^{18}O$ fractionation across a single rainfall event (e.g. Celle-Jeanton *et al*., 2004) and regionally, when considering the progressive vapor depletion of air parcels transiting through a region of enhanced precipitation (e.g. Cobb *et al*., 2007; Vimeux *et al*., 2011).

Several post-condensation processes also likely contribute to the observed amount effect relationship. For one, the evaporation of falling raindrops causes the residual rainfall to be relatively enriched — a process that is maximized in arid regions and during dry seasons (Dansgaard, 1964; Stewart, 1975; Gat, 1996; Lee and Fung, 2008; Risi *et al*., 2008a). In regions characterized by strong convection, the recycling of water vapor within the convective cell drives rainfall $\delta^{18}O$ lower during episodes of intense convection (Lawrence and Gedzelman, 1996; Lawrence *et al*., 2004; Risi *et al*., 2008a,

2008b). Numerous studies have identified additional processes, such as atmospheric mixing and/or changes in moisture sources and trajectories, that contribute to rainfall $\delta^{18}O$ variability at tropical and subtropical sites (Aggarwal *et al*., 2004; Cobb *et al.*, 2007; Tian *et al.,* 2007; Breitenbach *et al*., 2010, Gao *et al*., 2011).

Previous studies have referred to the amount effect in describing fractionation processes that act strictly locally (e.g Vuille *et al.,* 2005; Lee *et al*., 2009; LeGrande and Schmidt 2009) as well as fractionation processes that integrate across larger spatial scales and longer time periods (e.g. Cobb *et al*., 2007; Risi *et al.,* 2008b; Kurita *et al*., 2009; Kurita *et al*., 2011; Tremoy *et al*., 2012). For the sake of clarity, we will differentiate between a "local" versus "regional" amount effect in our study, based on the inferred spatial scale of the fractionation mechanism in question.

Isotope-equipped general circulation models (GCMs) allow for the systematic investigation of the various dynamics regulating rainfall isotopic composition (Joussaume *et al.*, 1984; Jouzel *et al.* 1987; Hoffmann *et al*., 1998; Noone and Simmonds, 2002; Schmidt *et al*., 2007; Tindall *et al*., 2009; Risi *et al.,* 2010). Agreement between observations and model output has improved as models incorporate processes such as post-condensation raindrop re-evaporation and convective mixing (Field *et al*., 2010) and as higher spatial resolution affords more realistic model topographies and better representations of weather systems (Vimeux *et al*., 2011; Gao *et al.*, 2011). Recent studies using isotope-equipped GCMs find that the dominant drivers of rainfall isotopic variability vary from region to region (Lee *et al.*, 2007; Lewis *et al*., 2010; Conroy *et al., submitted*), with modeled $\delta^{18}O$ values reflecting the net sum of often competing processes (Field *et al.*, 2010). Models also reveal that the relationship between climate

and rainfall $\delta^{18}O$ at a given site may vary with time period (e.g LeGrande and Schmidt, 2009).

The dearth of high-resolution rainfall $\delta^{18}O$ isotope timeseries throughout the tropics makes it difficult to assess the accuracy of fractionation mechanisms that emerge in isotope-equipped model simulations. Most rainfall $\delta^{18}O$ studies rely on the International Atomic Energy Agency–Global Network of Isotopes in Precipitation database (IAEA-GNIP; International Atomic Energy Agency, 2006). As this network is comprised almost exclusively of monthly averaged rainfall $\delta^{18}O$ data, such studies are limited to investigating seasonal and longer timescales. As a result, relatively little is known about rainfall $\delta^{18}O$ variability on daily to intraseasonal (30-90 day) timescales and its connection to dominant intraseasonal climate modes, such as the Madden-Julian Oscillation (MJO; Madden and Julian, 1972; Zhang, 2005). Furthermore, the relatively sparse spatial coverage of the GNIP database in the deep tropics means that the relationship between interannual rainfall $\delta^{18}O$ variability and the El Niño Southern Oscillation (ENSO) is poorly constrained. Additional rainfall isotope timeseries from the tropics help to constrain the modern-day dynamical controls on rainfall $\delta^{18}O$ variability in the tropics, while providing much-needed interpretive frameworks for tropical rainfall $\delta^{18}O$ paleo-reconstructions.

Here we present a 5-year quasi-continuous collection of cumulative daily rainfall $\delta^{18}O$ from Gunung Mulu National Park (4° N, 114° E), located in northwestern Borneo, in the heart of the West Pacific Warm Pool (WPWP). We investigate the variability of northern Borneo rainfall $\delta^{18}O$ and its response to local and regional climate variations on synoptic to interannual timescales. We also investigate the evolution of rainfall $\delta^{18}O$

across a single rainfall event in order to constrain the sub-diurnal influences on rainfall $\delta^{18}O$ at our site. By comparing these rainfall $\delta^{18}O$ timeseries to local and regional climate variables as well as to indices of large-scale climate variability, we investigate the relationship of rainfall $\delta^{18}O$ in northern Borneo to both local and large-scale climate controls across a range of timescales. We also briefly present rainfall δD data from Gunung Mulu in to order to plot meteoric water lines and compute values of deuterium-excess, a parameter derived from $\delta^{18}O$ and δD (deuterium-excess = $\delta D - 8*\delta^{18}O$ [*Dansgaard*, 1964]) and hereafter referred to as 'd-excess.' There is no GNIP station on Borneo, so our study represents an important addition to the rainfall $\delta^{18}O$ data archive, while informing the climatic interpretation of numerous stalagmite $\delta^{18}O$-based paleoclimate records from our site (Partin *et al*., 2007; Meckler *et al.*, 2012; Carolin *et al*., submitted).

2.3. Methods

2.3.1. Site description

Gunung Mulu National Park receives over 5 m of precipitation annually, which exhibits significant intraseasonal (30-90 days) and interannual variability. The vast majority of this precipitation is delivered by discrete convective events that typically occur in the afternoon. Since northern Borneo lies within the migration path of the Intertropical Convergence Zone (ITCZ) year-round, seasonal variations in precipitation at Mulu are weak. As a result, the climate of northern Borneo is primarily controlled by intraseasonal and interannual precipitation variability associated with the MJO and ENSO respectively, with strong ENSO phases producing annual precipitation anomalies of up to ± 50% (Bell and Halpert, 1998). During El Nino events, anomalously warm sea surface

temperatures (SST) in the eastern and central tropical Pacific pull the center of deep atmospheric convection east of the Maritime continent (Rasmusson and Wallace, 1983), decreasing convection across the WPWP (Fig. A.1). Conversely, convective activity in the WPWP increases during La Niña events. Comprehensive descriptions of the climatic and geologic setting of Gunung Mulu National Park are presented in Cobb *et al*. (2007).

2.3.2. Rainfall $\delta^{18}O$ sampling procedure and analysis

Two distinct rainfall sampling campaigns were conducted for this study: (1) a daily collection of rainfall $\delta^{18}O$ at the Gunung Mulu airport from July 2006 to May 2011, and (2) a high-resolution sampling of an individual precipitation event at a remote field camp at Gunung Mulu on March 7, 2010. For the daily rainfall $\delta^{18}O$ collection (N = 1203), rainfall was collected in a splayed-bottom rain gauge (Casella model M114003; 254 mm diameter; ~1m above ground level) at the Mulu Meteorological Station headquartered at Mulu Airport (4.05° N, 114.81° E) and transferred to glass vials, leaving no headspace when precipitation amounts allowed, each morning at 8:00AM MYT. Precipitation amounts were logged at the same time – we refer to this timeseries as 'local Mulu precipitation' hereafter. Rainfall aliquots collected between July 2006 and February 2010 were stored in 4 mL glass vials with polyseal screw caps and sealed with parafilm. Aliquots collected from March 2010 onwards were stored in 3 mL glass serum vials and sealed with rubber stoppers and crimped aluminum closures, which provided a superior seal than the screw caps.

The use of an open-air rain gauge raises the possibility of isotopic enrichment of the rainfall samples by evaporation over the course of the day. To assess the impact of evaporative enrichment on rainfall isotopic values and to develop guidelines for

identifying potentially affected samples, several quality control assessments were performed (see Supplemental Section for details). Based on the findings of these assessments, rainfall samples associated with precipitation amounts less than 1.6 mm were excluded from the final dataset. Evaporation within a vial with headspace represents another source of post-deposition enrichment. As a result, samples stored in vials that were less than 4/5 full were also excluded from the final dataset. Together, this resulted in the exclusion of 176 samples. An additional 23 samples collected in December 2006 were excluded due to documented sampling errors by Mulu personnel. In total, 199 rainfall $\delta^{18}O$ samples were excluded from the final dataset tally ($N = 1004$). The exclusion of these samples did not significantly alter the variability of the 5-year timeseries (Fig. A.5).

We also conducted detailed rainfall sampling across a single precipitation event on March 7, 2010 at Camp 5 (4.14° N, 114.89° E), located approximately 12km NE of Gunung Mulu National Park headquarters. Rainfall $\delta^{18}O$ samples were collected manually at one to four minute intervals (depending on rainfall intensity) throughout the event, for a total of 19 samples. The event lasted for approximately one hour, including a 20-minute break in rainfall. Lacking any way to quantitatively measure rainfall rates at the remote field camp, we recorded relative rainfall intensity at the time of each sample collection, where '1' represented a light drizzle and '10' represented the heaviest of downpours. Samples were stored in 3 mL glass serum vials sealed with rubber stoppers and crimped aluminum closures.

Rainfall $\delta^{18}O$ and δD were measured at the Georgia Institute of Technology via cavity ring-down spectroscopy (Picarro L1102-i water isotope analyzer). To calibrate the

isotopic composition of the rainfall samples, three internal water standards, each calibrated against NIST-VSMOW, NIST-GISP, and NIST-SLAP, were analyzed at the beginning and end of each analysis. An internal water standard was analyzed after every nine rainfall samples to monitor instrument drift. Memory corrections were applied to each measurement based on empirical, instrument-specific memory coefficients. The long-term reproducibility of this technique is better than ± 0.1‰ for $\delta^{18}O$ and ± 0.8‰ for δD (1σ). In the case of the screw-top vials, sampling and storage contributed an additional uncertainty of ± 0.1‰ (1σ) for $\delta^{18}O$ and ± 0.7‰ (1σ) for δD, as determined by measuring 34 pairs of duplicate rainfall samples. Crimp-top vial duplicates provided indistinguishable $\delta^{18}O$ and δD values. As such, a conservative estimate of uncertainty of ± 0.2‰ (1σ) is attributed to each rainfall $\delta^{18}O$ measurement and ± 1.5‰ (1σ) to each δD measurement. We report an uncertainty of ± 1.5‰ for d-excess values, calculated from the quadratic combination of the uncertainties for $\delta^{18}O$ and δD.

2.3.3. Gridded climate datasets

We use daily and monthly values of both the Tropical Rainfall Measuring Mission (TRMM 3B42 V6 and 3B43 V6 respectively; 0.25° x 0.25°) precipitation data (Huffman *et al.*, 2007) and NOAA Interpolated Outgoing Longwave Radiation dataset (OLR; 2.5° x 2.5°; Liebmann and Smith, 1996) to investigate regional convective activity, following Arkin and Ardanuy (1989). SST-derived indices of ENSO variability (i.e. NIÑO3, NIÑO3.4, and NIÑO4) are derived from monthly NOAA Optimum Interpolation Sea Surface Temperature (OISST V2; Reynolds *et al*., 2002). The significance of correlations between Mulu rainfall $\delta^{18}O$, local Mulu precipitation amount, and the gridded climate

datasets listed above is assessed via the Student's *t*-test using effective degrees of freedom, following Bretherton *et al*. (1999).

2.4. Results

2.4.1. Rainfall isotope timeseries across a single convective event

The timeseries of rainfall $\delta^{18}O$ and d-excess across the March 7, 2010 rainfall event are shown in Fig. 2.1a. Over a one-hour period, rainfall $\delta^{18}O$ ranges from -1.5 to +0.8‰, and δD ranges from +1.8 to +10‰ (not shown), with the highest isotopic values observed in the first minutes of the event. Rainfall isotope values reach their lowest values after fifteen minutes and then gradually increase thereafter, following a "V-shaped" progression documented at higher latitude sites (Rindsberger *et al.*, 1990; Celle-Jeanton *et al.*, 2004).

Fig. 2.1b illustrates the strong inverse relationship between rainfall $\delta^{18}O$ and relative rainfall intensity (R = -0.82) across the March 7th precipitation event, consistent with the amount effect. The strong correlations between d-excess, which is an indicator of kinetic fractionation (Dansgaard, 1964; Gat, 1996; Risi *et al.*, 2010), and both rainfall $\delta^{18}O$ (R = -0.98) and rainfall intensity (R = 0.80) suggest that the partial re-evaporation of falling raindrops likely drives the amount effect during this event. When raindrops undergo evaporation in low relative humidity conditions, the d-excess value of the evaporate increases, leaving the raindrops with lower d-excess, as seen mostly in the beginning of the March 7th event (Fig. 2.1a). Further support for post-condensation evaporation is provided by the relatively low slope (~ 4) for rainfall δD vs $\delta^{18}O$ variations for this event (Fig. 2.2), which is typical of evaporation and differs appreciably from the

equilibrium $\delta D/\delta^{18}O$ slope of 8 associated with the global meteoric water line (GMWL; Dansgaard, 1964). These data support a central role for post-condensation evaporation during the March 7th convective event, whereby a raindrop is isotopically enriched during its transit from cloud to ground. Such a mechanism also explains the occurrence of several positive rainfall $\delta^{18}O$ values during this event. Together, these results strongly

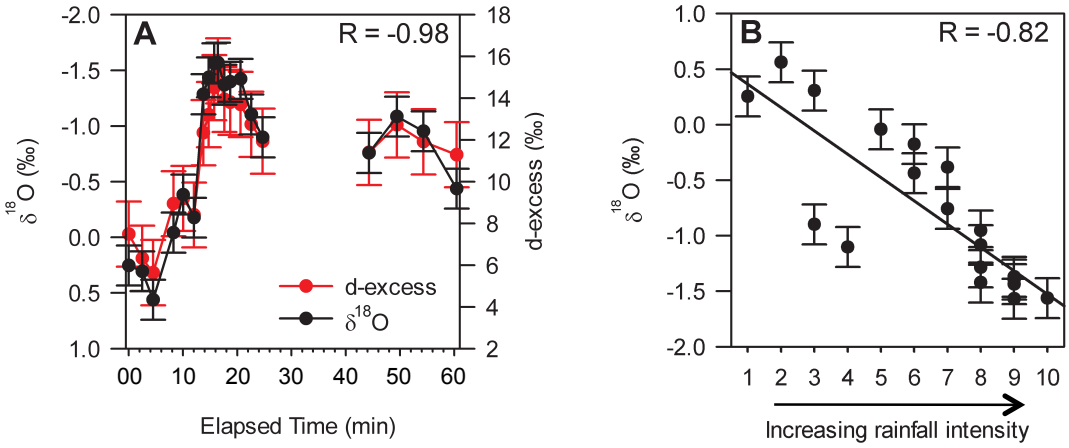

Fig. 2.1. Intra-storm rainfall $\delta^{18}O$ variability. a) Mulu rainfall $\delta^{18}O$ (black circles) and d-excess (red circles) during the March 7, 2010 convective event, plotted with error bars of ± 0.2‰ (1σ) for Mulu rainfall $\delta^{18}O$ and ± 1.5‰ (1σ) for d-excess. Note that axes for $\delta^{18}O$ and d-excess are inverted. b) Relationship between rainfall $\delta^{18}O$ and relative precipitation intensity during the March 7th convective event, where '1' represents a light drizzle and '10' represents the most intense downpour based on qualitative assessment of relative precipitation intensities. Error bars represent ± 0.2‰ (1σ).

suggest that post-condensation evaporative processes drive the observed "local" amount effect, and rainfall $\delta^{18}O$ variability in general, during this convective event. Our results provide further observational support for recent studies of an idealized microphysical model (Lee and Fung, 2008) and a single column model (Risi *et al*, 2008a), which both suggest that post-condensation evaporation is an important contributor to the amount

effect within individual rainfall events. Additional high-resolution sampling of water isotopes across discrete convective events is needed, however, to confirm whether these results are representative of precipitation events at our site.

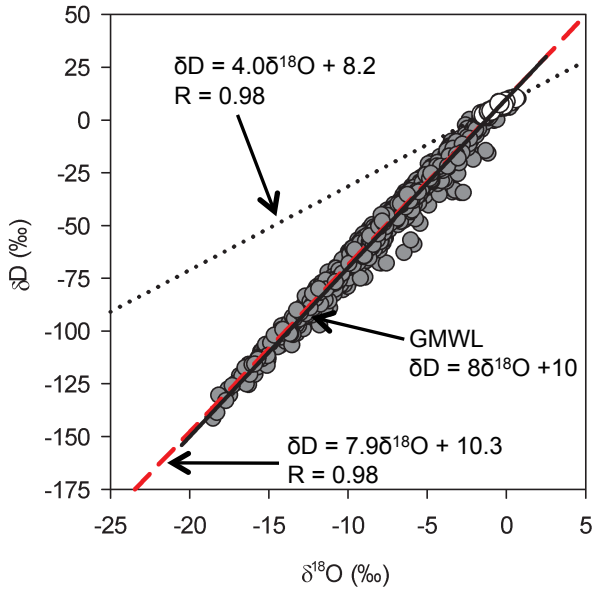

Fig. 2.2. Mulu local meteoric water line. Mulu rainfall $\delta^{18}O$ versus δD for the daily 5-year timeseries (gray circles) and the March 7, 2010 convective event (white circles). The dashed red line represents a linear fit for the 5-year timeseries of daily Mulu rainfall samples. The dotted black line represents a linear fit for the March 7, 2010 event samples. The global meteoric water line (solid black line) is plotted for reference (Craig, 1961).

2.4.2. Multi-year timeseries of daily rainfall $\delta^{18}O$

Daily rainfall $\delta^{18}O$ values vary considerably throughout the 5-year timeseries, ranging from +0.7 to -18.5‰ (Fig. 2.3). Daily rainfall $\delta^{18}O$ values average -7.8 ± 3.6‰ (1σ, N = 1004), and δD values average -51.7 ± 28.9‰ (1σ, N = 1004, not shown). The precipitation amount-weighted $\delta^{18}O$ timeseries is nearly identical to the raw $\delta^{18}O$ timeseries (Fig. A.5), except that its mean $\delta^{18}O$ value is shifted lower by roughly -0.5‰ because higher precipitation days are also, on average, lower rainfall $\delta^{18}O$ days. Several

daily rainfall $\delta^{18}O$ values fall to the right of the local meteoric water line (LMWL; Fig 2.2), providing evidence for a role, albeit limited, of evaporative forcing on daily rainfall $\delta^{18}O$ at the site (Dansgaard, 1964). Overall, however, the Mulu LMWL is indistinguishable from the GMWL, indicating that local post-condensation evaporation has minimal impact on cumulative daily rainfall $\delta^{18}O$ (Fig. 2.2). This finding is further supported by a near-zero correlation between daily rainfall $\delta^{18}O$ and d-excess ($R = -0.01$).

2.4.2.1. The amount effect at daily and longer timescales

As shown in Fig. 2.4a, the inverse correlation between daily rainfall $\delta^{18}O$ and daily precipitation amount at Mulu is significant but relatively weak ($R = -0.19$, $p < 0.05$). Correlations between rainfall $\delta^{18}O$ and local Mulu precipitation amount are higher on monthly timescales ($R = -0.56$, $p < 0.01$; Fig. 2.4b). Indeed, Fig. 2.4c further illustrates that the correlation between rainfall $\delta^{18}O$ and Mulu precipitation increases with increased temporal averaging. Correlations with Mulu rainfall $\delta^{18}O$ are even higher for TRMM precipitation and OLR integrated across a 2.5° x 2.5° gridbox centered at 5° N, 115° E containing Gunung Mulu, indicating that regional convective activity explains a larger fraction of Mulu rainfall $\delta^{18}O$ variability at daily and longer timescales than local precipitation. Basin-wide correlations between daily Mulu rainfall $\delta^{18}O$ and gridded TRMM precipitation amount further demonstrate that daily variations in Mulu rainfall $\delta^{18}O$ are closely tied to regional-scale processes (Fig. 2.5a). This spatial map can be contrasted to the map of correlations between Mulu precipitation amount and gridded TRMM precipitation amount, in which high correlations are confined to the immediate vicinity of the site (Fig. 2.5b).

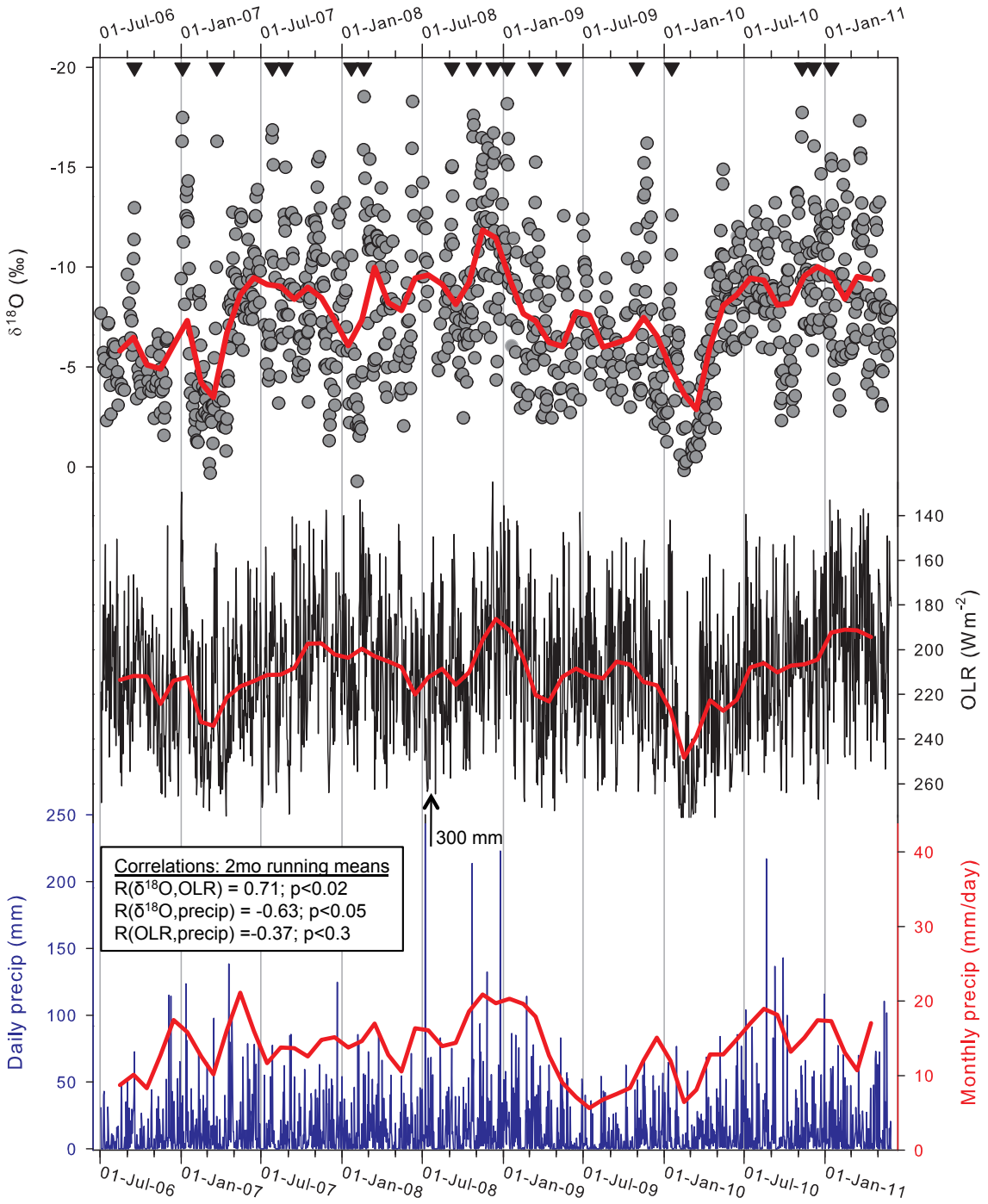

Fig. 2.3. 5-year timeseries of local Mulu rainfall $\delta^{18}O$, outgoing longwave radiation, and precipitation amount. (top) Timeseries of daily Mulu rainfall $\delta^{18}O$ (gray circles), plotted with a 2-month running mean (red line). Note that the 2-month running mean value plotted for December 2006 represents a linear interpolation of monthly values for November 2006 and January 2007. Intraseasonal rainfall $\delta^{18}O$ depletion events identified

with our statistical filter (see Section 3.2.2) are denoted by black triangles along the upper x-axis. (middle) Daily NOAA interpolated OLR at 5°N, 115°E (black line), plotted with a 2-month running mean (red line). Axes for $\delta^{18}O$ and OLR are inverted. (bottom) Daily local Mulu precipitation amount (blue line), plotted with a 2-month running mean (red line, plotted on the right-hand y-axis). Note that one of the daily precipitation entries (300mm) exceeds the scale plotted here, and is flagged accordingly. Correlations among the 2-month running means of the three timeseries are also provided.

While daily Mulu rainfall $\delta^{18}O$ variations are weakly correlated to daily Mulu precipitation amount, they are highly correlated to Mulu precipitation averaged over the previous 8 days (R=-0.46; Fig 2.4d). Similar results are found using TRMM precipitation and OLR but with correlations peaking with ~5 days of averaging (Fig 2.4d). This result reflects the time-integrative nature of rainfall $\delta^{18}O$ that previous studies have observed (Risi *et al*., 2008b; Vimeux *et al*., 2011) and modeled (Sturm *et al*., 2007; Risi *et al*., 2008a). It should be noted that a simple 8-day lag of local Mulu precipitation (as opposed to an 8-day integration of Mulu precipitation) is not correlated to daily Mulu rainfall $\delta^{18}O$ values (R=-0.07), indicating that a simple lag relationship is not responsible for these observations. The time-integrative nature of Mulu rainfall $\delta^{18}O$ is also illustrated by high auto-correlation of the $\delta^{18}O$ timeseries (R_{AC}=0.45) compared with that for local Mulu precipitation (R_{AC}=0.23). We hypothesize that the week-long 'memory' of rainfall $\delta^{18}O$ may reflect an approximately week-long atmospheric residence time of water vapor at Mulu.

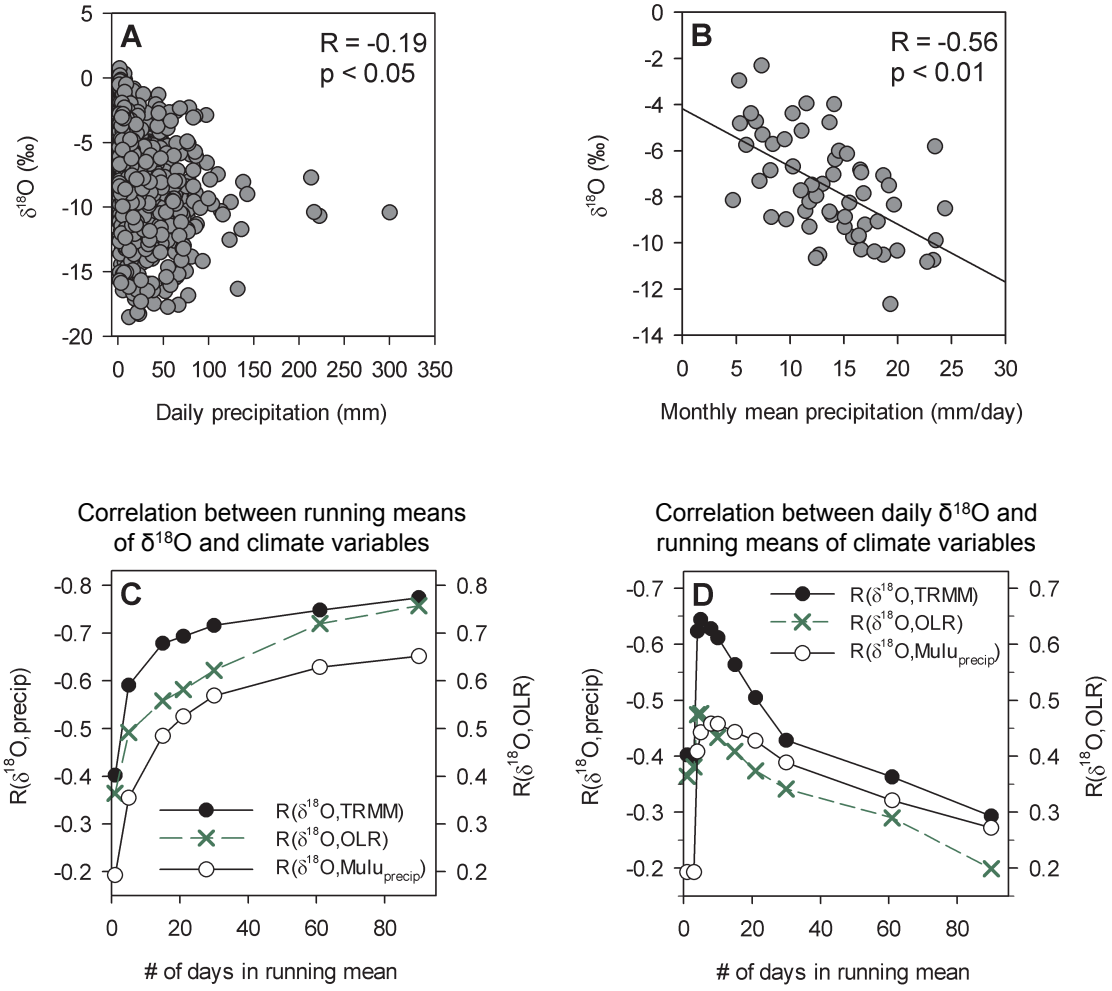

Fig. 2.4. Relationship between Mulu rainfall $\delta^{18}O$ and hydrological variables. a) Relationship between daily Mulu rainfall $\delta^{18}O$ and daily Mulu precipitation amount. b) Relationship between monthly-averaged Mulu rainfall $\delta^{18}O$ and monthly-averaged local Mulu precipitation amount. Solid black line represents linear best fit. c) Correlation between 'x'-day running means of Mulu rainfall $\delta^{18}O$ and 'x'-day running means of Mulu precipitation amount (open circles, solid line), satellite-derived TRMM 3B42 precipitation amount (black circles, solid line), and NOAA interpolated OLR (green crosses, dashed line). d) Correlation between daily Mulu rainfall $\delta^{18}O$ and 'x'-day minus-projected running means of local Mulu precipitation amount (open circles, solid line), TRMM 3B42 precipitation amount (black circles, solid line), and OLR (green crosses, dashed line), after Risi *et al*. (2008a). TRMM and OLR in both (c) and (d) are spatial averages integrated over a 2.5°x2.5° gridbox centered about 5°N, 115°E.

2.4.2.2. Intraseasonal variability of rainfall $\delta^{18}O$

The daily rainfall $\delta^{18}O$ timeseries is characterized by several exceptionally large (~10‰) negative excursions that occur every 30-90 days and last for several days to one week (Fig. 2.3). In order to characterize the evolution of these dramatic excursions and investigate their dynamical origins, we isolated eighteen of the largest excursions, hereafter referred to as 'depletion events,' by applying a statistical filter that selected excursions based on their amplitude and abruptness (Table A.1; see Supplemental Section for selection criteria). The resulting 'depletion events' are marked by triangles along the upper x-axis of Fig. 2.3.

A composite of the eighteen rainfall $\delta^{18}O$ 'depletion events' reveals consistent relationships between rainfall $\delta^{18}O$, local Mulu precipitation amount, and OLR across the duration of these events (Fig. 2.6). Rainfall $\delta^{18}O$ becomes gradually more depleted in the three days leading up to the minimum $\delta^{18}O$ value of -15.4 ± 2.4‰ (1σ) on 'Day 0' in Fig. 2.6, and gradually returns to average values three days after peak $\delta^{18}O$ depletion. Local Mulu precipitation amount, however, is characterized by a more abrupt transition to above average precipitation rates, with a near doubling of the long-term average precipitation amount four days prior to the minimum rainfall $\delta^{18}O$ value. Precipitation rates remain anomalously high until the day of lowest rainfall $\delta^{18}O$ (Day 0), after which they abruptly drop to below average rates for six days. The temporal evolution of OLR across a rainfall $\delta^{18}O$ depletion event falls somewhere between that of rainfall $\delta^{18}O$ and local Mulu precipitation.

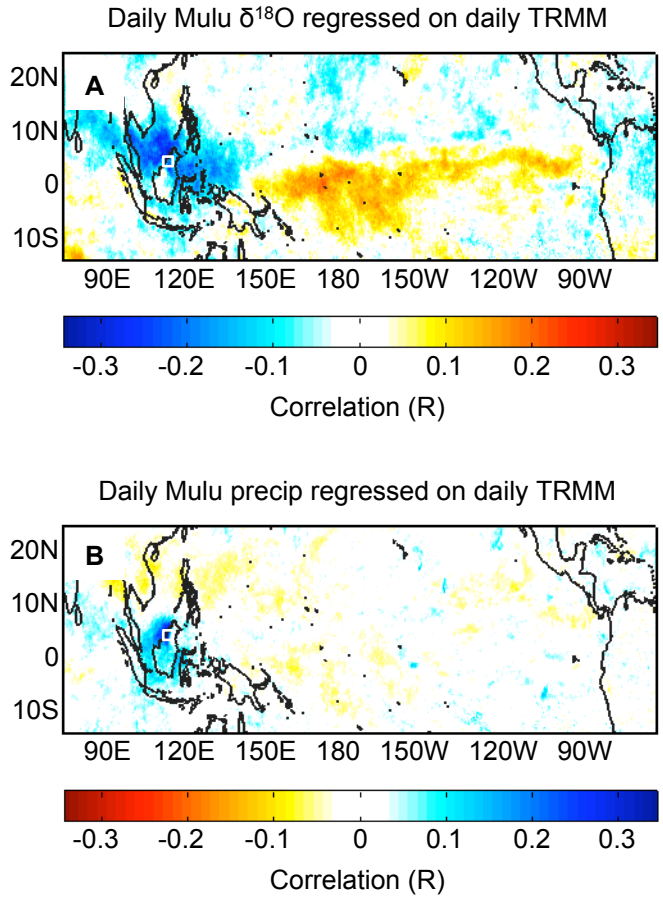

Fig. 2.5. Correlation maps of daily Mulu rainfall $\delta^{18}O$ and local Mulu precipitation amount with daily TRMM precipitation product 3B42 for July 2006 – May 2011 constructed using ordinary least squares regression. a) Correlation between daily Mulu rainfall $\delta^{18}O$ and gridded TRMM precipitation. b) Same as (a) but with daily local Mulu precipitation amount. The white box in each panel marks the location of our study site at Gunung Mulu National Park (4°N, 114°E).

The systematic relationships between Mulu rainfall $\delta^{18}O$, local Mulu precipitation, and OLR across the large rainfall $\delta^{18}O$ depletion events imply that they share a common origin. Indeed, a Hovmöller diagram of OLR confirms that the rainfall $\delta^{18}O$ depletion events occur during or immediately after the passage of organized regional convective activity from west to east (Fig. 2.7). The spatio-temporal signature of these OLR anomalies strongly resembles that of the MJO. Indeed, the majority of rainfall $\delta^{18}O$ depletion events do coincide with defined active (i.e. wet) phases of the MJO (Table

A.1). We conclude that the MJO strongly influences the intraseasonal variability of Mulu rainfall $\delta^{18}O$ and contributes to a "regional" amount effect relationship at intraseasonal timescales, as inferred by Cobb *et al.* (2007). In this case, the "regional" amount effect derives from the advection of depleted water vapor from regions to the west (upstream) of Mulu.

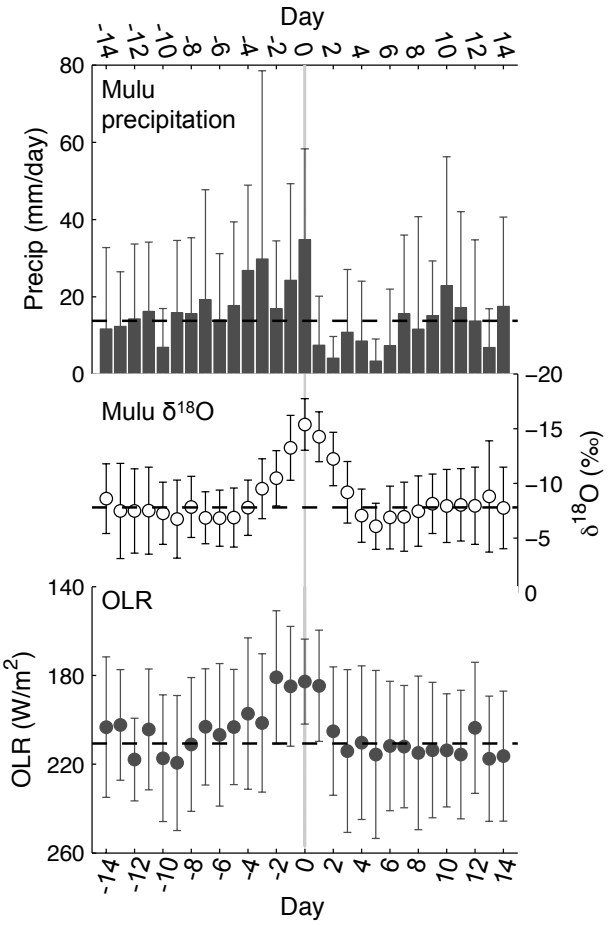

Fig. 2.6. Composite intraseasonal variability in local Mulu precipitation amount, Mulu rainfall $\delta^{18}O$, and outgoing longwave radiation. Composites of (top) daily Mulu precipitation amount, (middle) daily Mulu rainfall $\delta^{18}O$, and (bottom) daily OLR at 5°N, 115°E during the eighteen intraseasonal rainfall $\delta^{18}O$ depletion events centered about Day '0', which represents the minimum rainfall $\delta^{18}O$ value of the depletion events. Error bars reflect the 1σ spread for each daily average. Dashed horizontal lines represent the long-term daily average value of each parameter over the 5-year study period (13.8 ± 23.2 mm/day [1σ] for local Mulu precipitation, -7.8 ± 3.6‰ [1σ] for Mulu rainfall $\delta^{18}O$, and 210.7 ± 30.4 Wm^{-2} [1σ] for OLR). Note that axes for $\delta^{18}O$ and OLR are inverted.

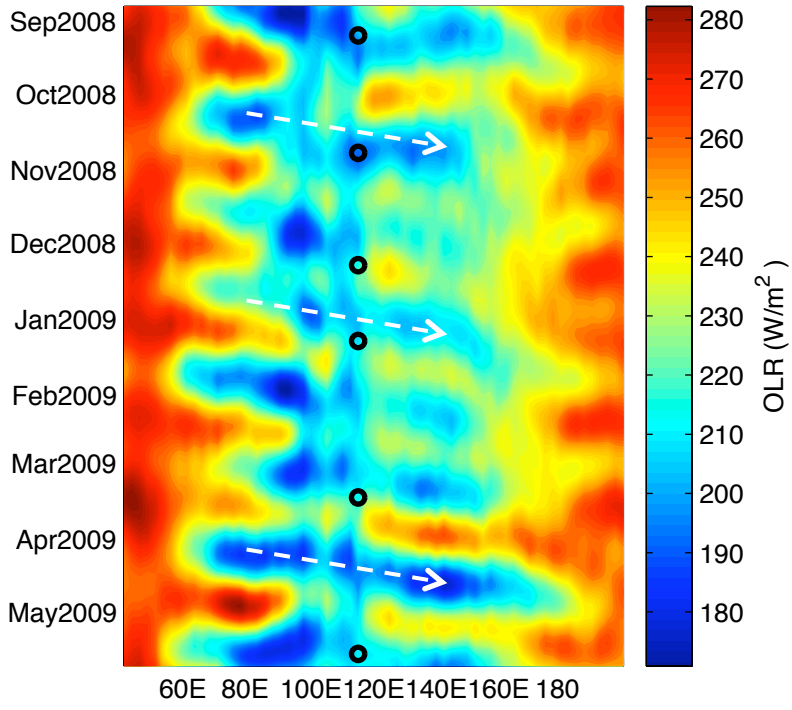

Fig. 2.7. Time-longitude map of daily NOAA interpolated OLR filtered with a 30-96 day bandpass filter and averaged over 0 – 5°N for the time window spanning 8/26/2008 to 5/23/2009. Open circles mark the timing of intraseasonal rainfall $\delta^{18}O$ depletion events that occur during the time window. White dashed arrows highlight examples of eastward-propagating enhanced convection.

2.4.2.3. Seasonal variability of rainfall $\delta^{18}O$

Long-term monthly mean rainfall $\delta^{18}O$ values reveal a weak semi-annual seasonal cycle with an amplitude of ~2-3‰ that accounts for roughly 20% of the total variance in monthly rainfall $\delta^{18}O$ (Fig. 2.8). Two relative rainfall $\delta^{18}O$ minima occur in June-July and November-January, and two relative maxima occur in February-April and August-October. It is important to note that removing potential ENSO influences from the 5-year rainfall $\delta^{18}O$ timeseries does not alter the rainfall $\delta^{18}O$ seasonal cycle (Fig. 2.8). Mulu rainfall $\delta^{18}O$ bears little resemblance to neither local nor regional precipitation on

seasonal timescales, suggesting that seasonal variations in Mulu rainfall $\delta^{18}O$ are driven by a combination of more remote effects.

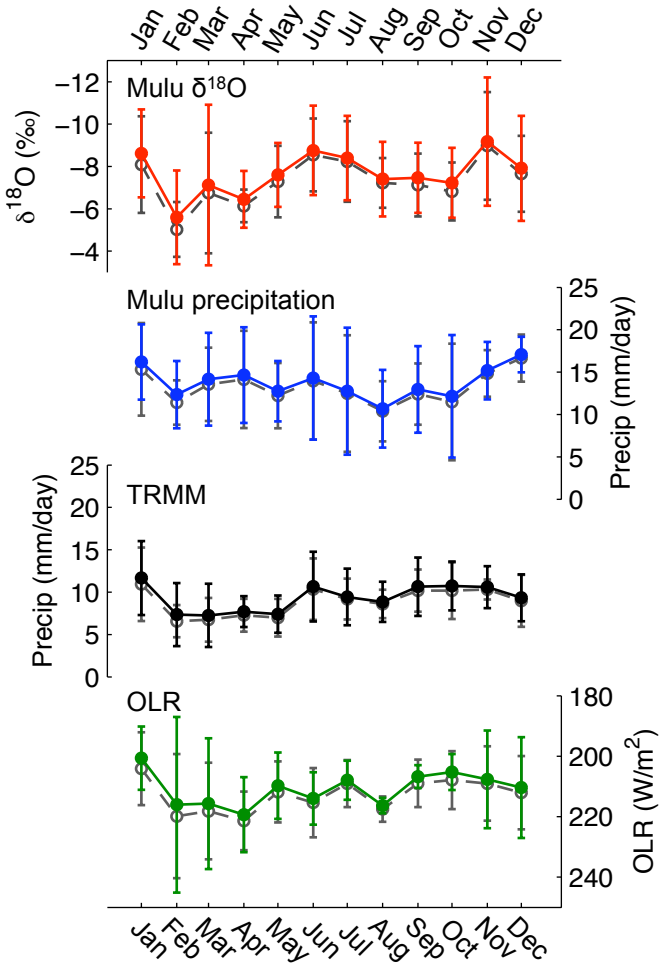

Fig. 2.8. Long-term monthly mean Mulu rainfall $\delta^{18}O$ (red), local Mulu precipitation amount (blue), satellite-measured TRMM 3B43 precipitation amount (black), and NOAA interpolated OLR (green) from July 2006 – May 2011. TRMM and OLR are spatial averages integrated over a 2.5° x 2.5° gridbox centered about 5°N, 115°E. Also plotted are versions of each long-term monthly mean with ENSO-related variability removed (gray). Error bars represent the 1σ spread of each month's mean value. Note that axes for $\delta^{18}O$ and OLR are inverted.

The semi-annual seasonal rainfall $\delta^{18}O$ composite presented here represents a significant revision to the annual seasonal cycle of rainfall $\delta^{18}O$ inferred by Cobb *et al.* (2007) from a much smaller sample size. Cobb *et al*. (2007) invoked seasonal changes in the degree of orographic fractionation to explain a relative $\delta^{18}O$ maximum (minimum) in boreal summer (winter). Such a mechanism may contribute to the complexity of seasonal rainfall $\delta^{18}O$ at Mulu, but our new results require a mechanism that leads to relatively high rainfall $\delta^{18}O$ values during the shoulder seasons of February/March/April and August/September/October (Fig. 2.8). Regional winds are relatively weak during these times, as the ITCZ transits directly over northern Borneo. We hypothesize that during these seasons, the adjoining sea surface is the dominant source of water vapor to Mulu, providing for shorter water vapor trajectories and therefore less cumulative isotopic fractionation. A detailed investigation of the causes of seasonal variations in Mulu rainfall $\delta^{18}O$, however, is beyond the scope of the present manuscript.

2.4.2.4. Interannual variability of rainfall $\delta^{18}O$

The 5-year Mulu rainfall $\delta^{18}O$ timeseries contains appreciable interannual variations of 6-8‰ that account for approximately 70% of the total monthly variance in rainfall $\delta^{18}O$. Interannual rainfall $\delta^{18}O$ variations are significantly correlated to both local Mulu precipitation ($R=-0.63$, $p < 0.05$; Fig. 2.9a) and large-scale ENSO indices (e.g. $R=0.64$, $p < 0.05$ for NIÑO4; Fig. 2.9c). Compared to western Pacific ENSO indices, eastern Pacific indices are more weakly correlated to Mulu rainfall $\delta^{18}O$ (Table A.3). Local Mulu precipitation amount is characterized by lower correlations to ENSO indices (e.g. $R = -0.50$, $p < 0.1$ for NIÑO4; Fig. 2.9f). These findings strongly suggest that,

compared to Mulu precipitation, Mulu rainfall $\delta^{18}O$ is a better tracer of ENSO variability, owing to its time- and space-integrative properties.

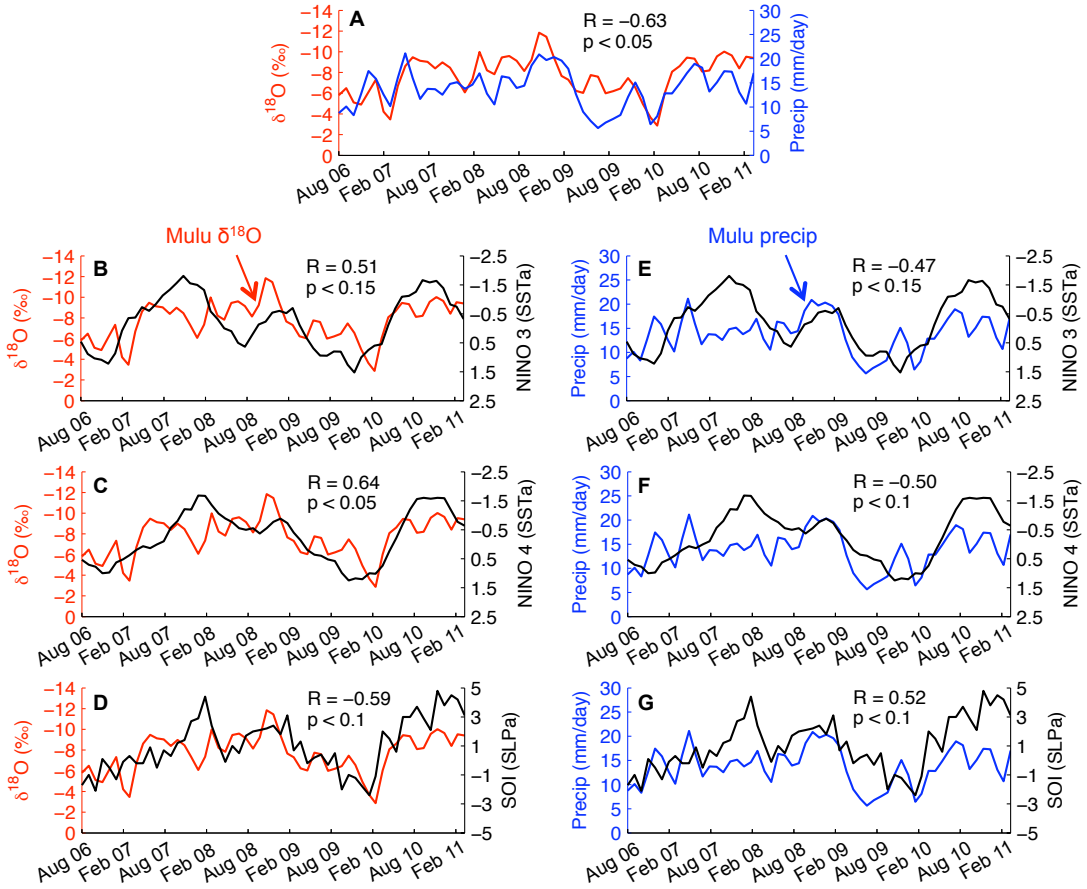

Fig. 2.9. Comparison of monthly averaged Mulu rainfall $\delta^{18}O$, local precipitation amount, and ENSO indices. a) Timeseries of 2-month running mean Mulu rainfall $\delta^{18}O$ and local Mulu precipitation amount. b-d) Comparisons of 2-month running mean Mulu rainfall $\delta^{18}O$ with (b) NIÑO 3, (c) NIÑO 4, and (d) SOI. e-g) Same as (b-d) but for 2-month running mean Mulu precipitation amount. Axes for rainfall $\delta^{18}O$ and NIÑO indices are inverted (with the exception of SOI). NIÑO and SOI indices obtained from http://www.cpc.ncep.noaa.gov/data/indices/.

Regression maps of Mulu rainfall $\delta^{18}O$ and basin-scale precipitation (Fig 2.10a) and OLR (Fig. 2.10b) reveal significant correlations that extend from the western to central Pacific. The spatial pattern of these correlations strongly resembles the first EOF of global precipitation, which is attributed to ENSO variability (e.g. Fig 1 of Furtado *et al*., 2009). These results support the existence of a strong "regional" amount effect associated with ENSO variability, whereby regionally suppressed convection in the western Pacific leads to higher rainfall isotopes during El Niño conditions, and vice versa during La Nina events. It is worth noting that these statistically robust relationships were extracted from a time series that contained only one "strong" ENSO event (i.e. the 2010/2011 La Niña), thus underscoring the sensitivity of rainfall $\delta^{18}O$ at our site to small/moderate changes in the ENSO state.

In contrast to Mulu rainfall $\delta^{18}O$, which closely tracks basin-scale ocean-atmosphere interactions associated with ENSO, Mulu precipitation amount is correlated to regional precipitation in a much smaller area. The fact that Mulu rainfall $\delta^{18}O$ is more sensitive than Mulu precipitation amount to basin-scale ENSO variability indicates that the rainfall $\delta^{18}O$-ENSO relationship is primarily transmitted through regional-scale, rather than local, convective activity. In other words, interannual variations in the overall convective state of the WPWP imprint water vapor with an isotopic ENSO signal prior to the vapor's arrival at northern Borneo, while ENSO-related changes in convective activity at our site may subsequently serve to amplify the far-field ENSO signal in rainfall $\delta^{18}O$.

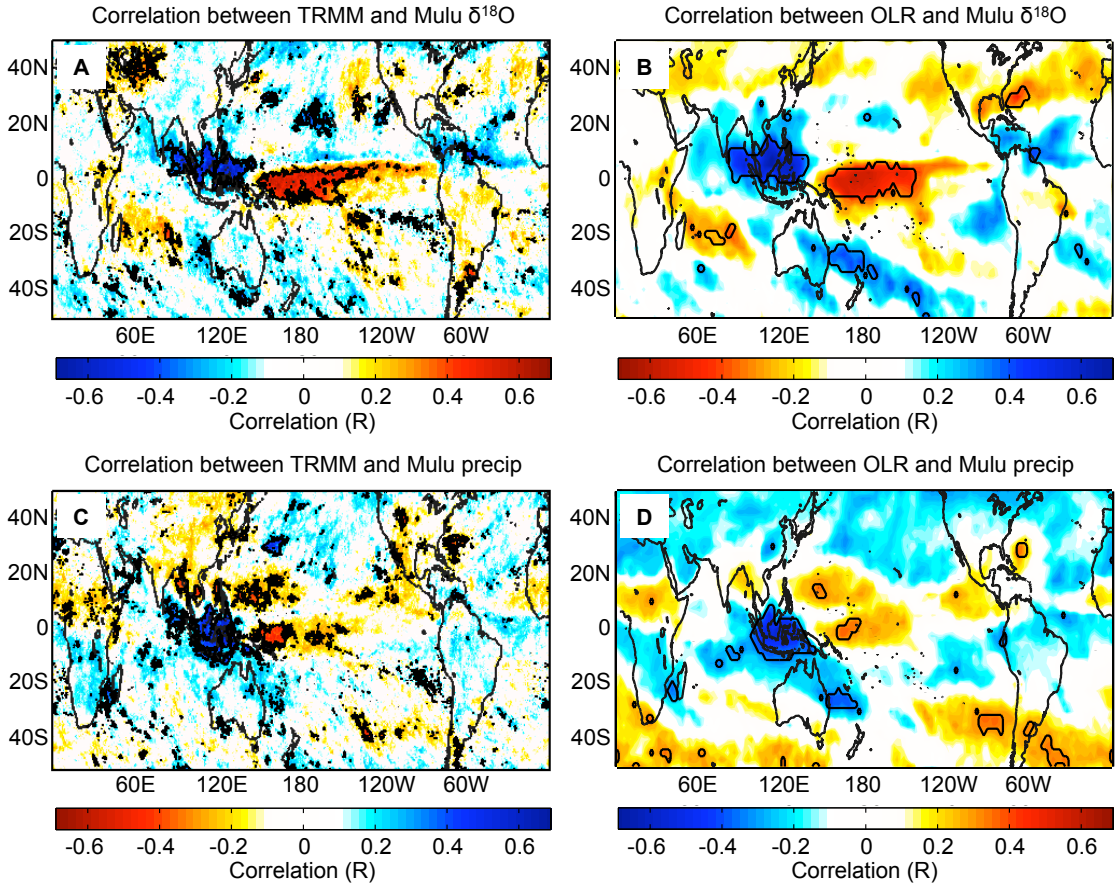

Fig. 2.10. Correlation maps of monthly mean Mulu rainfall $\delta^{18}O$ and local Mulu precipitation amount with monthly TRMM precipitation product 3B43 and monthly NOAA interpolated OLR for July 2006 – May 2011 constructed using ordinary least squares regression. a) Correlation between monthly mean Mulu rainfall $\delta^{18}O$ and gridded TRMM precipitation. b) Same as (a) but with gridded OLR. c) Correlation between monthly mean Mulu precipitation amount and gridded TRMM precipitation. d) Same as (c) but with gridded OLR. Black contour lines indicate 95% significance regions as determined by the student's *t*-test using effective degrees of freedom (Bretherton *et al*., 1999). Color scales for panels (b) and (c) are inverted.

2.5. Discussion

2.5.1. Spatial and temporal signatures of the amount effect

Across nearly all timescales studied, Mulu rainfall $\delta^{18}O$ is inversely related to precipitation variability, consistent with the tropical amount effect. While we find evidence for a "local" amount effect across a single convective event, we demonstrate that rainfall $\delta^{18}O$ variability on diurnal to interannual timescales at Mulu is tied to a "regional" amount effect.

Within an individual storm, we find evidence that local processes, specifically below-cloud evaporation of falling raindrops, cause the observed inverse correlation between rainfall $\delta^{18}O$ and precipitation rate. This relationship arises because the degree of kinetic fractionation during the evaporation of a raindrop depends on the humidity of the atmosphere through which it falls, with higher humidity suppressing evaporative enrichment (Dansgaard, 1964; Stewart, 1975). The response of rainfall $\delta^{18}O$ to changes in the efficiency of below-cloud evaporation is essentially instantaneous at the intra-storm timescale. These findings provide observational confirmation of numerical modeling results invoking post-condensation evaporative enrichment as a primary control on rainfall isotopes during individual precipitation events (Lee and Fung, 2008; Risi *et al*., 2008a).

At the diurnal timescale, several lines of evidence suggest that isotopic fractionation associated with the "local" amount effect is dwarfed by $\delta^{18}O$ variations that reflect regional convective activity. For one, our results indicate that post-condensation evaporation of falling raindrops, which amounts to variations of ~1-2‰ within the March 7, 2010 convective event, is relatively small compared to day-to-day rainfall $\delta^{18}O$

variations of ~2-10‰. Indeed, previous observational and GCM-based studies also find that local post-condensation evaporation has relatively little impact on rainfall $\delta^{18}O$ values on daily and longer timescales in wet tropical regions (Kurita *et al*., 2009; Breitenbach *et al*., 2010; Field *et al*., 2010). Secondly, the weak correlation between daily rainfall $\delta^{18}O$ and daily Mulu precipitation amount further suggests that local rainout has relatively little impact on cumulative daily Mulu rainfall $\delta^{18}O$ values. Similarly weak correlations between daily rainfall $\delta^{18}O$ and local precipitation amount are also observed at other tropical and subtropical sites (e.g. Yamanaka *et al*., 2004; Risi *et al*., 2008b, Kurita *et al.* 2009, Breitenbach *et al*., 2010; Vimeux *et al*., 2011).

The weak daily rainfall $\delta^{18}O$-precipitation relationship can be attributed to the time- and space- integrative properties of rainfall $\delta^{18}O$, illustrated by the high correlation between daily rainfall $\delta^{18}O$ and regional precipitation amount averaged over the preceding week (Fig. 2.4d). The 5-8-day vapor residence time that we observe at Mulu, suggests that isotopic signals persist within the atmospheric vapor above Mulu for several days. These findings are consistent with those of studies at other tropical sites, which explain the time-integrative behavior of rainfall $\delta^{18}O$ via a repeated atmospheric vapor recycling process, in which low-level vapor depleted by earlier convective activity is fed into successive convective systems (Risi *et al*., 2008a, 2008b; Vimeux *et al*., 2011). In this way, the isotopic composition of the recycled water vapor – and that of the resultant rainfall – reflects the cumulative intensity of the previous days' convective activity, thus causing daily rainfall $\delta^{18}O$ to be poorly correlated with daily precipitation amount. Taken together, these results suggest that diurnal rainfall $\delta^{18}O$ variability at our site is more dependent on the isotopic composition of the water vapor from which it condenses than

the local fractionation processes that occur during individual rainfall events. The space-integrative property of daily Mulu rainfall $\delta^{18}O$, illustrated by the strong correlations between Mulu rainfall $\delta^{18}O$ and regional precipitation amount in Figs. 2.4c and 2.4d, suggests that Mulu vapor $\delta^{18}O$ is also significantly influenced by regional-scale convective processes. This is further supported by Fig. 2.5, which shows that correlations between daily gridded TRMM precipitation amount and daily Mulu rainfall $\delta^{18}O$ are far more regionally extensive than they are for daily Mulu precipitation amount.

The large multi-day rainfall $\delta^{18}O$ depletion events observed at Mulu typically coincide with the passage of mesoscale convective systems associated with the MJO (Fig. 2.7). We infer that these large-scale convective systems deliver anomalously depleted water vapor $\delta^{18}O$ to Mulu, thus resulting in depleted rainfall $\delta^{18}O$. Indeed, Kurita *et al*. (2011) and Berkelhammer *et al*. (2012) observe large negative anomalies in water vapor δD as active MJO events pass over the northern Borneo area. However, the most depleted Mulu rainfall $\delta^{18}O$ occurs towards the end of the passage of a regional convective system rather than at the onset (Figs. 2.6 and 2.7). Risi *et al*. (2008b) similarly observe a multi-day delay in maximum rainfall $\delta^{18}O$ depletion with respect to the onset of enhanced convective activity associated with the monsoon in west Africa. In our case, maximum rainfall $\delta^{18}O$ depletion occurs after ~3-4 days of above-average local precipitation. As water vapor residence times are 5-8 days at our site, this relatively rapid depletion suggests that additional vapor fractionation occurs as a result of on-site convective activity. Thus, the largest, sharpest rainfall $\delta^{18}O$ depletions observed in our timeseries can be ascribed to two processes: 1) regionally-enhanced convection associated with the MJO delivers already depleted water vapor to Gunung Mulu, and 2) intense local convective

activity distills the vapor pool over a period of several days, amplifying the advected negative isotopic anomaly. In this way, Mulu rainfall $\delta^{18}O$ variations on intraseasonal timescales reflect contributions from both regional and local convective activity.

The close relationship between regional hydrology and Mulu rainfall $\delta^{18}O$ is most evident on interannual timescales, when weak to moderate El Niño events are associated with significantly higher rainfall $\delta^{18}O$ at Mulu, and vice versa during La Niña events. In this context, it is striking that Mulu rainfall $\delta^{18}O$ is a better indicator than local Mulu precipitation of basin-scale atmospheric circulation on interannual timescales. This reinforces the notion that water vapor $\delta^{18}O$ has an integrating effect, averaging the convective activity experienced during its transport history through both space and time. As such, the ENSO signal captured by Mulu rainfall $\delta^{18}O$ reflects the sensitivity of Mulu rainfall $\delta^{18}O$ to regional climatic conditions on monthly timescales.

2.5.2 Implications for $\delta^{18}O$ – based paleoclimate reconstructions

The present study demonstrates that changes in regional convective activity are reflected in rainfall $\delta^{18}O$ variations at our site, providing further empirical support for the amount effect framework used to interpret $\delta^{18}O$-based paleo-reconstructions from northern Borneo stalagmites (Partin *et al.,* 2007; Meckler *et al*., 2012). As such, any changes over time in the background state of regional-scale hydrology, such as variability in the strength and/or location of deep convection in the WPWP, would likely impact rainfall $\delta^{18}O$ at Mulu. More generally, the ability of rainfall $\delta^{18}O$ to integrate regional convective activity across space and time makes it a much better indicator of large-scale hydrology than local precipitation amount, which contains much more noise. Therefore, while precipitation variability from nearby sites may be poorly correlated (Dayem *et al*.,

2010), rainfall $\delta^{18}O$ variability from nearby sites may indeed be highly correlated due to the integrative properties of rainfall $\delta^{18}O$. This explains why stalagmite $\delta^{18}O$ records from caves that are hundreds of kilometers apart reflect the same regional-scale hydroclimate influences (e.g. Yuan *et al*., 2004; Wang *et al*., 2001). Likewise, well-reproduced cave stalagmite records from a single site can be interpreted as robust indicators of regional-scale hydroclimate variability (e.g. Partin *et al.,* 2007).

When considering how to relate rainfall $\delta^{18}O$ variability to stalagmite calcite $\delta^{18}O$ variability, one must keep in mind that several processes mediate the cloud-to-calcite transformation of rainfall $\delta^{18}O$ signals. First, the infiltration of rainwaters through the karst environment inevitably leads to some measure of signal attenuation from mixing, as well as signal delay depending on water residence times in the karst. In comparing several Mulu dripwater $\delta^{18}O$ timeseries with rainfall $\delta^{18}O$ timeseries, Cobb *et al*. (2007) argue for dripwater residence times of 2-3 months, based on the preservation of a weak seasonal cycle in dripwater $\delta^{18}O$. However, owing to logistical difficulties in collecting timeseries of dripwater $\delta^{18}O$ from slow to ultra-slow drips that typically form stalagmites, residence time estimates for the most relevant drips remain poorly constrained. A new 5-yr-long timeseries of dripwater $\delta^{18}O$ from both fast and slow Mulu drips will help quantify groundwater transit times across a broad range of drip environments (Moerman *et al*., 2012). A complementary approach involves pursuing a "calibration" of annual to sub-annual stalagmite $\delta^{18}O$ with climatic timeseries over the 20th century. The latter approach requires unusually fast-growing stalagmites and small chronological errors afforded by either annual layer counting and/or many U/Th dates (e.g. Frappier *et al*., 2002, 2007; Fleitman et al., 2004; Treble *et al.,* 2005;) and, as such, are relatively rare.

Such calibrations generally confirm the interpretation of stalagmite $\delta^{18}O$ reconstructions as hydroclimate reconstructions, but highlight key uncertainties surrounding the cloud-to-calcite transformation of rainfall $\delta^{18}O$ signals.

Our study suggests that as records of paleo-rainfall $\delta^{18}O$, stalagmite $\delta^{18}O$ records reflect changes in regional convective activity, which in turn is related to a variety of climatic processes operating across a range of timescales. The Mulu rainfall $\delta^{18}O$ timeseries exhibits variability at intraseasonal, seasonal, and interannual timescales, each linked to a distinct climatic phenomenon. Therefore, low-frequency stalagmite $\delta^{18}O$ signals at Mulu could conceivably represent a change in the frequency and/or amplitude of MJO-related variability, a change in the seasonal rainfall cycle (i.e. the ITCZ), and/or a change in the tropical Pacific's zonal SST gradient (i.e. ENSO). This ambiguity illustrates the need to transition from reliance on single-site stalagmite $\delta^{18}O$ reconstructions to networks of paleoclimate records that span the geographic range of the climatic phenomenon of interest. Indeed, small networks of stalagmite $\delta^{18}O$ records have recently been applied to investigate changes in the ITCZ by Griffiths et al. (2009) with a north-south transect from southeast Asia to Indonesia. Such an approach could be used to investigate changes in the zonal convective gradient across the equatorial tropical Pacific. Networks such as these would provide important benchmarks for newly available paleoclimate simulations of coupled GCMs, some of which are equipped with water isotope modules (e.g. LeGrande *et al*., 2006; Sturm *et al*., 2010; Risi *et al*., 2010). Such data-model comparisons provide an opportunity to advance our understanding of the mechanisms of global climate change on decadal to millennial timescales and how well these processes are represented in state-of-the-art climate models.

2.6. Conclusions

Our analyses demonstrate that the inverse relationship between rainfall $\delta^{18}O$ and precipitation amount, known as the amount effect, is a strong control on the oxygen isotopic composition of rainfall in northern Borneo over the majority of the timescales examined. Studying a single precipitation event at high temporal resolution, we find evidence for local fractionation processes driving intra-storm rainfall $\delta^{18}O$ variability, whereas the majority of diurnal to interannual rainfall $\delta^{18}O$ variability originates from regional-scale hydrological processes. Daily rainfall $\delta^{18}O$ variations best reflect cumulative regional precipitation occurring over the preceding week. Intraseasonal rainfall $\delta^{18}O$ variability, which is particularly large at our site with up to ~16‰ shifts, is closely associated with the MJO – the dominant mode of intraseasonal climatic variability in the tropics – and exhibits influences from both local and far-field fractionation processes. Interannual rainfall $\delta^{18}O$ variability at Mulu is significantly correlated to ENSO, whereby a basin-scale reorganization of atmospheric circulation patterns during El Niño and La Niña events affects regional convective activity and in turn the regional isotopic composition of the atmospheric water vapor. In this context, Mulu rainfall $\delta^{18}O$ is superior to local Mulu precipitation amount as a proxy for ENSO variability.

Taken together, our study documents a robust amount effect relationship between regional precipitation and Mulu rainfall $\delta^{18}O$ that is most evident at intraseasonal and interannual timescales. Our results lend strong support to the interpretation of $\delta^{18}O$-based reconstructions from northern Borneo stalagmites as regional hydroclimate proxies, with

significant influences from intraseasonal and interannual variability, and to a lesser extent, seasonal variability. More generally, our study illustrates that the processes governing the climate-rainfall $\delta^{18}O$ relationship are space- and time-dependent. As such, our results support the generation of multi-year, daily-resolved timeseries of rainfall isotopes in order to identify the dynamical controls on rainfall $\delta^{18}O$ variability at sites where accurate interpretations of paleoclimate $\delta^{18}O$ reconstructions are especially critical.

2.7. Acknowledgements

The authors gratefully acknowledge the Mulu Meteorological Station staff for overseeing the collection of the daily rainfall samples, as well as Jenny Malang, Syria Lejau, and the staff at Gunung Mulu National Park for their dedicated assistance during fieldtrips. Permits for this work were granted by the Malaysian Economic Planning Unit, the Sarawak State Planning Unit, and the Sarawak Forestry Department. We also thank Aaron van Pelt of Picarro, Inc., Bruce Vaughn of INSTARR at UC Boulder, and Krystle Stewart for their invaluable assistance during sample analysis and Dr. Emanuele Di Lorenzo for his assistance with the TRMM dataset. This research was supported by NSF grant 0645291 to KMC, and JWM was funded by a NSF Graduate Research Fellowship.

2.8. REFERENCES

Aggarwal, P., Frohlich, K., Kulkarni, K., Gourcy, L., 2004. Stable isotope evidence for moisture sources in the Asian summer monsoon under present and past climate regimes. Geophys. Res. Lett. 31, L08203.

Araguas-Araguas, L., Froehlich, K., Rozanski, K., 1998. Stable isotope composition of precipitation over southeast Asia. J. Geophys. Res. Atmos. 103, 28721–28742.

Arkin, P.A., Ardanuy, P.E., 1989. Estimating climatic-scale precipitation from space: A review. J. Climate 2, 1229–1238.

Bar-Matthews, M., Ayalon, A., Kaufman, A., 1997. Late Quaternary paleoclimate in the Eastern Mediterranean region from stable isotope analysis of speleothems at Soreq Cave, Israel. Quat. Res. 47, 155-168.

Bell, G.D., Halpert, M.S., 1998. Climate assessment for 1997. Bull. Amer. Meteor. Soc. 79, 1014–1014.

Berkelhammer, M., Risi, C., Kurita, N., Noone, D., 2012. The moisture source and sequence for the Madden-Julian Oscillation as derived from satellite retrievals of HDO and H_2O. J. Geophys. Res. 117, D03106.

Breitenbach, S., Adkins, J., Meyer, H., Marwan, N., Kumar, K., Haug, G., 2010. Strong influence of water vapor source dynamics on stable isotopes in precipitation observed in Southern Meghalaya, NE India. Earth Planet. Sci. Lett. 292, 212-220.

Bretherton, C.S., Widmann, M., Dymnikov, V.P., Wallace, J.M., Bladè, I., 1999. Effective number of degrees of freedom of a spatial field. J. Clim. 12, 1990–2009.

Burns, S.J., Matter, A., Frank, N., Mangini, A., 1998. Speleothem-based paleoclimate record from northern Oman. Geology 26 (6), 499-502.

Carolin, S.A., Cobb, K.M., Adkins, J.F., Tuen, A.A., Clark, B., Lejau, S., Malang, J., Varied response of western Pacific hydrology to abrupt climate change events. Science *submitted.*

Celle-Jeanton, H., Gonfiantini, R., Travi, Y., Sol, B., 2004. Oxygen-18 variations of rainwater during precipitation: application of the Rayleigh model to selected rainfalls in southern France. J. Hydrol. 289, 165-177.

Cobb, K.M., Adkins, J.F., Partin, J.W., Clark, B., 2007. Regional-scale climate influences on temporal variations of rainwater and cave dripwater oxygen isotopes in northern Borneo. Earth Planet. Sci. Lett. 263, 207-220.

Conroy, J.L., Cobb, K.M., Noone, D., Comparison of precipitation isotope variability across the tropical Pacific in observations and SWING2 model simulations. J. Geophys. Res. Atmos. *submitted*.

Craig, H., 1961. Isotopic variations in meteoric waters. Science 133, 1702-1703.

Dansgaard, W., 1964. Stable isotopes in precipitation. Tellus 16 (4), 436–468.

Dayem, K., Molnar, P., Battisti, D., Roe, G., 2010. Lessons learned from oxygen isotopes in modern precipitation applied to interpretation of speleothem records of paleoclimate from eastern Asia. Earth Planet. Sci. Lett. 295, 219-230.

Dykoski, C.A., Edwards, R.L., Cheng, H., Yuan, D.X., Cai, Y.J., Zhang, M.L., Lin, Y.S., Qing, J.M., An, Z.S., Revenaugh, J., 2005. A high-resolution, absolute-dated Holocene and deglacial Asian monsoon record from Dongge Cave, China. Earth Planet. Sci. Lett. 233, 71–86.

Field, R., Jones, D., Brown, D., 2010. Effects of postcondensation exchange on the isotopic composition of water in the atmosphere. J. Geophys. Res. 115, D24305.

Fleitmann, D., Burns, S.J., Neff, U., Mudelsee, M., Mangini, A., Matter, A., 2004. Palaeoclimatic interpretation of high-resolution oxygen isotope profiles derived from annually laminated speleothems from Southern Oman. Quat. Sci. Rev. 23, 935-945.

Frappier, A., Sahagian, D., Gonzalez, L.A., Carpenter, S.J., 2002. El Niño events recorded by stalagmite carbon isotopes. Science 298, 565.

Frappier, A., Sahagian, D., Carpenter, S., Gonzalez, L., Frappier, B., 2007. Stalagmite stable isotope record of recent tropical cyclone events. Geology 35 (2), 111-114.

Furtado, J.C., Di Lorenzo, E., Cobb, K.M., Bracco, A., 2009. Paleoclimate reconstructions of tropical sea surface temperatures from precipitation proxies: Methods, uncertainties, and nonstationarity. J. Clim. 22, 1104-1123.

Gao, J., Masson-Delmotte, V., Yao, T., Tian, L., Risi, C., Hoffmann, G., 2011. Precipitation water stable isotopes in the south Tibetan plateau: Observations and modeling. J. Clim. 24, 3161-3178.

Gat, J.R., 1996. Oxygen and hydrogen isotopes in the hydrologic cycle. Annual Rev. Earth Planet. Sci. 24, 225–262.

Griffiths, M., Drysdale, R., Gagan, M., Zhao, J.-x., Ayliffe, L., Hellstrom, J., Hantoro, W., Frisia, S., Feng, Y.-x., Cartwright, I., St. Pierre, E., Fischer, M., Suwargadi, B., 2009. Increasing Australian-Indonesian monsoon rainfall linked to early Holocene sea-level rise. Nature Geosci. 2, 636-639.

Hoffmann, G.,Werner, M., Heimann, M., 1998.Water isotope module of the ECHAM atmospheric general circulation model: a study on timescales from days to several years. J. Geophys. Res. Atmos. 103, 16871–16896.

Hoffmann, G., Ramirez, E., Taupin, J., Francou, B., Ribstein, P., Delmas, R., Dürr, H., Gallaire, R., Simões, J., Schotterer, U., Stievenard, M., Werner, M. 2003. Coherent isotope history of Andean ice cores over the last century. Geophys. Res. Lett. 30 (4), 1179.

Huffman, G., Adler, R., Bolvin, D., Gu, G., Nelkin, E., Bowman, K., Hong, Y., Stocker, E., Wolff, D., 2007. The TRMM multisatellite precipitation analysis (TMPA): Quasi-global, multiyear, combined-sensor precipitation estimates at fine scales. J. Hydrometeorol. 8, 38-55.

International Atomic Energy Agency 2006. Isotope Hydrology Information System. The ISOHIS Database. Accessible at http://isohis.iaea.org.

Joussaume, S., Sadourny, R., and Jouzel, J., 1984. A General-circulation model of water isotope cycles in the atmosphere. Nature 311, 24-29.

Jouzel, J., Russell, G.L., Suozzo, R.J., Koster, R.D., White, J.W.C., Broecker, W.S., 1987. Simulations of the HDO and H2 O-18 atmospheric cycles using the NASA GISS general-circulation model - the seasonal cycle for present-day conditions. J. of Geophys. Res. Atmos. 92 (D12), 14739-14760.

Kurita, N., Ichiyanagi, K., Matsumoto, J., Yamanaka, M., Ohata, T., 2009. The relationship between the isotopic content of precipitation and precipitation amount in tropical regions. J. Geochem. Explor. 102, 113-122.

Kurita, N., Noone, D., Risi, C., Schmidt, G. A., Yamada, H., Yoneyama, K., 2011. Intraseasonal isotopic variation associated with the Madden-Julian Oscillation. J. Geophys. Res. 116, D24101.

Lawrence, J., Gedzelman, S., 1996. Low stable isotope ratios of tropical cyclone rains. Geophys. Res. Lett. 23 (5), 527-530.

Lawrence, J.R., Gedzelman, S.D., Dexheimer, D., Cho, H.K., Carrie, G.D., Gasparini, R., Anderson, C.R., Bowman, K.P., Biggerstaff, M.I., 2004. Stable isotopic composition of water vapor in the tropics. J. Geophys. Res. Atmos. 109, D06115.

Lee, J.-E., Fung, I., DePaolo, D., Henning, C., 2007 Analysis of the global distribution of water isotopes using the NCAR atmospheric general circulation model. J. Geophys. Res. 112, D16306.

Lee, J.-E., Fung, I., 2008. “Amount effect” of water isotopes and quantitative analysis of post-condensation processes. Hydrol. Process. 22, 1-8.

Lee, J.-E., Johnson, K., Fung, I., 2009. Precipitation over South America during the Last Glacial Maximum: An analysis of the ‘‘amount effect’’ with a water isotope-enabled general circulation model. Geophys. Res. Lett. 36, L19701.

LeGrande, A., Schmidt, G., Shindell, D., Field, C., Miller, R., Koch, D., Faluvegi, G., Hoffmann, G., 2006. Consistent simulations of multiple proxy responses to an abrupt climate change event. Proc. Natl. Acad. Sci. 103, 837-842.

LeGrande, A., Schmidt, G., 2009. Sources of Holocene variability of oxygen isotopes in paleoclimate archives. Clim. Past 5, 441-445.

Lewis, S., LeGrande, A., Kelley, M., Schmidt, G., 2010. Water vapor source impacts on oxygen isotope variability in tropical precipitation during Heinrich events. Clim. Past. 6, 325-340.

Liebmann B, Smith, C., 1996. Description of a complete (interpolated) outgoing longwave radiation dataset. Bull. Am. Meteorol. Soc. 77, 1275-1277.

Madden, R.A., Julian, P.R., 1972. Description of global-scale circulation cells in tropics with a 40–50day period. J. Atmos. Sci. 29, 1109–1123.

Meckler, A., Clarkson, M., Cobb, K., Sodemann, H., Adkins, J., 2012. Interglacial hydroclimate in the tropical west Pacific through the late Pleistocene. Science 336, 1301-1304.

Moerman, J.W., Cobb, K.M., Adkins, J.F., Sodemann, H., Clark, B., Tuen, A.A., 2012. Local and regional climatic controls on high-resolution rainfall and cave dripwater oxygen isotopes in northern Borneo. Abstract PP33A-2094 presented at 2012 Fall MeetingAmerican Geophysical Union, San Francisco, Calif., 3-7 Dec.

Noone, D., Simmonds, I., 2002. Associations between delta O-18 of water and climate parameters in a simulation of atmospheric circulation for 1979–95. J. Clim. 15, 3150–3169.

Partin, J.W., Cobb, K.M., Adkins, J.F., Fernandez, D.P., Clark, B., 2007. Millennial-scale trends in West Pacific Warm Pool hydrology from the Last Glacial Maximum to present. Nature 499, 452–455.

Rasmusson, E.M.,Wallace, J.M., 1983. Meteorological aspects of the El Niño/Southern Oscillation. Science 222, 1195–1202.

Reynolds, R.W., Rayner, N.A., Smith, T.M., Stokes, D.C., Wang, W., 2002. An improved in situ and satellite SST analysis for climate. J. Clim. 15, 1609-1625.

Risi, C., Bony, S., Vimeux, F., 2008a. Influence of convective processes on the isotopic composition ($\delta^{18}O$ and δD) of precipitation and water vapor in the Tropics, Part 2: physical interpretation of the amount effect. J. Geophysical Res. 113, D19306.

Risi, C., Bony, S., Vimeux, F., Descroix, L., Boubacar, I., Lebreton, E., Mamadou, I., Sultan, B., 2008b. What controls the isotopic composition of the African monsoon precipitation? Insights from event-based precipitation collected during the 2006 AMMA field campaign. Geophys. Res. Lett. 35, L24808.

Risi, C., Bony, S., Vimeux, F., Jouzel, J., 2010. Water-stable isotopes in the LMDZ4 general circulation model: Model evaluation for present-day and past climates and applications to climatic interpretations of tropical isotopic records. J. Geophys. Res. 115, D12118.

Rindsberger, M., Jaffe, S., Rahamim, S., Gat, J., 1990. Patterns of the isotopic composition of precipitation in time and space: Data from the Israeli storm collection program. Tellus 42B, 263-271.

Rozanski, K., Araguas-Araguas, L., Gonfiantini, R., 1993. Isotopic patterns in modern global precipitation. In: Swart, P.K., Lohmann, K.C., McKenzie, J. (Eds.), Climate Change in Continental Isotopic Records. Geophysical Monograph, vol. 78. American Geophysical Union, Washington D.C., pp. 1–36.

Sachs, J., Sachse, D., Smittenberg, R., Zhang, Z., Battisti, D., Golubic, S., 2009. Southward movement of the Pacific intertropical convergence zone AD 1400-1850. Nature Geosci. 2, 519-525.

Schmidt, G., LeGrande, A., Hoffman, 2007. Water isotope expressions of intrinsic and forced variability in a coupled ocean-atmosphere model. J. Geophys. Res. 112, D10103.

Stewart, M., 1975. Stable isotope fractionation due to evaporation and isotopic exchange of falling waterdrops: Applications to atmospheric processes and evaporation of lakes. J. Geophys. Res. 80 (9), 1133-1146.

Sturm, C., Vimeux, F., Krinner, G., 2007. Intraseasonal variability in South America recorded in stable water isotopes. J. Geophys. Res. 112, D20118.

Sturm, C., Zhang, Q., Noone, D., 2010. An introduction to stable water isotopes in climate models: Benefits of forward proxy modeling for paleoclimatology. Clim. Past 6, 115-129.

Tian, L., Yao, T., MacClune, K., White, J., Schilla, A., Vaughn, B., Vachon, R., Ichiyanagi, K., 2007. Stable isotope variations in west China: a consideration of moisture sources. J. Geophys. Res. 112, D10112.

Tierney, J., Oppo, D., Rosenthal, Y., Russell, J., Linsley, B., 2010. Coordinated hydrological regimes in the Indo-Pacific region during the past two millennia. Paleoceanogr. 25, PA1102.

Tindall, J., Valdes, P., Sime, L., 2009. Stable water isotopes in HadCM3: Isotopic signature of El Niño Southern Oscillation and the tropical amount effect. J. Geophys. Res. Atmos. 114, D04111.

Treble, P.C., Chappell, J., Gagan, M.K., McKeegan, K.D., Harrison, T.M., 2005. In situ measurement of seasonal delta O-18 variations and analysis of isotopic trends in a modem speleothem from southwest Australia. Earth Planet. Sci. Lett. 233, 17–32.

Tremoy, G., Vimeux, F., Mayaki, S., Souley, I., Cattani, O., Risi, C., Favreau, G., Oi, M., 2012. A 1-year long $\delta^{18}O$ record of water vapor in Niamey (Niger) reveals insightful atmospheric processes at different timescales. Geophys. Res. Lett. 39, L08805.

Vimeux, F., Ginot, P., Schwikowski, M., Vuille, M., Hoffmann, G., Thompson, L.G., Schotterer, U., 2009. Climate variability during the last 1000 years inferred from Andean ice cores: A review of methodology and recent results. Palaeogeogr. Palaeoclimatol. Palaeoecol. 281, 229-241.

Vimeux, F., Tremoy, G., Risi, C., Gallaire, R., 2011. A strong control of the South American SeeSaw on the intra-seasonal variability of the isotopic composition of precipitation in the Bolivian Andes. Earth Planet. Sci. Lett. 307, 47-58.

Vuille, M., Werner, M., Bradley, R.S., Keimig, F., 2005. Stable isotopes in precipitation in the Asian monsoon region. J. Geophys. Res. 110, D23108.

Wang, Y.J., Cheng, H., Edwards, R.L., An, Z.S., Wu, J.Y., Shen, C.C., Dorale, J.A., 2001. A high-resolution absolute-dated Late Pleistocene monsoon record from Hulu Cave, China. Science 294, 2345–2348.

Yamanaka, T., Shimada, J., Hamada, Y., Tanaka, T., Yang, Y.H., Zhang, W.J., and Hu C.S., 2004. Hydrogen and oxygen isotopes in precipitation in the northern part of the north china plain: Climatology and interstorm variability. Hydrol. Process. 18 (12), 2211–2222.

Yuan, D.X., Cheng, H., Edwards, R.L., Dykoski, C.A., Kelly, M.J., Zhang, M.L., Qing, J.M., Lin, Y.S., Wang, Y.J., Wu, J.Y., Dorale, J.A., An, Z.S., Cai, Y.J., 2004. Timing, duration and transition of the last interglacial Asian Monsoon. Science 304, 575–578.

Zhang, C., 2005. Madden-Julian Oscillation. Rev. Geophys. 43, RG2003.

CHAPTER 3

TRANSFORMATION OF ENSO-RELATED RAINWATER TO DRIPWATER $\delta^{18}O$ VARIABILITY BY VADOSE WATER MIXING

This chapter is published in:

J.W. Moerman, Cobb, K.M., Partin, J.W., Meckler, A.N., Carolin, S.A., Adkins, J.F., Malang, J., Lejau, S., Clark, B., Tuen, A.A. (2014) Transformation of ENSO-related rainwater to dripwater $\delta^{18}O$ variability by vadose water mixing. *Geophysical Research Letters.* **41**. 7907–7915.

3.1. Abstract

Speleothem oxygen isotopes ($\delta^{18}O$) are often used to reconstruct past rainfall $\delta^{18}O$ variability, and thereby hydroclimate changes, in many regions of the world. However, poor constraints on the karst hydrological processes that transform rainfall signals into cave dripwater add significant uncertainty to interpretations of speleothem-based reconstructions. Here we present several 6.5-year, biweekly dripwater $\delta^{18}O$ timeseries from northern Borneo and compare them to local rainfall $\delta^{18}O$ variability. We demonstrate that vadose water mixing is the primary rainfall-to-dripwater transformation process at our site, where dripwater $\delta^{18}O$ reflects amount-weighted rainfall $\delta^{18}O$ integrated over the previous 3-10 months. We document large interannual dripwater $\delta^{18}O$ variability related to the El Niño-Southern Oscillation (ENSO), with amplitudes inversely correlated to dripwater residence times. According to a simple stalagmite forward model, asymmetrical ENSO extremes produce significant offsets in stalagmite $\delta^{18}O$ timeseries

given different dripwater residence times. Our study highlights the utility of generating multi-year, paired timeseries of rainfall and dripwater $\delta^{18}O$ to aid interpretations of stalagmite $\delta^{18}O$ reconstructions.

3.2. Introduction

The broad geographic availability of speleothems has allowed for the generation of continuous high-resolution, absolutely-dated paleoclimate reconstructions from oxygen isotopes ($\delta^{18}O$) across the globe. As a key tropical link between high-latitude, high-resolution ice core and tropical, low-resolution marine sediment records, speleothems have served to constrain the global extent of glacial terminations [e.g. *Cheng et al.*, 2009; *Meckler et al.*, 2012], characterize millennial-scale abrupt climate changes [e.g. *Carolin et al.*, 2013; *Wang et al.*, 2001], provide evidence of inter-hemispheric antiphasing in terrestrial hydroclimate [e.g. *Ayliffe et al.*, 2013; *Cruz et al.*, 2005a; *Griffiths et al.*, 2009; *Wang et al.*, 2006] and reconstruct centennial-scale variability over the last millennium [e.g. *Partin et al.*, 2013e; *Sinha et al.*, 2007; *Zhang et al.*, 2008]. Annually- and subannually-resolved speleothem $\delta^{18}O$ records also track high-frequency tropical modes, such as the El Niño-Southern Oscillation (ENSO) [e.g. *Lachniet*, 2004], monsoon variability [e.g. *Berkelhammer et al.*, 2010; *Fleitmann et al.*, 2004], and tropical cyclones [e.g. *Frappier et al.*, 2007].

The amount effect – whereby rainfall $\delta^{18}O$ in lower latitudes is inversely correlated to rainfall amount [*Dansgaard*, 1964; *Rozanski*, 1993] – forms the basis for interpretations of low-latitude speleothem $\delta^{18}O$ as records of past hydroclimate variability. More recently, attention has turned towards site-specific investigations of the isotope-climate relationship through time, using long-term observational monitoring

programs [e.g. *Cobb et al.*, 2007; *Kurita et al.*, 2009; *Moerman et al.*, 2013; *Vimeux et al.*, 2011] and isotope-equipped general circulation models (GCMs) [e.g. *LeGrande and Schmidt*, 2009; *Lewis et al.*, 2010; *Schmidt et al.*, 2007]. While broadly supporting the amount effect relationship in the tropics, these studies and others [e.g. *Lawrence et al.*, 2004] suggest that $\delta^{18}O$ variability is best interpreted as a reflection of regional-scale, rather than local, hydrological variability. GCM and observation-based studies by *Schmidt et al.* [2007] and *Moerman et al.* [2013], respectively, further document that local rainfall $\delta^{18}O$ outperforms local precipitation amount as an indicator of large-scale atmospheric circulation. Such studies lend strong support to the use of speleothem-based reconstructions of rainfall $\delta^{18}O$ for tracking low-frequency modes of hydroclimate variability.

Surface-to-cave infiltration modifies the original rainfall $\delta^{18}O$ signal, yet this transformation is poorly constrained for all but a few karst systems. *Baker et al.* [2012] suggest that karst hydrology may even be a stronger control on speleothem $\delta^{18}O$ variability than climate, in extreme cases, highlighting the need for additional studies on this topic. Dominant transformation processes include evaporation of water within the soil and epikarst layers [e.g. *Ayalon et al.*, 1998; *Bradley et al.*, 2010], biases in hydrologically effective recharge toward high-volume rainfall events and/or wet seasons [e.g. *Jex et al.*, 2010; *Pape et al.*, 2010; *Partin et al.*, 2012], mixing in the vadose zone [e.g. *Genty et al.*, 2014; *Partin et al.*, 2012], and variable water routing [e.g. *Baker et al.*, 2012; *Jex et al.*, 2013; *Treble et al.*, 2013]. Non-stationary and nonlinear flow behavior may further obscure the relationship between rainfall and dripwater $\delta^{18}O$ [*Baker et al.*, 2013; *Bradley et al.*, 2010]. As no two cave systems are alike, temporal monitoring of

dripwater $\delta^{18}O$ at individual paleoclimate sites is essential to constrain the unique influence of karst hydrology on speleothem $\delta^{18}O$ and improve interpretations of past climate variations.

Here we present a new 6.5-yr-long biweekly-collected timeseries of dripwater $\delta^{18}O$ from the Mulu karst system in northern Borneo, where tropical hydroclimate has been reconstructed over the past 500,000 years [*Carolin et al.*, 2013; *Meckler et al.*, 2012; *Partin et al.*, 2007]. Building upon previous work by *Cobb et al.* [2007] and *Partin et al.* [2013a], this paper seeks to characterize Mulu karst hydrology and its impact on the dripwater $\delta^{18}O$ variability that is ultimately archived in Borneo speleothem $\delta^{18}O$. By comparing Mulu rainfall and dripwater $\delta^{18}O$ timeseries, we identify the dominant karst transformation processes at Mulu, estimate water transit times, and demonstrate how different residence times can influence speleothem $\delta^{18}O$.

3.3. Geological and climatic setting

The caves of Gunung Mulu National Park are found in northwestern Borneo (4°N, 114°E) within the Melinau Limestone Formation – a Late Eocene to Early Miocene shallow marine carbonate platform [*Wannier*, 2009; *Wilford*, 1961]. The site receives approximately 5m of precipitation annually, which supports lush tropical rainforests with relatively thin topsoil. Seasonality in both precipitation amount and rainfall $\delta^{18}O$ is weak due to the site's year-round position within the ITCZ [*Cobb et al.*, 2007; *Moerman et al.*, 2013]. The largest anomalies in precipitation amount and rainfall $\delta^{18}O$ occur intraseasonally in association with the Madden Julian-Oscillation (MJO; 30-90 days) and interannually in association with ENSO (2-7 years), with La Niña (El Niño) events

delivering anomalously wet (dry) conditions to the region [*Moerman et al.*, 2013]. Recharge for the Mulu karst system can be broadly divided into three categories: (1) autogenic infiltration of precipitation falling directly onto the Melinau limestone; (2) allogenic runoff from the adjoining sandstone mountain Gunung Mulu (2377 m); and (3) occasional flooding of the Melinau River alluvial plain [*Waltham and Brook*, 1980].

3.4. Methods

Two distinct dripwater sampling programs were launched for this study: (1) a biweekly collection of dripwater at three individual drip sites from May 2006 to November 2012; and (2) spatial surveys of stalagmite-forming drips throughout multiple caves and chambers during three field expeditions in August 2008 (N = 36), February-March 2010 (N = 54), and October-November 2012 (N = 135).

For the 6.5-year dripwater timeseries, discrete samples were collected by park staff approximately every two weeks. Drip rate was measured manually via stopwatch. Two of the dripwater timeseries were collected from Wind Cave and the third from Lang's Cave, approximately 5km to the south [*Partin et al.*, 2013a]. The two Wind Cave drips are located 50-75 m from the entrance and overlain by ~100 m of bedrock. The first drip site, named Wind Slow (WS), has a relatively slow drip rate of 7 ± 1 dpm (drips per minute; 1σ) and drips onto bedrock detritus (Figure B.1). The second site, named Wind Fast (WF), has a relatively fast drip rate of 35 ± 6 dpm (1σ) and drips into a small pool within a speleothem (Figure B.1). The Lang's Cave drip site (L2) is located approximately 140 m from the entrance and overlain by ~200 m of bedrock. L2 has an average drip rate of 14 ± 3 dpm (1σ) and drips onto a 2m-tall stalagmite (Figure B.1).

This study also extends the Mulu rainfall $\delta^{18}O$ timeseries presented in *Moerman et al.* [2013] by 1.5 years. All rainfall and dripwater samples were collected in 3mL glass vials and sealed with rubber stoppers and crimp-top aluminum closures to safeguard against post-collection evaporation. Rainfall and dripwater $\delta^{18}O$ and δD were analyzed via cavity ring-down spectroscopy (Picarro L1102-i water isotope analyzer), which has a long-term reproducibility of ± 0.1‰ for $\delta^{18}O$ and ± 0.8‰ for δD (1σ) [*Moerman et al.*, 2013].

3.5. Results

3.5.1. Observed Mulu dripwater $\delta^{18}O$ variability

The oxygen isotopic composition of the three dripwater timeseries varies coherently through time despite considerable diversity in drip-type, drip-rate, and geographic location (Figure 1c). Despite the large difference in drip-rate, the Wind Cave drips WF and WS exhibit the same range of $\delta^{18}O$ variability (-4.9 to -11.6‰) and nearly identical mean isotopic values (-8.2 ± 1.2‰ [1σ] and -8.0 ± 1.2‰ [1σ], respectively). Drip L2 in Lang's Cave has a similar mean $\delta^{18}O$ value of -8.4 ± 0.6‰ (1σ), but the amplitude of the variability (-7.2 to -10.0‰) is roughly half that of WF and WS. Variations in drip rate are poorly correlated to dripwater $\delta^{18}O$ variability (Figure 3.1c,d; $R < 0.1$).

The isotopic maximum for each timeseries occurs during the moderate 2009/2010 El Niño event, whereas the isotopic minimum coincides with a weak La Nina event in 2008/2009 (Figure 3.1a,c). Rainfall and dripwater $\delta^{18}O$ anomalies related to El Niño events are larger in magnitude, shorter in duration, and decay more rapidly than those

associated with La Niña events, reflecting asymmetry in the duration and magnitude of El Niño versus La Niña events themselves [e.g. *McPhaden and Zhang*, 2009; *Okumura and Deser*, 2010]. The El Niño-related anomalies in WF and WS are 2-3‰ heavier than those observed in L2. The La Niña-related dripwater $\delta^{18}O$ anomalies are more similar across the drip sites, clustering within 1‰ of each other during moderate to strong La Niña events (Figure 3.1c).

A succession of several intense precipitation events in late 2008/early 2009 associated with a particularly active MJO [*Moerman et al.*, 2013] contributes to the minimum in dripwater $\delta^{18}O$ observed during this time. This package of relatively frequent, large precipitation events is unique in the timeseries, and its relationship to the concurrent La Niña event is unclear, as the other weak La Niña event (2011/2012) covered in the study period is not associated with particularly active MJO activity. Generally speaking, however, intraseasonal rainfall $\delta^{18}O$ anomalies of ~10‰ [*Moerman et al.*, 2013] are largely homogenized in the resulting dripwater $\delta^{18}O$ timeseries, leaving a predominantly interannual signal related to ENSO variability.

The three dripwater $\delta^{18}O$ timeseries reflect smoothed, lagged versions of amount-weighted Mulu rainfall $\delta^{18}O$ (Figure 3.1b,c). Relative to the 6-8‰ ENSO-related variations in Mulu rainfall $\delta^{18}O$ (Figure 3.1b; *Moerman et al.* [2013]), interannual variability is reduced to ~5‰ in the Wind Cave drips and to ~2.5‰ in L2. The timing of dripwater $\delta^{18}O$ maxima and minima also lags rainfall $\delta^{18}O$ by 2-3 months. Taken together, this suggests that mixing of infiltrating waters is a dominant influence on the resultant isotopic composition of dripwater at the monitored sites. Potential biases in recharge rates during wet versus dry times, as well as potential evaporative enrichment of

soil water, both appear to have limited influence on dripwater $\delta^{18}O$, as evidenced by (i) the close match between mean amount-weighted Mulu rainfall $\delta^{18}O$ (-8.6 ± 3.5‰ [1σ]) and the combined mean isotopic value for the three dripwater timeseries (-8.2 ± 1.0‰ [1σ]; Figure 3.1c) and (ii) the lack of consistent evaporation tails in plots of dripwater $\delta^{18}O$ versus δD (Figure B.2).

3.5.2. Residence time analysis

To further probe karst hydrology as it relates to the rainfall-to-dripwater $\delta^{18}O$ transformation, we model dripwater $\delta^{18}O$ from the daily Mulu rainfall $\delta^{18}O$ timeseries. We begin by considering a simple recharge model wherein a single reservoir is fed by the autogenic infiltration of percolating precipitation. We simulate the effect of different mixing rates on dripwater $\delta^{18}O$ variability by averaging daily amount-weighted rainfall $\delta^{18}O$ over the previous *n* weeks (e.g. backwards-projected running mean). In this way, we generate a suite of modeled dripwater $\delta^{18}O$ timeseries corresponding to different residence times (Figure B.3) and infer the actual residence time to be the number of weeks used in the modeled dripwater timeseries that best correlates with the observed timeseries for each drip site (Figure B.4).

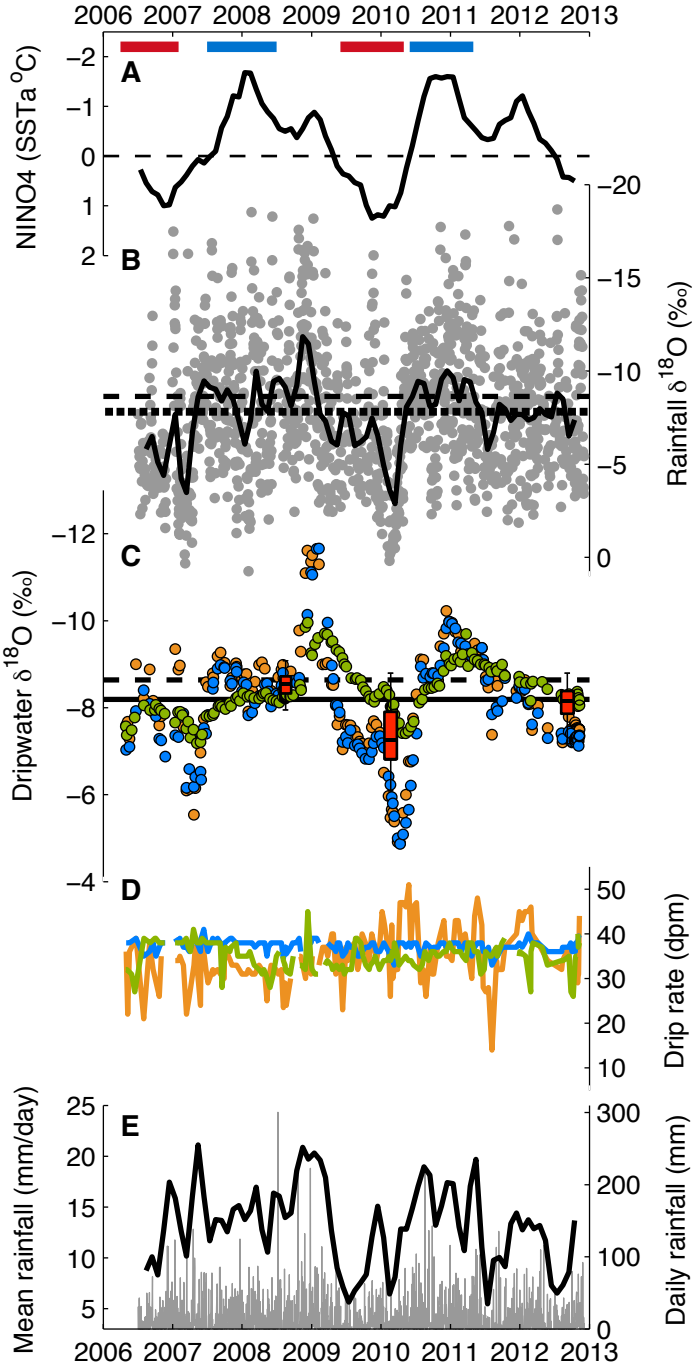

Figure 3.1: **Comparison of Mulu dripwater $\delta^{18}O$ to rainfall $\delta^{18}O$ and local and regional climate variables**. (a) Monthly NINO4 SST anomalies [*Reynolds et al.*, 2002]. Red and blue bars along the upper x-axis represent weak-to-moderate El Niño and moderate-to-strong La Niña events as defined by the Oceanic Niño Index (http://www.cpc.ncep.noaa.gov/products/analysis_monitoring/ensostuff/ensoyears.shtml). (b) Non-amount-weighted daily Mulu rainfall $\delta^{18}O$ (gray circles) shown with a 2-month running average (black line), and non-amount-weighted (dotted line) and amount-weighted (dashed line) means of the entire timeseries. (c) Mulu dripwater $\delta^{18}O$ from drips WF (orange), WS (blue), and L2 (green) plotted with the composite mean of the three dripwater $\delta^{18}O$ timeseries (black line) and mean amount-weighted rainfall $\delta^{18}O$ from

panel (b) (dashed line). Box-and-whisker plots represent the median (bold bar), 25-75% quartile range (red box), and maximum and minimum $\delta^{18}O$ values (whiskers) for system-wide field-expedition surveys of stalagmite-forming dripwaters conducted in August 2008 (n=36), February-March 2010 (n=54), and October-November 2012 (n=135). (d) Drip rates from drip sites WF (orange), WS (blue), and L2 (green). Note WS drip rate has been shifted by +30 dpm and L2 by +20 dpm. (e) Rain gauge measurements of daily Mulu precipitation amount (gray bars) plotted with a 2-month running average (black line). Y-axes in panels (a-c) are inverted.

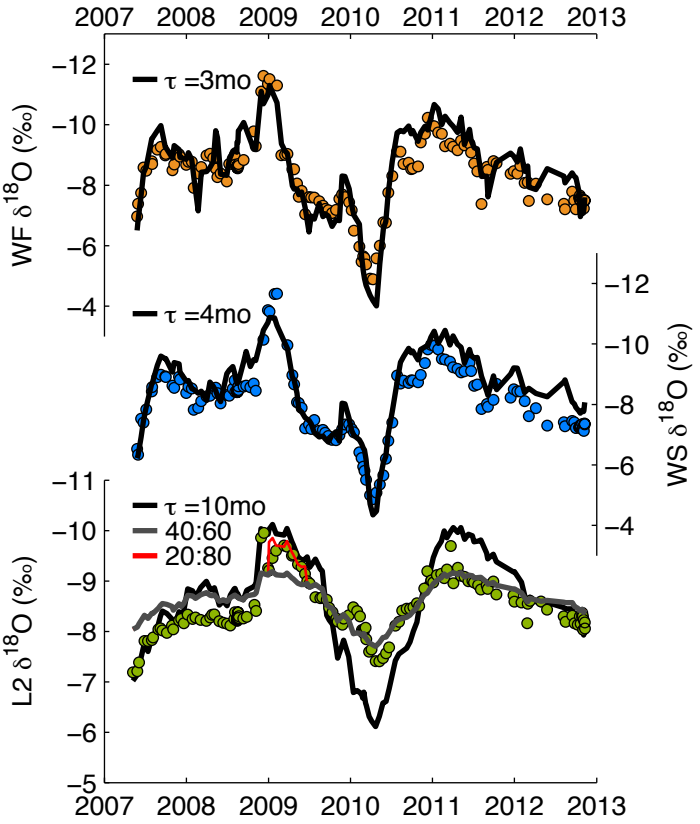

Figure 3.2: Observed dripwater $\delta^{18}O$ (circles) for drips WF (orange), WS (blue), and L2 (green) compared with best-fit modeled dripwater $\delta^{18}O$ (solid lines) using amount-weighted Mulu rainfall $\delta^{18}O$ as input. Bold black lines represent dripwater simulated by the autogenic recharge model with a residence times of ~3 months for WF, ~4 months for WS, and ~10 months for L2. Bivariate mixing model results for drip L2 modeled as 40% of Reservoir A with an ~10-month residence time and 60% of Reservoir B reflecting mean amount-weighted rainfall $\delta^{18}O$ are plotted as a gray line. During the October 2008 – June 2009 interval, the red line reflects modeled dripwater $\delta^{18}O$ assuming contributions of 20% from Reservoir A and 80% from Reservoir B. Y-axes are inverted in all panels.

We estimate residence times of 3-4 months for reservoirs feeding drips WF and WS. Observed dripwater $\delta^{18}O$ variations in WF are best reproduced by averaging amount-weighted rainfall $\delta^{18}O$ over the previous 13 weeks or ~3 months (R = 0.92; Figure 3.2), while WS is best correlated to the modeled timeseries with an 18-week or ~4-month averaging interval (R = 0.94; Figure 3.2). For these two drips, our simple autogenic recharge model reproduces both the variability and amplitude of variance extremely well and captures the observed lag between rainfall and dripwater $\delta^{18}O$ minima and maxima.

While the autogenic recharge model reproduces the timing of L2 dripwater $\delta^{18}O$ minima and maxima, it overestimates the amplitude of the drip's $\delta^{18}O$ variations (Figure 3.2). Amount-weighted rainfall $\delta^{18}O$ averaged over the previous 42 weeks (~10 months) best reflects the timing of dripwater $\delta^{18}O$ maxima and minima observed in L2 (R = 0.84), but the predicted variations are roughly 1‰ higher than observed (Figure 3.2). This suggests that the flow pathway to this drip site is more complicated than that feeding WF and WS. L2's amplitude attenuation suggests a likely contribution from a second, well-mixed reservoir, which we model using a bivariate mixing model,

$$\mathbf{X_M} = \mathbf{X_A}(1 - f_B) + \mathbf{X_B} f_B \qquad \text{(Eqn. 1)}$$

where $\mathbf{X_A}$ is the isotopic composition of Reservoir A, $\mathbf{X_B}$ is the isotopic composition of Reservoir B, and f_B is the mixing parameter. Modeled dripwater $\delta^{18}O$ simulated by the autogenic recharge model with an ~10-month residence time represents Reservoir A. In the interest of simplicity, we set the isotopic composition of Reservoir B as amount-weighted Mulu rainfall $\delta^{18}O$ averaged across the study period (-8.6‰). At $f_B = 0.6$, the residuals between the modeled and observed L2 timeseries are minimized. With this

model configuration, the muted variability in L2 is reproduced particularly well during the 2009-2012 ENSO cycle (Figure 3.2), suggesting that two distinct reservoirs likely feed L2 – one with a residence time of ~10 months that is recharged autogenically (Reservoir A) and a second with a significantly longer residence time (Reservoir B). However, prior to 2009, the above parameters over-damp the variability, resulting in a poor fit between the modeled and observed timeseries. Increasing the Reservoir A flux from 40% to 80% (i.e. $f_B = 0.2$) during late 2008/early 2009 greatly improves model-data fit, suggesting an abrupt switch in flow to L2 during this period (Figure 3.2). Indeed, Reservoir A may represent 100% of flow in December 2008. Throughout 2008, modeled dripwater $\delta^{18}O$ is ~0.5‰ more negative than observed L2 values, indicating that either i) the isotopic composition of Reservoir B varies over the study period and/or ii) that our simple two-reservoir model fails to capture the complexity of flow feeding L2. Longer timeseries of rainwater and dripwater $\delta^{18}O$ are required to differentiate between these scenarios.

The isotopic spread of hundreds of stalagmite-forming drips collected during field expeditions falls within the variability of the dripwater $\delta^{18}O$ timeseries (Figure 3.1c), indicating that the three timeseries drips are broadly representative of system-wide shifts in isotopic composition. The relatively small spread in both the 2008 and 2012 expedition datasets (~0.3‰ [1σ]) suggests that residence times for stalagmite-forming drips in Mulu are long enough to homogenize large intraseasonal shifts in rainfall $\delta^{18}O$ of ~10‰ [*Moerman et al.*, 2013], establishing a lower bound for residence times of stalagmite-forming drips of approximately 1-2 months. Likewise, residence times for many stalagmite-forming drips appear to be less than 2yrs, as only 25% of the 2010 expedition

drip distribution overlaps that of the 2008 expedition (Figure 3.1c). This remains true even when a subset of the slowest dripping samples (< 2dpm) is considered.

3.5.3. ENSO-related pseudo-stalagmite $\delta^{18}O$ variability

To explore how ENSO variability may be recorded in high- and low-resolution stalagmite $\delta^{18}O$ reconstructions, we generate pseudo-stalagmites from the dripwater $\delta^{18}O$ timeseries and sample them at a variety of temporal resolutions. First, we transform the NINO3.4 SST index over the last 150 years into pseudo-dripwater $\delta^{18}O$ space using scalings obtained from drip WS or L2 (WF is similar to WS, for these purposes). Specifically, we perform a peak-to-peak linear regression between observed dripwater $\delta^{18}O$ timeseries and the NINO3.4 SST index over the study period [Figure S5; *Kaplan et al.*, 1998]. Next, we sample the pseudo-dripwater $\delta^{18}O$ timeseries at annual to multi-decadal resolutions to reflect typical stalagmite growth rates. As our approach assumes that pseudo-stalagmite $\delta^{18}O$ is a perfect recorder of ENSO dripwater $\delta^{18}O$ variability, this analysis represents an upper bound on possible ENSO-related stalagmite $\delta^{18}O$ variability.

Differences in dripwater residence time lead to large differences between the WS and L2 pseudo-stalagmite $\delta^{18}O$ timeseries (Figure 3.3). When sampled at annual resolution, ENSO variability in pseudo-stalagmite WS is as large as 4‰ versus 1.5‰ for pseudo-stalagmite L2, as positive El Niño-related $\delta^{18}O$ anomalies are damped more effectively in L2 (Figure 3.3b). At decadal sampling resolution, individual ENSO events are largely unresolvable in the pseudo-stalagmites (Figure 3.3c), as expected. However, for decadal sampling, periods of high ENSO variance (e.g. 1970-2000) result in pseudo-stalagmite $\delta^{18}O$ values that are lower than those during ENSO quiescent periods (e.g. 1920 – 1960). The asymmetrical nature of the ENSO phenomenon, whereby El Niño

events produce higher amplitude anomalies than La Niña events [e.g. *McPhaden and Zhang*, 2009], imparts a shift in mean pseudo-stalagmite $\delta^{18}O$ during high- versus low-variance periods.

At all sampling resolutions, the mean $\delta^{18}O$ value for pseudo-stalagmite L2 is ~0.8‰ heavier than pseudo-stalagmite WS, similar to mean $\delta^{18}O$ offsets of up to ~0.7‰ observed between individual Borneo stalagmite records [*Carolin et al.*, 2013; *Partin et al.*, 2007]. To determine the cause of this offset, we generate pseudo-stalagmites from modeled dripwater $\delta^{18}O$ with different parameterization schemes to isolate the effects of 1) dripwater residence time, 2) multiple reservoirs, and 3) precipitation amount-weighting (Figure B.6; see Auxiliary Material for details). We find that dripwater residence time accounts for the majority of the observed offset, whereby drips with longer residence times are biased towards lower, La Niña-like $\delta^{18}O$ values, given the asymmetry of the ENSO phenomenon. Amount-weighting of rainfall $\delta^{18}O$ also contributes to the observed offset by driving pseudo-stalagmite L2 towards even lower $\delta^{18}O$ values (Figure B.6), as La Niña events are associated with higher precipitation amount at the site. As such, we conclude that the observed offset can be attributed to the combination of different dripwater residence times, ENSO asymmetry, and the latter's impact on amount-weighted rainfall $\delta^{18}O$.

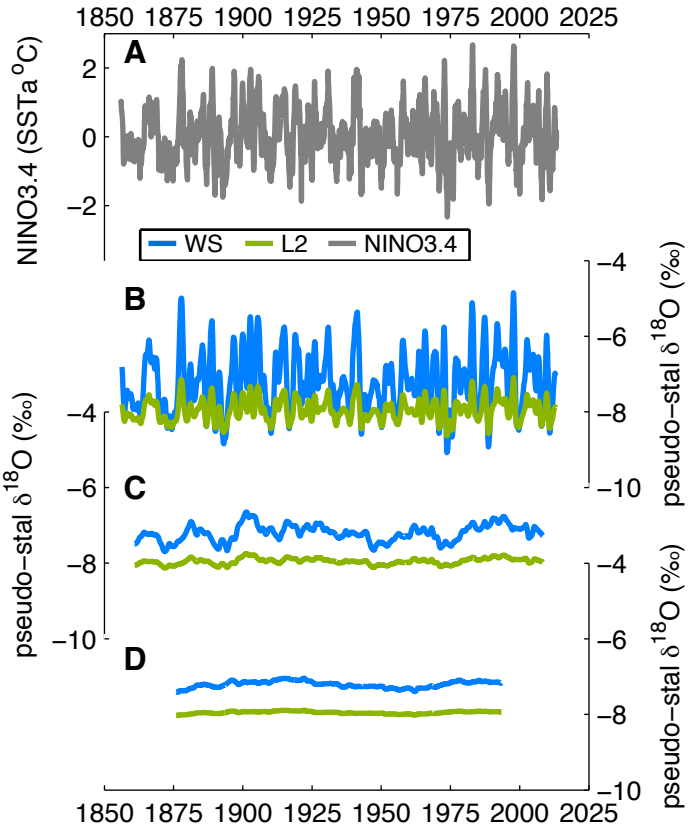

Figure 3.3: Pseudo-stalagmite $\delta^{18}O$ timeseries obtained by converting the NINO3.4 SST index into a timeseries of dripwater $\delta^{18}O$ using the observed relationship between NINO3.4 and dripwater $\delta^{18}O$ timeseries during the study interval. (a) Extended NINO3.4 index retrieved from http://iridl.ldeo.columbia.edu/SOURCES/.Indices/.nino/ [*Reynolds et al.*, 2002] (b) Annually-resolved, (c) 10-year resolution, (d) 40-year resolution pseudo-stalagmite $\delta^{18}O$ modeled from observed WS (blue) and L2 (green) dripwater $\delta^{18}O$.

3.6. Discussion

This study is one of the first to capture individual ENSO events in dripwater $\delta^{18}O$. Previous work by *McDonald* [2004] documented ENSO variability in dripwater trace metal composition, while *Frappier et al.* [2002] found clear evidence of ENSO in a

high-resolution stalagmite $\delta^{13}C$ record. The large range of variability exhibited in Mulu dripwater $\delta^{18}O$ (3-7‰) stems from relatively short residence times (3-10 months) compared to the dominant input frequency (i.e. interannual). While similarly large dripwater $\delta^{18}O$ variations are reported elsewhere [e.g. *Ayalon et al.*, 1998; *Oster et al.*, 2012], these sites typically involve rapid flow through karst conduits and joints, such that dripwater $\delta^{18}O$ timeseries reflect discrete rainfall events. Flow to the temporally monitored drips at Mulu, however, is likely delivered by diffuse seepage flow [*Cobb et al.*, 2007; *Partin et al.*, 2013a]. Given the dominance of seasonal variability at most other cave monitoring sites with diffuse flow, large seasonal variations in rainfall $\delta^{18}O$ (>4‰) are largely smoothed out by residence times greater than a year, generating dripwater $\delta^{18}O$ variability of only ~1‰ [e.g. *Cruz et al.*, 2005c; *Genty et al.*, 2014; *Mickler et al.*, 2004; *Pape et al.*, 2010; *Partin et al.*, 2012; *Treble et al.*, 2013].

Given the preservation of resolvable ENSO-related variations in dripwater $\delta^{18}O$, annual and higher resolution $\delta^{18}O$ records from fast-growing Borneo stalagmites are likely to capture ENSO-related variability. However, our analyses indicate that several factors may influence the variance of interannual stalagmite $\delta^{18}O$ signals. Most significantly, we find that different flow pathways and mixing rates can produce different dripwater $\delta^{18}O$ timeseries, even given the same rainfall $\delta^{18}O$ input, consistent with karst system modeling studies [e.g. *Baker et al.*, 2012; 2013; *Bradley et al.*, 2010] and observations elsewhere [e.g. *Ayalon et al.*, 1998; *Genty et al.*, 2014; *Treble et al.*, 2013]. Specifically, longer transit times attenuate dripwater $\delta^{18}O$ variance more effectively and enhance temporal lags between the original rainfall $\delta^{18}O$ (climate) signal and the dripwater $\delta^{18}O$ (speleothem) signal. Therefore, stalagmites fed by water with a relatively

short residence time will exhibit higher ENSO-related $\delta^{18}O$ variance than those associated with longer transit times, as demonstrated by our pseudo-stalagmite model. As such, stalagmite $\delta^{18}O$ is best suited for inferring relative changes in ENSO variance, assuming that dripwater residence time is relatively stable through time. There is evidence that sustained bursts of strong MJO-related convective activity may produce dripwater $\delta^{18}O$ anomalies on the order of those associated with a strong La Niña event (i.e. -2 to -3‰), but such events are rare in the observed timeseries. The contribution of higher- and lower-frequency climate signals to dripwater $\delta^{18}O$ variability awaits the generation of longer rainfall and dripwater $\delta^{18}O$ timeseries.

Our study provides compelling evidence that some drips are characterized by nonstationary flow regimes, which would complicate the interpretation of climate-related signals in the resulting stalagmite $\delta^{18}O$ records. Potential drivers of non-stationary flow include changes in the nature of rainfall events delivering infiltrating waters, changes in karst water balance, and reservoir volume thresholds that may bias flow along certain pathways [*Baker et al.*, 2013; *Bradley et al.*, 2010]. Indeed, a change in water routing to drip L2 in late 2008 following unusually wet conditions resulted in more negative dripwater $\delta^{18}O$ values than expected under stationary flow conditions. This abrupt change in flow suggests that some drips at Mulu may be sensitive to karst water balance and/or thresholds in reservoir volume. Additionally, the fact that karst hydrology alters the amplitude and timing of water isotopic extrema in a non-uniform, and potentially nonlinear, manner introduces the possibility that relationships between climate-related fields and stalagmite $\delta^{18}O$ may not always be stationary over time. This is an important consideration for high-resolution studies that rely on modern calibrations between

rainfall, dripwater, or stalagmite $\delta^{18}O$ and instrumental climate variables to derive quantitative estimates of past climatic conditions from high-resolution stalagmite $\delta^{18}O$ reconstructions, as emphasized elsewhere [e.g. *Baker et al.*, 2013; *Bradley et al.*, 2010; *Jex et al.*, 2013]. The generation of multiple stalagmite $\delta^{18}O$ records that overlap in time allows for the separation of climatic versus non-climatic influences on stalagmite $\delta^{18}O$, under the assumption that climate-related $\delta^{18}O$ variations are well-replicated across samples [*Dorale and Liu*, 2009].

At multidecadal and longer timescales, Borneo stalagmite $\delta^{18}O$ likely reflects the long-term mean of amount-weighted rainfall $\delta^{18}O$. Our pseudo-stalagmite analysis demonstrates that multidecadal changes in ENSO variance on the order of those observed during the instrumental record [*Kleeman and Power*, 2000] can produce lower-frequency isotopic variability of similar magnitude to the ~0.5‰ centennial-scale variations observed in low-resolution Borneo stalagmite $\delta^{18}O$ records [*Carolin et al.*, 2013; *Partin et al.*, 2007]. However, the rectification of changes in ENSO variance cannot explain the 1-3‰ variations of stalagmite $\delta^{18}O$ documented on millennial to orbital timescales [*Carolin et al.*, 2013; *Meckler et al.*, 2012; *Partin et al.*, 2007]. That said, our study confirms the sensitivity of rainfall and dripwater $\delta^{18}O$ variations in northern Borneo to zonal shifts in the location of deep convection in the western Pacific [*Moerman et al.*, 2013], which may occur on decadal to orbital timescales [*Emile-Geay et al.*, 2013; e.g. *Lea et al.*, 2000; *Mann et al.*, 2009; *Stott et al.*, 2002]. It thus stands to reason that zonal shifts in the mean position of deep convection may drive a significant fraction of observed millennial- to orbital-scale variability in Mulu stalagmite $\delta^{18}O$ records.

3.7. Conclusion

Vadose water mixing is the primary karst process that governs the transformation of rainfall to dripwater $\delta^{18}O$ at Gunung Mulu in northern Borneo. The Mulu karst system acts as a low-pass filter of 3-10+ months, with dripwater $\delta^{18}O$ reflecting a smoothed version of amount-weighted local rainfall $\delta^{18}O$. Relatively rapid water transit times allow for large ENSO-related variations in local rainfall $\delta^{18}O$ of 6-8‰ to be preserved as dripwater $\delta^{18}O$ variations of 2.5-5‰, enabling the reconstruction of past ENSO variability from sufficiently fast-growing Borneo stalagmites. Variations in dripwater residence time, precipitation amount-weighting, and ENSO asymmetry likely contribute to systematic offsets between overlapping stalagmite $\delta^{18}O$ records documented at our site [*Carolin et al.*, 2013; *Partin et al.*, 2007]. Longer dripwater $\delta^{18}O$ timeseries, as well as a larger set of monitored drips, are required to assess the role of potential non-linearities in karst flow patterns through time.

This study demonstrates the power of generating modern rainfall and dripwater isotope timeseries at sites where paleoclimate reconstructions from stalagmites exist. In addition to highlighting the utility of site-specific monitoring of water isotopes for stalagmite $\delta^{18}O$ interpretation, our results demonstrate the importance of replicating stalagmite $\delta^{18}O$ records, especially for quantitative reconstructions of ENSO variance.

3.8. Acknowledgements

The authors wish to thank the Gunung Mulu National Park staff, Eleanor Middlemas, Danja Mewes, Sang Chen, and Niko Sluzki for their assistance during fieldwork and the Mulu Meteorological Station staff for overseeing the collection of the daily rainfall

samples. We also gratefully acknowledge the Mulu Caves Project for providing invaluable information about the Mulu karst system and an anonymous reviewer for comments that greatly improved the manuscript. Permits for this work were granted by the Malaysian Economic Planning Unit, the Sarawak State Planning Unit, and the Sarawak Forestry Department. This work was supported by NSF Grant 0645291 to KMC, and JWM was funded by a NSF Graduate Research Fellowship. Observational datasets of Mulu rainfall and dripwater isotopes used in this study can be found in the Auxiliary Material.

3.9 REFERENCES

Ayalon, A., M. Bar-Matthews, and E. Sass (1998), Rainfall-recharge relationships within a karstic terrain in the eastern Mediterranean semi-arid region, Israel: delta O-18 and delta D characteristics, *J. Hydro.*, *207*(1-2), 18-31.

Ayliffe, L. K., et al. (2013), Rapid interhemispheric climate links via the Australasian monsoon during the last deglaciation, *Nat Commun*, *4*, 2908.

Baker, A., C. Bradley, S. J. Phipps, M. Fischer, I. J. Fairchild, L. Fuller, C. Spötl, and C. Azcurra (2012), Millennial-length forward models and pseudoproxies of stalagmite δ18O an example from NW Scotland, *Clim. Past.*, *8*(4), 1153-1167.

Baker, A., C. Bradley, and S. J. Phipps (2013), Hydrological modeling of stalagmite δ18O response to glacial-interglacial transitions, *Geophys. Res. Lett.*, *40*(12), 3207-3212.

Berkelhammer, M., A. Sinha, M. Mudelsee, H. Cheng, R. L. Edwards, and K. Cannariato (2010), Persistent multidecadal power of the Indian Summer Monsoon, *Earth Planet. Sci. Lett.*, *290*(1-2), 166-172.

Bradley, C., A. Baker, C. N. Jex, and M. J. Leng (2010), Hydrological uncertainties in the modelling of cave drip-water δ18O and the implications for stalagmite palaeoclimate reconstructions, *Quat. Sci. Rev.*, *29*(17-18), 2201-2214.

Carolin, S. A., K. M. Cobb, J. F. Adkins, B. Clark, J. L. Conroy, S. Lejau, J. Malang, and A. A. Tuen (2013), Varied response of western Pacific hydrology to climate forcings over the last glacial period, *Science*, *340*(6140), 1564-1566.

Cheng, H., R. L. Edwards, W. S. Broecker, G. H. Denton, X. Kong, Y. Wang, R. Zhang, and X. Wang (2009), Ice age terminations, *Science*, *326*(5950), 248-252.

Cobb, K. M., J. F. Adkins, J. W. Partin, and B. Clark (2007), Regional-scale climate influences on temporal variations of rainwater and cave dripwater oxygen isotopes in northern Borneo, *Earth Planet. Sci. Lett.*, *263*(3-4), 207-220.

Cruz, F. W., S. J. Burns, I. Karmann, W. D. Sharp, M. Vuille, A. O. Cardoso, J. A. Ferrari, P. L. S. Dias, and O. Viana (2005a), Insolation-driven changes in atmospheric circulation over the past 116,000 years in subtropical Brazil, *Nature*, *434*(7029), 63-66.

Cruz, F. W., I. Karmann, O. Viana, S. J. Burns, J. A. Ferrari, M. Vuille, A. N. Sial, and M. Z. Moreira (2005b), Stable isotope study of cave percolation waters in subtropical Brazil: Implications for paleoclimate inferences from speleothems, *Chem. Geol.*, *220*(3-4), 245-262.

Dansgaard, W. (1964), Stable isotopes in precipitation, *Tellus*, *16*(4), 436-468.

Dorale, J. A., and Z. H. Liu (2009), Limitations of Hendy test criteria in judging the paleoclimatic suitability of speleothems and the need for replication, *J. Cave Karst Stud.*, *71*(1), 73-80.

Emile-Geay, J., K. M. Cobb, M. E. Mann, and A. T. Wittenberg (2013), Estimating Central Equatorial Pacific SST Variability over the Past Millennium. Part I: Methodology and Validation, *J. Clim.*, *26*(7), 2302-2328.

Fleitmann, D., S. J. Burns, U. Neff, M. Mudelsee, A. Mangini, and A. Matter (2004), Palaeoclimatic interpretation of high-resolution oxygen isotope profiles derived from annually laminated speleothems from Southern Oman, *Quat. Sci. Rev.*, *23*(7-8), 935-945.

Frappier, A., D. Sahagian, L. A. Gonzalez, and S. J. Carpenter (2002), El Nino events recorded by stalagmite carbon isotopes, *Science*, *298*(5593), 565-565.

Frappier, A. B., D. Sahagian, S. J. Carpenter, L. A. González, and B. R. Frappier (2007), Stalagmite stable isotope record of recent tropical cyclone events, *Geology*, *35*(2), 111.

Genty, D., et al. (2014), Rainfall and cave water isotopic relationships in two South-France sites, *Geochim. Cosmochim. Acta*, *131*, 323-343.

Griffiths, M. L., et al. (2009), Increasing Australian–Indonesian monsoon rainfall linked to early Holocene sea-level rise, *Nature Geoscience*, *2*(9), 636-639.

Jex, C. N., A. Baker, I. J. Fairchild, W. J. Eastwood, M. J. Leng, H. J. Sloane, L. Thomas, and E. Bekaroğlu (2010), Calibration of speleothem δ18O with instrumental climate records from Turkey, *Global Planet. Change*, *71*(3-4), 207-217.

Jex, C. N., S. J. Phipps, A. Baker, and C. Bradley (2013), Reducing uncertainty in the climatic interpretations of speleothem δ18O, *Geophys. Res. Lett.*, *40*(10), 2259-2264.

Kaplan, A., M. A. Cane, Y. Kushnir, A. C. Clement, M. B. Blumenthal, and B. Rajagopalan (1998), Analyses of global sea surface temperature 1856-1991, *Journal of Geophysical Research-Oceans*, *103*(C9), 18567-18589.

Kleeman, R., and S. B. Power (2000), Modulation of ENSO variability on decadal and longer timescales, in *El Niño and the Southern Oscillation: Multiscale Variability and Global and Regional Impacts*, edited by H. F. Diaz and V. Markgraf, pp. 413–442, Cambridge University Press.

Kurita, N., K. Ichiyanagi, J. Matsumoto, M. D. Yamanaka, and T. Ohata (2009), The relationship between the isotopic content of precipitation and the precipitation amount in tropical regions, *Journal of Geochemical Exploration*, *102*(3), 113-122.

Lachniet, M. S. (2004), A 1500-year El Niño/Southern Oscillation and rainfall history for the Isthmus of Panama from speleothem calcite, *J. Geophys. Res.*, *109*(D20).

Lawrence, J. R., S. D. Gedzelman, D. Dexheimer, H. K. Cho, G. D. Carrie, R. Gasparini, C. R. Anderson, K. P. Bowman, and M. I. Biggerstaff (2004), Stable isotopic composition of water vapor in the tropics, *J. Geophys. Res.-Atmos.*, *109*(D6), 16.

Lea, D. W., D. K. Pak, and H. J. Spero (2000), Climate impact of late quaternary equatorial Pacific sea surface temperature variations, *Science*, *289*(5485), 1719.

LeGrande, A. N., and G. A. Schmidt (2009), Sources of Holocene variability of oxygen isotopes in paleoclimate archives, *Clim. Past.*, *5*(3), 441-455.

Lewis, S. C., A. N. LeGrande, M. Kelley, and G. A. Schmidt (2010), Water vapour source impacts on oxygen isotope variability in tropical precipitation during Heinrich events, *Clim. Past.*, *6*(3), 325-343.

Mann, M. E., Z. Zhang, S. Rutherford, R. S. Bradley, M. K. Hughes, D. Shindell, C. Ammann, G. Faluvegi, and F. Ni (2009), Global signatures and dynamical origins of the Little Ice Age and Medieval Climate Anomaly, *Science*, *326*(5957), 1256.

McDonald, J. (2004), The 2002–2003 El Niño recorded in Australian cave drip waters: Implications for reconstructing rainfall histories using stalagmites, *Geophys. Res. Lett.*, *31*(22).

McPhaden, M. J., and X. B. Zhang (2009), Asymmetry in zonal phase propagation of ENSO sea surface temperature anomalies, *Geophys. Res. Lett.*, *36*, 6.

Meckler, A. N., M. O. Clarkson, K. M. Cobb, H. Sodemann, and J. F. Adkins (2012), Interglacial hydroclimate in the tropical West Pacific through the Late Pleistocene, *Science*, *336*(6086), 1301-1304.

Mickler, P. J., J. L. Banner, L. Stern, Y. Asmerom, R. L. Edwards, and E. Ito (2004), Stable isotope variations in modern tropical speleothems: Evaluating equilibrium vs. kinetic isotope effects, *Geochim. Cosmochim. Acta*, *68*(21), 4381-4393.

Moerman, J. W., K. M. Cobb, J. F. Adkins, H. Sodemann, B. Clark, and A. A. Tuen (2013), Diurnal to interannual rainfall δ18O variations in northern Borneo driven by regional hydrology, *Earth Planet. Sci. Lett.*, *369-370*, 108-119.

Okumura, Y. M., and C. Deser (2010), Asymmetry in the Duration of El Niño and La Niña, *J. Clim.*, *23*(21), 5826-5843.

Oster, J. L., I. P. Montañez, and N. P. Kelley (2012), Response of a modern cave system to large seasonal precipitation variability, *Geochim. Cosmochim. Acta*, *91*, 92.

Pape, J. R., J. L. Banner, L. E. Mack, M. Musgrove, and A. Guilfoyle (2010), Controls on oxygen isotope variability in precipitation and cave drip waters, central Texas, USA, *J. Hydro.*, *385*(1-4), 203-215.

Partin, J. W., K. M. Cobb, J. F. Adkins, B. Clark, and D. P. Fernandez (2007), Millennial-scale trends in west Pacific warm pool hydrology since the Last Glacial Maximum, *Nature*, *449*(7161), 452-455.

Partin, J. W., et al. (2012), Relationship between modern rainfall variability, cave dripwater, and stalagmite geochemistry in Guam, USA, *Geochem. Geophys. Geosys.*, *13*(3), n/a-n/a.

Partin, J. W., K. M. Cobb, J. F. Adkins, A. A. Tuen, and B. Clark (2013a), Trace metal and carbon isotopic variations in cave dripwater and stalagmite geochemistry from northern Borneo, *Geochem. Geophys. Geosys.*, *14*(9), 3567-3585.

Partin, J. W., et al. (2013b), Multidecadal rainfall variability in South Pacific Convergence Zone as revealed by stalagmite geochemistry, *Geology*, *41*(11), 1143-1146.

Reynolds, R. W., N. A. Rayner, T. M. Smith, D. C. Stokes, and W. Q. Wang (2002), An improved in situ and satellite SST analysis for climate, *J. Clim.*, *15*(13), 1609.

Rozanski, K. A.-A., L.; Gonfiantini, R. (1993), Isotopic patterns in modern global precipitation, *Geophys. Monogr. Ser.* , *78*, 1-36.

Schmidt, G. A., A. N. LeGrande, and G. Hoffmann (2007), Water isotope expressions of intrinsic and forced variability in a coupled ocean-atmosphere model, *J. Geophys. Res.*, *112*(D10).

Sinha, A., K. G. Cannariato, L. D. Stott, H. Cheng, R. L. Edwards, M. G. Yadava, R. Ramesh, and I. B. Singh (2007), A 900-year (600 to 1500 A.D.) record of the Indian summer monsoon precipitation from the core monsoon zone of India, *Geophys. Res. Lett.*, *34*(16).

Stott, L., C. Poulsen, S. Lund, and R. Thunell (2002), Super ENSO and global climate oscillations at millennial time scales, *Science*, *297*(5579), 222-226.

Treble, P. C., C. Bradley, A. Wood, A. Baker, C. N. Jex, I. J. Fairchild, M. K. Gagan, J. Cowley, and C. Azcurra (2013), An isotopic and modelling study of flow paths and storage in Quaternary calcarenite, SW Australia: implications for speleothem paleoclimate records, *Quat. Sci. Rev.*, *64*, 90-103.

Vimeux, F., G. Tremoy, C. Risi, and R. Gallaire (2011), A strong control of the South American SeeSaw on the intra-seasonal variability of the isotopic composition of precipitation in the Bolivian Andes, *Earth Planet. Sci. Lett.*, *307*(1-2), 47-58.

Waltham, A. C., and D. B. Brook (1980), Symposium on the geomorphology of the Mulu Hills.8. Cave development in the Melinau limestone of the Gunung-Mulu National-Park, *Geogr. J.*, *146*, 258–266.

Wang, X., A. S. Auler, R. L. Edwards, H. Cheng, E. Ito, and M. Solheid (2006), Interhemispheric anti-phasing of rainfall during the last glacial period, *Quat. Sci. Rev.*, *25*(23-24), 3391-3403.

Wang, Y. J., H. Cheng, R. L. Edwards, Z. S. An, J. Y. Wu, C. C. Shen, and J. A. Dorale (2001), A high-resolution absolute-dated Late Pleistocene monsoon record from Hulu Cave, China, *Science*, *294*(5550), 2345-2348.

Wannier, M. (2009), Carbonate platforms in wedge-top basins: An example from the Gunung Mulu National Park, Northern Sarawak (Malaysia), *Mar. Petrol. Geol.*, *26*(2), 177-207.

Wilford, G. E. (1961), The geology and mineral resources of Brunei and adjacent parts of Sarawak, with description of the Seria and Miri oilfields., *British Borneo Geological Survey Memoirs*, *10*.

Zhang, P., et al. (2008), A test of climate, sun, and culture relationships from an 1810-year Chinese cave record, *Science*, *322*(5903), 940-942.

APPENDIX A

SUPPLEMENTARY MATERIAL FOR "DIURNAL TO INTERANNUAL RAINFALL $\delta^{18}O$ VARIATIONS IN NORTHERN BORNEO DRIVEN BY REGIONAL HYDROLOGY"

1. Precipitation anomalies associated with the El Niño Southern Oscillation (ENSO) during study period (July 2006 – May 2011)

ENSO activity during the 5-year study period is characterized by the weak 2006/2007 El Niño, moderate 2009/2010 El Niño, and strong 2010/2011 La Niña. The spatial pattern of the regressions of TRMM and OLR onto the NINO3.4 index in Fig. A1 below indicates regional drying in the west Pacific and regionally wet conditions in the central Pacific during El Niño events and the opposite effect during La Niña events. The strong resemblance of the spatial patterns in Fig. A1 to the first EOF of global precipitation (Fig. 1 of Furtado *et al*., 2009) further indicates that precipitation anomalies experienced between July 2006 – May 2011 do indeed reflect ENSO variability in general rather than a specific set of SST conditions experienced in the Pacific during our study period.

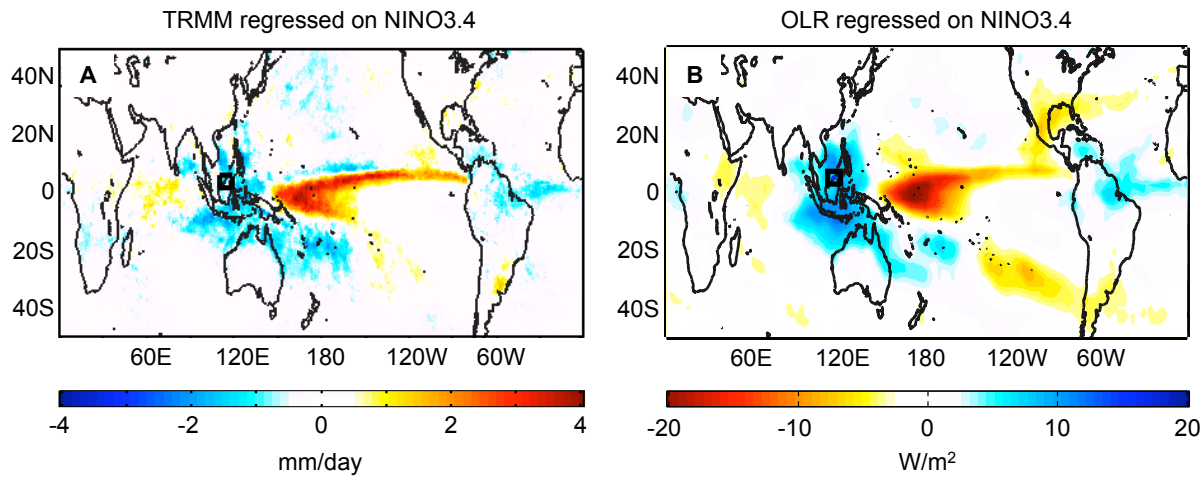

Fig. A.1. **Maps of monthly satellite-derived precipitation-related indices regressed onto the NIÑO3.4 index (http://www.cpc.ncep.noaa.gov/data/indices/) for the period July 2006-May 2011 using ordinary least squares regression**. (a) Regression of TRMM 3B43 V6 monthly precipitation (0.25° x 0.25°; Huffman *et al.*, 2007) on NIÑO 3.4. (b) Regression of monthly NOAA interpolated OLR (2.5° x 2.5°; Liebmann & Smith, 1996) on NIÑO 3.4. Note inverted color scale in (b). The black box in both (a) and (b) marks the location of the study site at Gunung Mulu National Park (4°N, 115°E).

2. Quality control assessment of daily rainfall $\delta^{18}O$ dataset

2.1 Description of quality control tests

During the 2010 field expedition to Gunung Mulu, daily rainfall samples (n = 7) were collected in several 250 mL HDPE separatory funnels deployed in open fields throughout the park. Approximately 20 mL of corn oil was added to each funnel to prevent evaporation prior to sampling. Samples were collected daily between 6 and 8 AM and stored in 3 mL glass serum vials sealed with rubber stoppers and crimped aluminum closures. Precipitation amounts during the 3-week sampling period ranged from 0.3 – 17.8 mm/day, as recorded at Mulu Meteorological Station. To identify the occurrence of evaporative enrichment in samples collected within the open-air rain gauge at Mulu Meteorological Station, the $\delta^{18}O$ of samples collected in the oil-capped separatory funnels were compared to that of contemporaneous samples collected in the rain gauges.

With the exception of two, all samples exposed to the air were more enriched than those capped with oil (Fig. A2a). As shown in Fig. A2a, the isotopic difference between the samples collected in the open-air rain gauge and the oil-type vessel increases exponentially as precipitation amount decreases.

To further constrain the relationship between $\delta^{18}O$ enrichment and sample water volume, additional quality control experiments were conducted at the Georgia Institute of Technology. Aliquots of tap water with volumes ranging from 500 mL to 10 mL were placed in a Casella splayed bottom rain gauge (Casella model M114003; 254 mm diameter; ~1m above ground level) and exposed to the atmosphere for 24 hours on the roof of a campus building in September and October 2010. The resulting values were compared to corresponding unexposed tap water $\delta^{18}O$ values in order to quantify any evaporative enrichment. Samples were stored in 3.5 mL glass vials sealed with rubber stoppers and crimped aluminum closures and refrigerated until analysis. All samples exhibited $\delta^{18}O$ enrichment following the 24-hour exposure period (Fig. A.2b). The magnitude of enrichment increased exponentially as water volume decreased, illustrating that the trend observed in the quality control test conducted at the field site is robust. To determine the effect of temperature and humidity on evaporative enrichment, several aliquots of 50mL each were monitored over 22 consecutive days (volume = 50 mL). The relatively poor relationships between evaporative $\delta^{18}O$ enrichment and temperature and humidity (Fig. A.2c,d) indicate that precipitation amount is a far more dominant control on the magnitude of evaporative enrichment than daily temperature and humidity conditions.

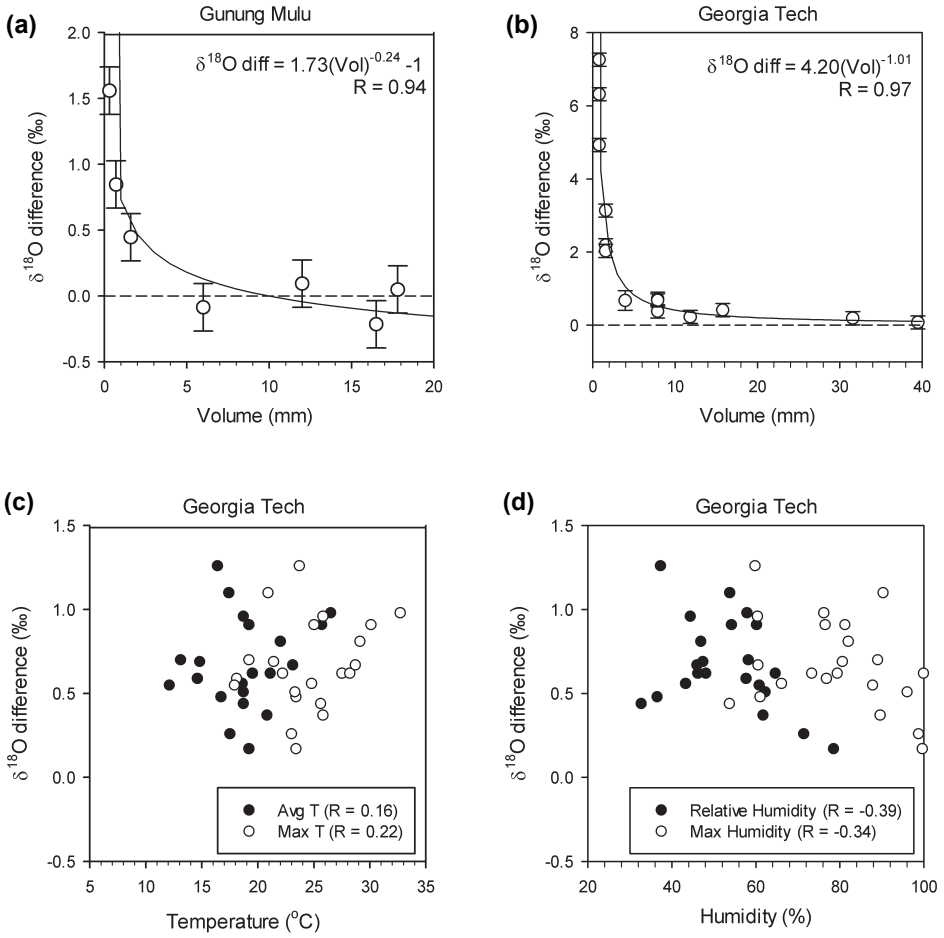

Fig. A.2: Quality control tests. (a) Results quality control test conducted at Gunung Mulu National Park, Sarawak, Malaysia in March 2010. The difference between $\delta^{18}O$ of rainfall samples collected in an open-air rain gauge and an oil-type vessel on the same day is plotted against daily precipitation amount measured at the Mulu Meteorological Station. Positive (negative) $\delta^{18}O$ values indicate that the rainfall sample collected in the open-air rain gauge is more enriched (depleted) than the sample collected in the oil-type vessel. (b) Results of quality control test conducted at Georgia Institute of Technology, GA, USA in September – October 2010. The difference between $\delta^{18}O$ of tap water sampled before and after 24 hours of atmospheric exposure in an open-air rain gauge is plotted against the amount of tap water added to the rain gauge prior to exposure. Positive $\delta^{18}O$ values indicate the exposed sample is more enriched than the unexposed sample. (c) Same as (b) but with $\delta^{18}O$ difference plotted against temperature. (d) Same as (b) but with $\delta^{18}O$ difference plotted against relative humidity. Error bars in panels (a) and (b) represent ± 0.2‰ (1σ).

2.2 Application of quality control results

Based on the findings of these quality control tests, rainfall $\delta^{18}O$ samples associated with precipitation amounts less than 1.6 mm and/or stored in vials that were less than 4/5 full were excluded from the final dataset, resulting in the removal of 176 samples from the unfiltered dataset (n = 1203). Twenty-three samples collected in December 2006 were also excluded due to improper sampling. Monthly averaged and two-month running mean rainfall $\delta^{18}O$ reported for December 2006 are thus derived from linear interpolations of November 2006 and January 2007 for the respective timeseries. With the exception of December 2006, the number of samples excluded from the dataset (n = 199) is fairly evenly distributed throughout the study period as shown in Fig. A.3 below.

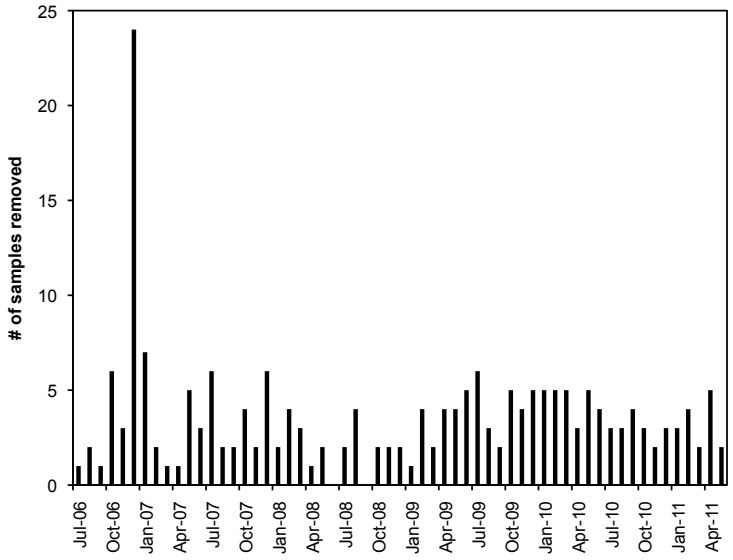

Fig. A.3: Number of daily rainfall samples excluded from each month of the five-year daily rainfall $\delta^{18}O$ timeseries

A comparison of the local meteoric water lines (LMWL) of the filtered and unfiltered datasets (Fig. A.4) illustrates that this filtering scheme effectively removes rainfall samples likely artificially enriched, as evidenced by the disappearance of the 'evaporation line' present in the unfiltered dataset. The exclusion of these samples results in a slight bias towards more depleted $\delta^{18}O$ relative to the unfiltered dataset (i.e. the difference in mean $\delta^{18}O$ for the filtered and unfiltered datasets is -0.4‰) but the fundamental variability of the timeseries remains unchanged (Fig. A.5). Fig. A.5 also illustrates that the underlying temporal variability of the $\delta^{18}O$ timeseries is also retained when $\delta^{18}O$ averages are weighted by precipitation amount.

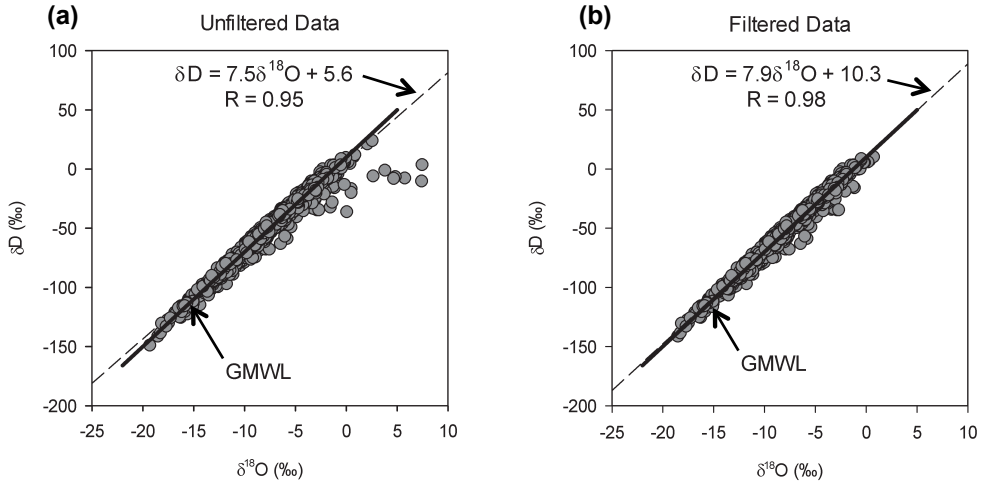

Fig. A.4: Local meteoric water line (LMWL) of filtered and unfiltered data. (a) LMWL of unfiltered rainfall $\delta^{18}O$ dataset (n = 1203). (b) LMWL of the filtered dataset (n = 1004). Dashed lines represent the LMWL determined by least squares regression. Solid line represents the global meteoric water line ($\delta D = 8\delta^{18}O + 10$; Craig, 1961).

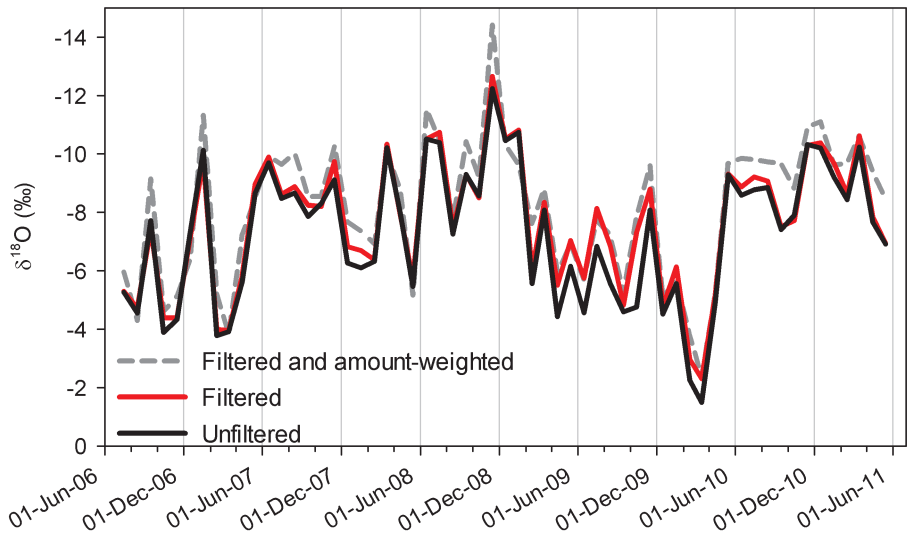

Fig. A.5: Monthly mean rainfall $\delta^{18}O$ for the unfiltered dataset (solid black line), filtered dataset (solid red line), and filtered and amount-weighted dataset (dashed gray line).

3. Identification of intraseasonal rainfall $\delta^{18}O$ depletion events in the 5-year daily timeseries

To objectively identify intraseasonal rainfall $\delta^{18}O$ depletion events in the 5-year rainfall $\delta^{18}O$ timeseries, the following statistical filter (Eqn. S1) was applied to the daily rainfall $\delta^{18}O$ dataset to screen for magnitude and abruptness of $\delta^{18}O$ variability:

$$\Delta(‰) = \text{max depletion} - \text{average}(\text{limb}_{pre}, \text{limb}_{post}) \qquad \text{Eqn. (S1)}$$

where 'max depletion' is the average $\delta^{18}O$ for Day 0 and Day +1, 'limb_{pre}' is the average $\delta^{18}O$ for Day -4 to Day -8, and 'limb_{post}' is the average $\delta^{18}O$ for Day +5 to Day +9. The schematic in Fig. A.6 illustrates the daily $\delta^{18}O$ values comprising the terms in Eqn. S1. Days with 'Δ' greater than or equal to -7.0‰ were designated as rainfall $\delta^{18}O$ 'depletion events.' Eighteen distinct intraseasonal rainfall $\delta^{18}O$ 'depletion events' were identified via this statistical filter and are listed in Table S1. In the instance that multiple consecutive days satisfied this criterion, the lowest daily $\delta^{18}O$ value was designated as 'Day 0.' The majority of the intraseasonal rainfall $\delta^{18}O$ depletion events (i.e. 60%), as

well as several large, less abrupt negative $\delta^{18}O$ excursions that did not qualify as 'depletion events,' occur during wet, active MJO phases. Table S2 lists the occurrence of MJO activity at Gunung Mulu over the 5-year study period, during which 18 active (i.e. wet) phases and 16 suppressed (i.e. dry) phases occurred, as identified following Wheeler and Weickmann (2001). Probability distributions of daily rainfall $\delta^{18}O$ during active and suppressed MJO phases shown in Fig. A.7 illustrate that rainfall $\delta^{18}O$ is generally more depleted than the long-term average during active MJO phases and more enriched during suppressed MJO phases.

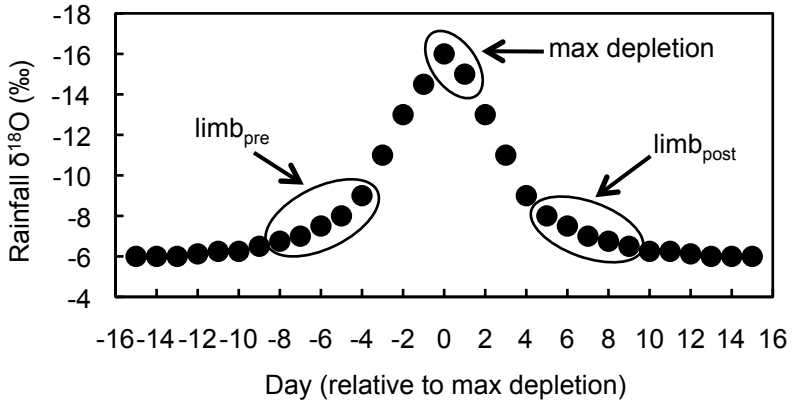

Fig. A.6: **Schematic of intraseasonal rainfall $\delta^{18}O$ depletion event.** Daily $\delta^{18}O$ values comprising terms in Eqn. S1 are denoted.

Table A.1: Date of maximum rainfall $\delta^{18}O$ depletion (Day 0) denoting intraseasonal rainfall $\delta^{18}O$ depletion events and whether they occur during active (i.e. wet) MJO phases, as determined following Wheeler and Weickmann (2001).

Depletion event	Day 0	Coincident with MJO?
1	09/17/06	Yes
2	01/04/07	Yes
3	03/23/07	Yes
4	07/27/07	Yes
5	08/26/07	No
6	01/23/08	No
7	02/20/08	Yes
8	09/07/08	Yes
9	10/25/08	Yes
10	12/10/08	No
11	01/10/09	No
12	03/15/09	No
13	05/18/09	No
14	10/31/09	No
15	01/18/10	Yes
16	11/10/10	No
17	12/07/10	Yes
18	01/14/11	Yes

Table A.2: Occurrence of MJO activity over 114°E (the longitude for Gunung Mulu National Park) during the 5-year study period.

MJO phase	Start date	End date	# of days
Active	09/10/06	09/29/06	20
Suppressed	10/05/06	10/31/06	27
Active	12/20/06	01/05/07	17
Active	06/10/07	06/25/07	16
Suppressed	07/01/07	07/15/07	15
Active	07/20/07	07/29/07	10
Suppressed	08/08/07	08/13/07	6
Suppressed	11/20/07	12/10/07	21
Active	12/15/07	01/06/08	23
Suppressed	01/08/08	01/29/08	22
Active	02/10/08	02/17/08	8
Active	03/18/08	03/25/08	7
Suppressed	04/02/08	04/16/08	15
Active	04/22/08	05/05/08	14
Suppressed	05/15/08	05/25/08	11
Active	09/01/08	09/15/08	15
Suppressed	09/23/08	10/08/08	16
Active	10/18/08	10/26/08	9
Suppressed	01/10/09	01/23/09	14
Active	01/31/09	02/12/09	14
Active	03/05/09	03/15/09	11
Suppressed	03/18/09	04/01/09	15
Active	04/05/09	04/20/09	16
Suppressed	04/25/09	05/05/09	11
Suppressed	10/18/09	11/03/09	17
Active	11/08/09	11/25/09	18
Suppressed	12/01/09	12/18/09	18
Active	12/25/09	01/18/10	25
Suppressed	01/23/10	02/10/10	19
Active	10/02/10	10/05/10	4
Active	12/02/10	12/10/10	9
Suppressed	01/10/11	01/13/11	4
Active	03/19/11	04/01/11	14
Suppressed	04/10/11	04/23/11	14

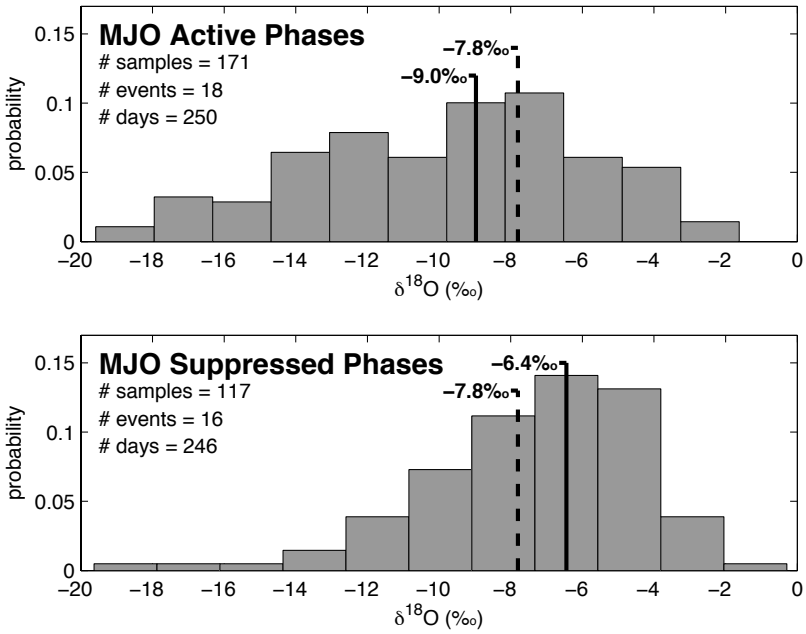

Fig. A.7: PDFs of $\delta^{18}O$ during (top) active and (bottom) suppressed MJO phases. Solid line marks the mean $\delta^{18}O$ value for the respective phase subset. Dashed line marks the long-term daily mean $\delta^{18}O$ value for the total 5-year timeseries.

4. Relationship between Mulu rainfall $\delta^{18}O$ and ENSO indices

The relationship between indices of ENSO and two-month running means of both Mulu rainfall $\delta^{18}O$ and Mulu local precipitation amount are examined in Table S3. For all indices, correlations with Mulu rainfall $\delta^{18}O$ are higher than those with local Mulu precipitation amount. The correlation between Mulu rainfall $\delta^{18}O$ and SST-based NINO indices increases the further west the index region lies. Mulu rainfall $\delta^{18}O$ is also well correlated with the SLP-based SOI index.

Table A.3: Correlations (R) between two-month running means of both Mulu rainfall $\delta^{18}O$ and local precipitation amount and ENSO indices.

Variable	NINO 4	NINO3.4	NINO3	NINO1+2	SOI
Rainfall $\delta^{18}O$	0.64	0.59	0.51	0.31	-0.59
Precipitation amount	-0.50	-0.48	-0.47	-0.36	0.52

REFERENCES

Craig, H., 1961. Isotopic variations in meteoric waters. Science 133, 1702-1703.

Furtado, J.C., Di Lorenzo, E., Cobb, K.M., Bracco, A., 2009. Paleoclimate Reconstructions of Tropical Sea Surface Temperatures from Precipitation Proxies: Methods, Uncertainties, and Nonstationarity. J. Clim. 22, 1104-1123.

Huffman, G., Adler, R., Bolvin, D., Gu, G., Nelkin, E., Bowman, K., Hong, Y., Stocker, E., Wolff, D., 2007. The TRMM multisatellite precipitation analysis (TMPA): Quasi-global, multiyear, combined-sensor precipitation estimates at fine scales. J. Hydrometeorol. 8, 38-55.

Liebmann B, Smith, C., 1996. Description of a complete (interpolated) outgoing longwave radiation dataset. Bull. Am. Meteorol. Soc. 77, 1275-1277.

Wheeler, M., Weickmann, K., 2001. Monitoring and prediction of modes of coherent synoptic to intraseasonal tropical variability. Monthly Weather Rev. 129, 2677-2694.

APPENDIX B

SUPPLEMENTARY MATERIAL FOR "TRANSFORMATION OF ENSO-RELATED RAINWATER TO DRIPWATER $\delta^{18}O$ VARIABILITY BY VADOSE WATER MIXING"

Meteoric water lines

The Mulu local meteoric water line (LMWL; $\delta D = 7.9*\delta^{18}O + 10.3$), calculated from all daily rainfall isotopic samples presented in this study, is nearly identical to the global meteoric water line (GMWL; $\delta D = 8*\delta^{18}O + 10$ from *Craig* [1961]), suggesting that sub-cloud evaporation of rainfall is limited (Figure B.2). Dripwater $\delta^{18}O$ vs. δD from all three drip sites plots slightly to the left of the Mulu LMWL, suggesting the possible contribution of recycled soil moisture [*Gat et al.*, 1994] or cave-surface condensates [*Genty et al.*, 2014] to seepage waters feeding WF, WS, and L2.

Stalagmite forward model development

To investigate how ENSO variability may be recorded in Borneo speleothem $\delta^{18}O$, we generate pseudo-stalagmites of varying growth rates that reflect ENSO-related dripwater $\delta^{18}O$ variability in drips WS and L2. We perform a peak-to-peak linear regression of Mulu dripwater $\delta^{18}O$ onto sea surface temperature (SST) anomalies in the NINO3.4 index by relating the maximum (minimum) dripwater $\delta^{18}O$ value between October – May during the 2006/2007 and 2009/2010 El Niño events (2007/2008 and 2010/2011 La Niña events) to maximum NINO3.4 SST anomalies for each event (Figure B.5a). We do not include the weak 2008/2009 La Niña in this calibration due to the influence of persistent enhanced intraseasonal variability. Inclusion of this data point

considerably reduces the correlation between NINO3.4 and dripwater $\delta^{18}O$ (Figure B.5b). We apply this calibration to the NINO3.4 extended index [*Kaplan et al.*, 1998] to obtain pseudo-dripwater $\delta^{18}O$ timeseries spanning 1856-2013. To generate speleothem $\delta^{18}O$, we smooth the pseudo-dripwater $\delta^{18}O$ timeseries with 1-yr, 10-yr, and 40-yr running means, representing different growth rates. As we are only interested in comparing relative $\delta^{18}O$ differences, we do not incorporate temperature-dependent water-to-calcite fractionation into this simple model. We also assume constant cave temperature.

Attribution analysis for mean $\delta^{18}O$ offsets between pseudo-stalagmites

To constrain the sources likely responsible for creating the ~0.8‰ offset in mean $\delta^{18}O$ between the WS and L2 pseudo-stalagmites, we utilize our dripwater forward model to generate pseudo-stalagmites from different versions of modeled dripwater $\delta^{18}O$ (Figure B.5c) and thus isolate potential influences – namely different residence times, contributions from well-mixed reservoirs, and precipitation amount-weighting. The variability in the observed L2 dripwater $\delta^{18}O$ timeseries, and thus the pseudo-stalagmite generated from it, is the product of two vadose zone reservoirs: (1) Reservoir A, which has with a residence time of ~10 months that is recharged autogenically, and (2) Reservoir B, which has a significantly longer residence time. Therefore, to differentiate the impact of these two influences on the mean $\delta^{18}O$ of pseudo-stalagmite L2, we isolate the contribution of Reservoir A by generating a pseudo-stalagmite reflecting modeled L2 dripwater d18O variability only with a 10-month residence time simulated using the autogenic recharge model, which we refer to as $L2_{res\text{-}A}$. The mean $\delta^{18}O$ value of pseudo-stalagmite $L2_{res\text{-}A}$ differs from that of pseudo-stalagmite L2 by only ~ 0.1‰, suggesting

that the impact of Reservoir B on pseudo-stalagmite L2 mean $\delta^{18}O$, and thus the offset with pseudo-stalagmite WS, is limited and that difference in residence time is likely a major influence.

Next, we investigate the role of precipitation amount-weighting by creating WS and L2 pseudo-stalagmites from non-amount-weighted modeled dripwater $\delta^{18}O$ timeseries with 4-month and 10-month residence times, respectively, referred to as $WS_{non\text{-}aw}$ and $L2_{non\text{-}aw}$. Whereas mean $\delta^{18}O$ for pseudo-stalagmite L2 is 0.75‰ heavier than $L2_{non\text{-}aw}$, mean $\delta^{18}O$ for pseudo-stalagmite WS is only 0.45‰ heavier than $WS_{non\text{-}aw}$ (Figure B.6). The unequal influence of amount-weighting on the isotopic composition of WS versus L2 thus contributes ~ 0.3‰ to the mean offset between pseudo-stalagmite WS and L2. The variable effect of amount-weighting on WS versus L2 dripwater $\delta^{18}O$ is illustrated in Figure B.7. While WS dripwater $\delta^{18}O$ modeled with amount-weighting is more depleted during La Niña events than when modeled without amount-weighting, as expected, amount-weighted L2 dripwater $\delta^{18}O$ is more depleted across the entire timeseries likely due to enhanced mixing given its longer residence time. As a result, the overall mean of amount-weighted L2 dripwater $\delta^{18}O$ is more negative than that for amount-weighted WS.

Based on this attribution analysis, we conclude that the majority of the ~0.8‰ offset in mean $\delta^{18}O$ between pseudo-stalagmites WS and L2 can be attributed to the interaction of asymmetry in ENSO extremes, variable residence times, and precipitation amount-weighting. It is important to note this offset in the pseudo-stalagmites is similar to actual mean $\delta^{18}O$ offsets of up to ~0.7‰ observed between Borneo stalagmite records [*Carolin et al.*, 2013; *Partin et al.*, 2007].

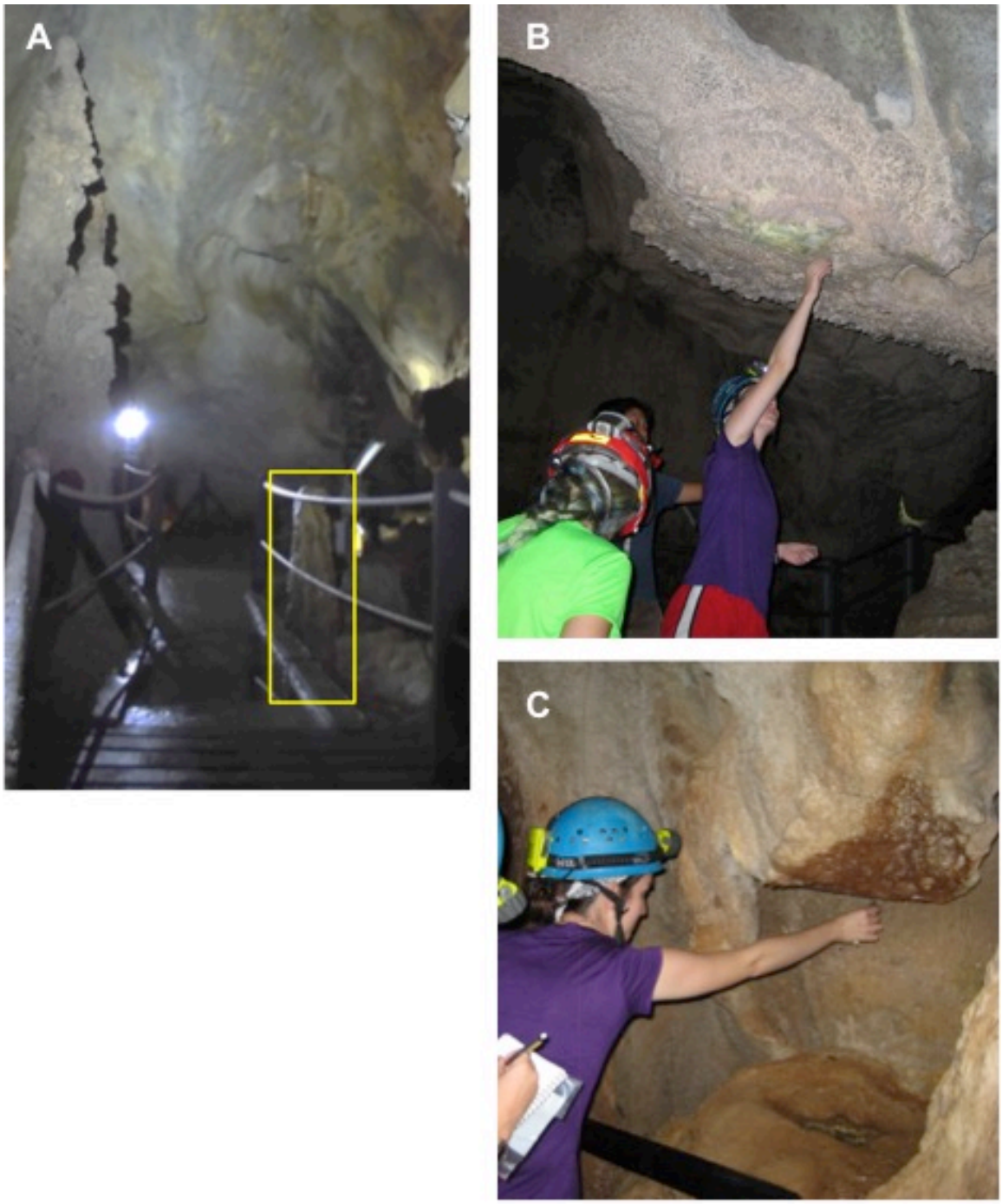

Figure B.1: Photos of timeseries drip sites (a) L2, (b) WS, and (c) WF. Note that WS drips onto detrital bedrock.

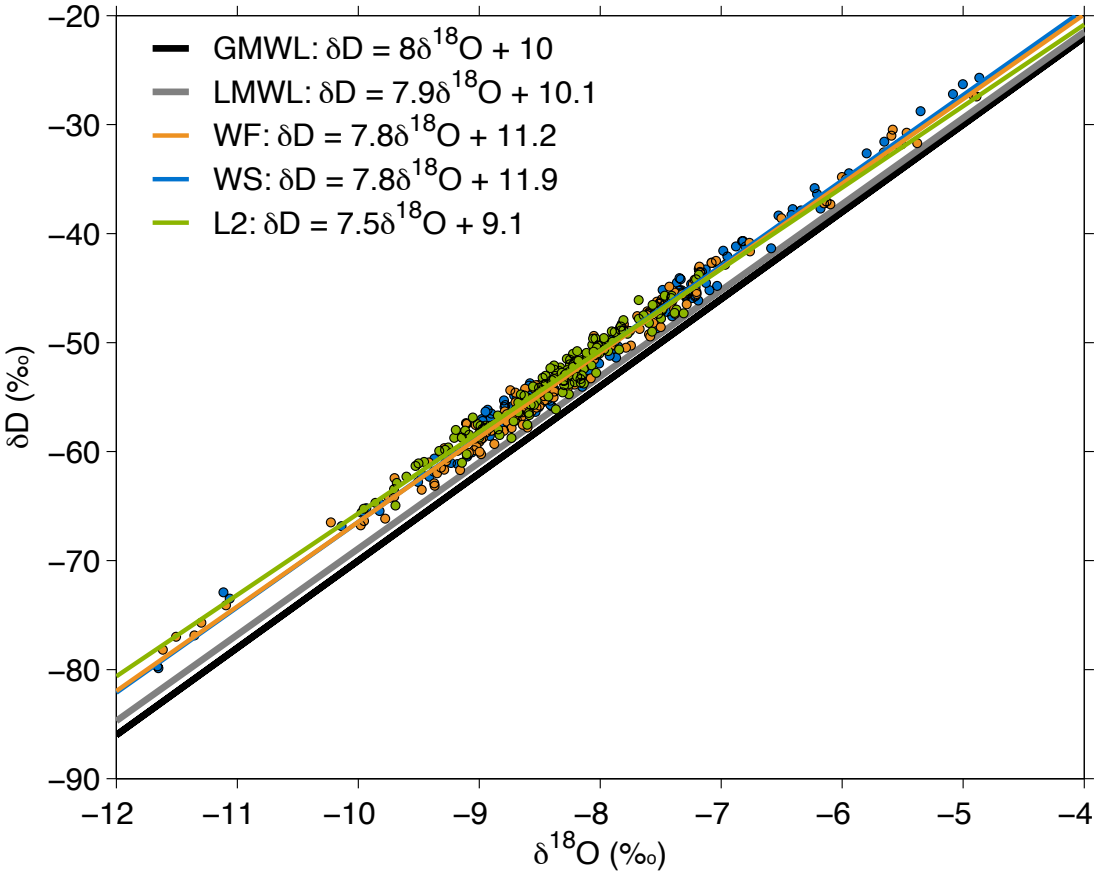

Figure B.2: Comparison of timeseries drip $\delta^{18}O$/ δD plots with Mulu LMWL (gray line; this study) and GMWL [black line; *Craig*, 1961]. Individual dripwater $\delta^{18}O$ versus δD values are plotted as orange circles for WF, blue circles for WS, and green circles for L2. Water lines for drips WF, WS, and L2 are shown as orange, blue, and green lines respectively.

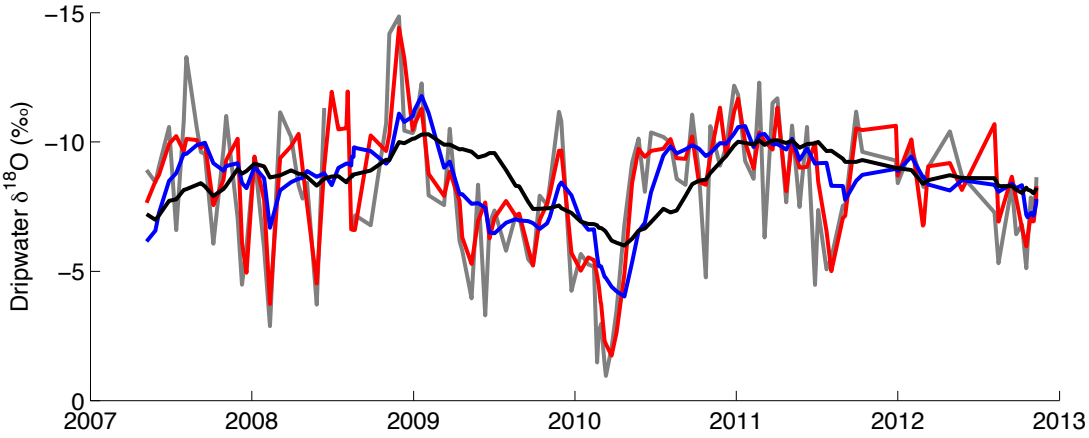

Figure B.3: **Selected modeled dripwater $\delta^{18}O$ timeseries.** Generated by inputting daily amount-weighted Mulu rainfall $\delta^{18}O$ into the autogenic recharge model and applying an averaging interval of two weeks (gray), one month (red), three months (blue), and nine months (black).

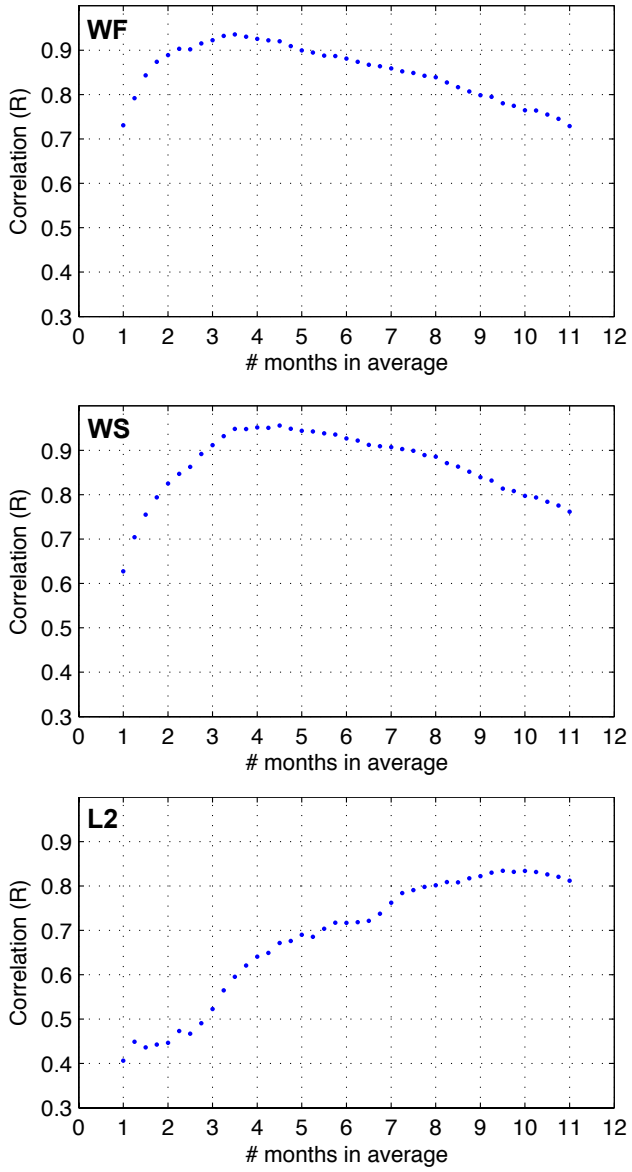

Figure B.4: Correlation between observed and modeled Mulu dripwater $\delta^{18}O$ plotted against corresponding averaging interval used in the autogenic recharge model to generate modeled dripwater $\delta^{18}O$ with different residence times.

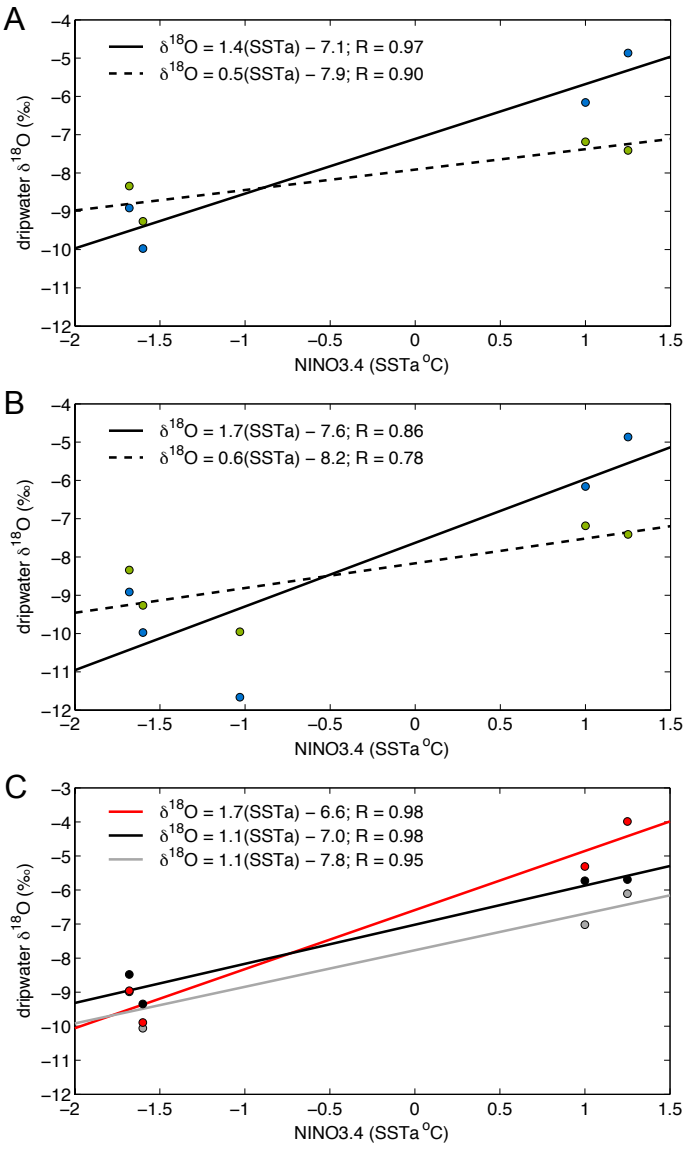

Figure B.5: Maximum dripwater $\delta^{18}O$ anomalies between October-May during ENSO events regressed onto maximum sea surface temperature anomalies (SSTa) in the NINO3.4 region across specified time periods. (a) Observed WS (blue circles) and L2 (green circles) dripwater $\delta^{18}O$ maximum anomalies for 2006/2007 and 2009/2010 El Niño and 2007/2008 and 2010/2011 La Niña events. Lines represent regression equations for WS (solid) and L2 (dashed). (b) same as (a) but includes 2007/2008 weak La Niña event. (c) same as (a) but for modeled dripwater $\delta^{18}O$ maximum anomalies (circles) and regression equations (lines) for amount-weighted modeled L2 dripwater $\delta^{18}O$ with a 10-month residence time (gray), non-amount-weighted modeled L2 dripwater $\delta^{18}O$ with a 10-month residence time (black), and non-amount-weighted modeled WS dripwater $\delta^{18}O$ with a 4-month residence time (red).

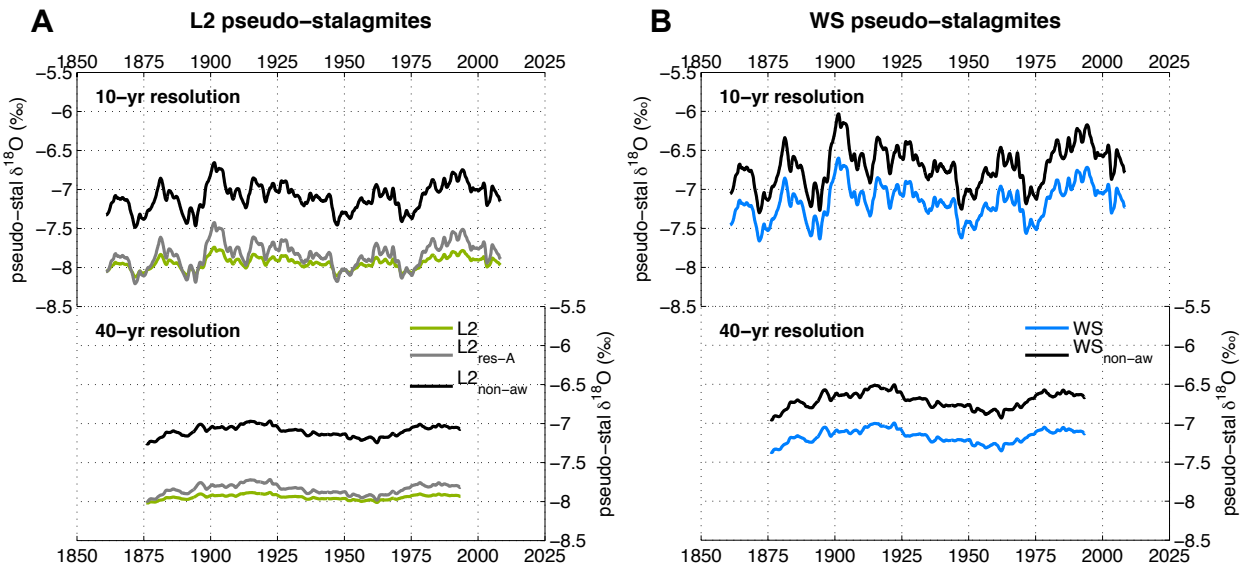

Figure B.6: Pseudo-stalagmite $\delta^{18}O$ timeseries generated from the peak-to-peak relationship between the NINO3.4 index and observed and modeled dripwater $\delta^{18}O$ timeseries. (a) L2 pseudo-stalagmite timeseries with a 10-year (top panel) and 40-year (bottom panel) sampling resolution generated from observed L2 dripwater $\delta^{18}O$ (green), amount-weighted L2 dripwater $\delta^{18}O$ modeled with an ~10-month residence time (gray), and non-amount-weighted L2 dripwater $\delta^{18}O$ modeled with an ~10-month residence time (black). (b) same as (a) but for WS pseudo-stalagmite timeseries generated from observed WS dripwater $\delta^{18}O$ (blue) and non-amount-weighted WS dripwater $\delta^{18}O$ modeled with an ~4-month residence time (black). All modeled dripwater $\delta^{18}O$ timeseries used to generate pseudo-stalagmites are simulated using the autogenic recharge model fed by a single reservoir with the specified residence time.

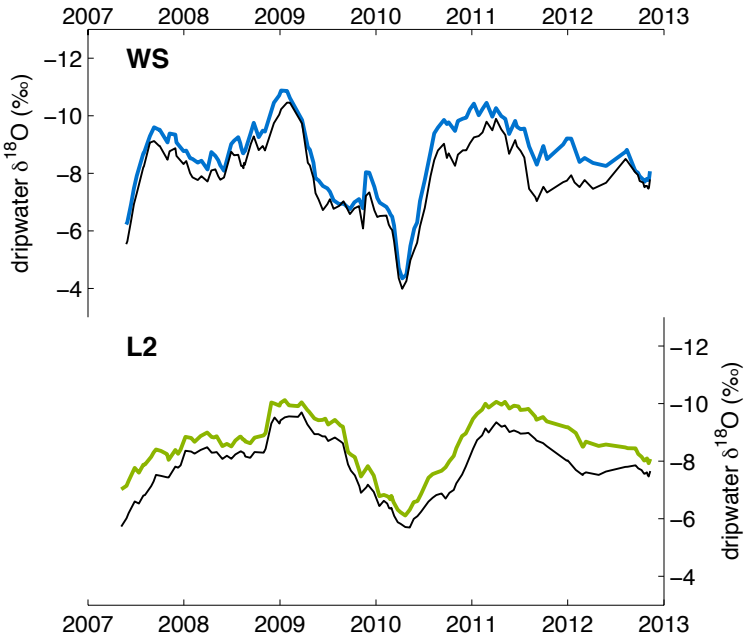

Figure B.7: Amount-weighted versus non-amount-weighted dripwater $\delta^{18}O$ timeseries modeled using the autogenic recharge model. (top) WS dripwater $\delta^{18}O$ timeseries modeled with a 4-month residence time with amount-weighting (blue) and without amount-weighting (black). (bottom) same as (top) but for L2 dripwater $\delta^{18}O$ timeseries modeled with a 10-month residence time and amount-weighting plotted in green.

REFERENCES

Carolin, S. A., K. M. Cobb, J. F. Adkins, B. Clark, J. L. Conroy, S. Lejau, J. Malang, and A. A. Tuen (2013), Varied response of western Pacific hydrology to climate forcings over the last glacial period, *Science*, *340*(6140), 1564-1566.

Craig, H. (1961), Isotopic variations in meteoric waters, *Science*, *133*(346), 1702-&.

Gat, J. R., C. J. Bowser, and C. Kendall (1994), The contribution of evaporation from the great-lakes to the continental atmosphere - estimate based on stable-isotope data, *Geophys. Res. Lett.*, *21*(7), 557-560.

Genty, D., et al. (2014), Rainfall and cave water isotopic relationships in two South-France sites, *Geochim. Cosmochim. Acta*, *131*, 323-343.

Kaplan, A., M. A. Cane, Y. Kushnir, A. C. Clement, M. B. Blumenthal, and B. Rajagopalan (1998), Analyses of global sea surface temperature 1856-1991, *Journal of Geophysical Research-Oceans*, *103*(C9), 18567-18589.

Partin, J. W., K. M. Cobb, J. F. Adkins, B. Clark, and D. P. Fernandez (2007), Millennial-scale trends in west Pacific warm pool hydrology since the Last Glacial Maximum, *Nature*, *449*(7161), 452-455.